Dup.

NASA
Reference
Publication
1126

August 1984

Lubrication of Machine Elements

Bernard J. Hamrock

NASA

NASA Reference Publication 1126

1984

Lubrication of Machine Elements

Bernard J. Hamrock

Lewis Research Center
Cleveland, Ohio

NASA

National Aeronautics
and Space Administration

Scientific and Technical Information Branch

Contents

Summary

By the middle of this century two distinct regimes of lubrication were generally recognized. The first of these was hydrodynamic lubrication. The development of the understanding of this lubrication regime began with the classical experiments of Tower (1883), in which the existence of a film was detected from measurements of pressure within the lubricant, and of Petrov (1883), who reached the same conclusion from friction measurements. This work was closely followed by Reynolds' (1886) celebrated analytical paper in which he used a reduced form of the Navier-Stokes equations in association with the continuity equation to generate a second-order differential equation for the pressure in the narrow, converging gap of a bearing contact. Such a pressure enables a load to be transmitted between the surfaces with very low friction since the surfaces are completely separated by a film of fluid. In such a situation it is the physical properties of the lubricant, notably the dynamic viscosity, that dictate the behavior of the contact.

The second lubrication regime clearly recognized by 1950 was boundary lubrication. The understanding of this lubrication regime is normally attributed to Hardy and Doubleday (1922a and b), who found that very thin films adhering to surfaces were often sufficient to assist relative sliding. They concluded that under such circumstances the chemical composition of the fluid is important, and they introduced the term "boundary lubrication." Boundary lubrication is at the opposite end of the lubrication spectrum from hydrodynamic lubrication. In boundary lubrication it is the physical and chemical properties of thin films of molecular proportions and the surfaces to which they are attached that determine contact behavior. The lubricant viscosity is not an influential parameter.

In the last 30 years research has been devoted to a better understanding and more precise definition of other lubrication regimes between these extremes. One such lubrication regime occurs in nonconformal contacts, where the pressures are high and the bearing surfaces deform elastically. In this situation the viscosity of the lubricant may rise considerably, and this further assists the formation of an effective fluid film. A lubricated contact in which such effects are to be found is said to be operating elastohydrodynamically. Significant progress has been made in our understanding of the mechanism of elastohydrodynamic lubrication, generally viewed as reaching maturity.

This report briefly describes the science of these three lubrication regimes (hydrodynamic, elastohydrodynamic, and boundary) and then demonstrates how this science is used in the design of machine elements.

Symbols

A_p	total projected pad area, m^2
a_b	groove width ratio
a_f	bearing pad load coefficient
B	total conformity of ball bearing
b	semiminor axis of contact, m; width of pad, m
$\bar{b}$	length ratio, b_s/b_r
b_g	length of feed groove region, m
b_r	length of ridge region, m
b_s	length of step region, m
C	dynamic load capacity, N
C_l	load coefficient, $F/p_a Rl$
c	radial clearance of journal bearing, m
c'	pivot circle clearance, m
c_b	bearing clearance at pad minimum film thickness (fig. 2.1-9), m
c_d	orifice discharge coefficient
D	distance between race curvature centers, m
$\tilde{D}$	material factor
D_x	diameter of contact ellipse along x-axis, m
D_y	diameter of contact ellipse along y-axis, m
d	diameter of rolling element or diameter of journal, m
d_a	overall diameter of ball bearing (fig. 2.6-2), m
d_b	bore diameter of ball bearing, m
d_c	diameter of capillary tube, m
d_i	inner-race diameter of ball bearing, m
d_o	outer-race diameter of ball bearing, m
$\bar{d}_o$	diameter of orifice, m
E	modulus of elasticity, N/m^2

E' effective elastic modulus, $2\Big/\left(\frac{1-\nu_a^2}{E_a}+\frac{1-\nu_b^2}{E_b}\right)$, N/m²

$\tilde{E}$ metallurgical processing factor

$\mathfrak{E}$ elliptic integral of second kind

e eccentricity of journal bearing, m

F applied normal load, N

F' load per unit length, N/m

$\tilde{F}$ lubrication factor

$\mathfrak{F}$ elliptic integral of first kind

F_c pad load component along line of centers (fig. 2.4-1), N

F_e rolling-element-bearing equivalent load, N

F_r applied radial load, N

F_s pad load component normal to line of centers (fig. 2.4-1), N

F_t applied thrust load, N

f race conformity ratio

f_c coefficient dependent on materials and rolling-element-bearing type (table 3.6-10)

G dimensionless materials parameter

$\tilde{G}$ speed effect factor

G_f groove factor

g_e dimensionless elasticity parameter, $W^{8/3}/U^2$

g_v dimensionless viscosity parameter, GW^3/U^2

H dimensionless film thickness, h/R_x

$\tilde{H}$ misalignment factor

H_a dimensionless film thickness ratio, h_s/h_r

H_b pad pumping power, N m/s

H_c power consumed in friction per pad, W

H_f pad power coefficient

$H_{\min}$ dimensionless minimum film thickness, $h_{\min}/R_x$

$\hat{H}_{\min}$ dimensionless minimum film thickness, $H_{\min}\,(W/U)^2$

H_p dimensionless pivot film thickness, h_p/c

H_t dimensionless trailing-edge film thickness, h_t/c

h film thickness, m

h_i inlet film thickness, m

$\bar{h}_i$ film thickness ratio, h_i/h_o

h_l leading-edge film thickness, m

$h_{\min}$ minimum film thickness, m

h_o outlet film thickness, m

h_p film thickness at pivot, m

h_r film thickness in ridge region, m

h_s film thickness in step region, m

h_t film thickness at trailing edge, m

h_0 film constant, m

J number of stress cycles

K load deflection constant

$\bar{K}$ dimensionless stiffness coefficient, cK_p/p_aRl

K_a dimensionless stiffness, $-c(\partial\bar{W}/\partial c)$

K_p film stiffness, N/m

K_1 load-deflection constant for a roller bearing

$K_{1.5}$ load-deflection constant for a ball bearing

$\bar{K}_\infty$ dimensionless stiffness, cK_p/p_aRl

k ellipticity parameter, D_y/D_x

k_c capillary tube constant, m³

k_o orifice constant, m⁴/s N$^{1/2}$

L fatigue life

L_a adjusted fatigue life

L_{10} fatigue life where 90 percent of bearing population will endure

L_{50} fatigue life where 50 percent of bearing population will endure

l bearing length, m

l_c length of capillary tube, m

l_r roller effective length, m

l_t roller length, m

l_v length dimension in stress volume, m

l_1 total axial length of groove, m

M probability of failure

$\bar{M}$ stability parameter, $\bar{m}p_ah_r^5/2R^5l\eta^2$

m number of rows of rolling elements

$\bar{m}$ mass supported by bearing, N s²/m

m_p preload factor

N rotational speed, rps

N_R Reynolds number

n number of rolling elements or number of pads or grooves

P dimensionless pressure, p/E'

P_d diametral clearance, m

P_e free endplay, m

p pressure, N/m²

p_a ambient pressure, N/m²

p_l lift pressure, N/m²

$p_{\max}$ maximum pressure, N/m²

p_r recess pressure, N/m²

p_s bearing supply pressure, N/m²

Q volume flow of lubricant, m³/s

$\bar{Q}$ dimensionless flow, $3\eta Q/\pi p_a h_r^3$

Q_c volume flow of lubricant in capillary, m³/s

Q_o volume flow of lubricant in orifice, m³/s

Q_s volume side flow of lubricant, m³/s

q constant, $\pi/2-1$

q_f bearing pad flow coefficient

R curvature sum on shaft or bearing radius, m

$\bar{R}$ groove length fraction, $(R_1 - R_g)/(R_1 - R_2)$

R_g groove radius (fig. 2.4-19), m

R_o orifice radius, m

R_x effective radius in x-direction, m

R_y effective radius in y-direction, m

R_1 outer radius of sector thrust bearing, m

R_2 inner radius of sector thrust bearing, m

r race curvature radius, m

r_c roller corner radius, m

S probability of survival

Sm Sommerfeld number for journal bearings, $\eta N d^3 l/4Fc^2$

Sm_t Sommerfeld number for thrust bearings, $\eta u b l^2/Fh_o^2$

s shoulder height, m

T tangential force, N

$\bar{T}$ dimensionless torque, $6T_r/\pi p_a(R_1^2+R_2^2)h_r\Lambda_c$

T_c critical temperature, °C

T_r torque, N m

U dimensionless speed parameter, $u\eta_0/E'R_x$

u mean surface velocity in direction of motion, m/s

v elementary volume, m^3

N dimensionless load parameter, $F/E'R_x^2$

$\bar{W}$ dimensionless load capacity, $F/p_a l(b_r+b_s+b_g)$

$\bar{W}_\infty$ dimensionless load, $1.5\ G_f F/\pi p_a(R_1^2-R_2^2)$

X, Y factors for calculation of equilvalent load

x,y,z coordinate system

$\bar{x}$ distance from inlet edge of pad to pivot, m

α radius ratio, R_y/R_x

α_a offset factor

α_b groove width ratio, $b_s/(b_r+b_s)$

α_p angular extent of pad, deg

α_r radius ratio, R_2/R_1

β contact angle, deg

β' iterated value of contact angle, deg

β_a groove angle, deg

β_f free or initial contact angle, deg

β_p angle between load direction and pivot, deg

Γ curvature difference

γ groove length ratio, l_1/l

Δ rms surface finish, m

δ total elastic deformation, m

ϵ eccentricity ratio, e/c

η absolute viscosity of lubricant, N s/m^2

η_k kinematic viscosity, η/ρ, m^2/s

η_0 viscosity at atmospheric pressure, N s/m^2

θ angle used to define shoulder height, deg

$\bar{\theta}$ dimensionless step location, $\theta_i/(\theta_i+\theta_o)$

θ_g angular extent of lubrication feed groove, deg

θ_i angular extent of ridge region, deg

θ_o angular extent of step region, deg

Λ film parameter (ratio of minimum film thickness to composite surface roughness)

Λ_c dimensionless bearing number, $3\eta\omega(R_1^2-R_2^2)/p_a h_r^2$

Λ_j dimensionless bearing number, $6\eta\omega R^2/p_a c^2$

Λ_t dimensionless bearing number, $6\eta u l/p_a h_r^2$

λ length-to-width ratio

λ_a length ratio, $(b_r+b_s+b_g)/l$

λ_b $(1+2/3\alpha)^{-1}$

μ coefficient of friction, T/F

ν Poisson's ratio

ξ pressure-viscosity coefficient of lubricant, m^2/N

ξ_p angle between line of centers and pad leading edge, deg

ρ lubricant density, N s^2/m^4

ρ_0 density at atmospheric pressure, N s^2/m^4

σ_{max} maximum Hertzian stress, N/m^2

τ shear stress, N/m^2

τ_o maximum shear stress, N/m^2

φ attitude angle in journal bearings, deg

φ_p angle between pad leading edge and pivot, deg

ψ angular location, deg

ψ_l angular limit of ψ, deg

ψ_s step location parameter, $b_s/(b_r+b_s+b_g)$

ω angular velocity, rad/s

ω_B angular velocity of rolling-element race contact, rad/s

ω_b angular velocity of rolling element about its own center, rad/s

ω_c angular velocity of rolling element about shaft center, rad/s

ω_d rotor whirl frequency, rad/s

$\bar{\omega}_d$ whirl frequency ratio, ω_d/ω_j

ω_j journal rotational speed, rad/s

Subscripts:

a solid a

b solid b

EHL elastohydrodynamic lubrication

e elastic

HL hydrodynamic lubrication

i inner

iv	isoviscous
o	outer
pv	piezoviscous
r	rigid
x,y,z	coordinate system

1 Lubrication Fundamentals

A lubricant is any substance that is used to reduce friction and wear and to provide smooth running and a satisfactory life for machine elements. Most lubricants are liquids (like mineral oils, the synthetic esters and silicone fluids, and water), but they may be solids (such as polytetrafluoroethylene) for use in dry bearings or gases (such as air) for use in gas bearings. An understanding of the physical and chemical interactions between the lubricant and the tribological surfaces is necessary if the machine elements are to be provided with satisfactory life. To help in the understanding of this tribological behavior, the first section describes some lubrication fundamentals.

1.1 Conformal and Nonconformal Surfaces

Hydrodynamic lubrication is generally characterized by surfaces that are conformal. That is, the surfaces fit snugly into each other with a high degree of geometrical conformity, as shown in figure 1.1-1, so that the load is carried over a relatively large area. Furthermore, the load-carrying surface remains essentially constant while the load is increased. Fluid-film journal bearings (fig. 1.1-1) and slider bearings exhibit conformal surfaces. In journal bearings the radial clearance between the shaft and bearing is typically one-thousandth of the shaft diameter; in slider bearings the inclination of the bearing surface to the runner is typically one part in a thousand. These converging surfaces, coupled with the fact that there is relative motion and a viscous fluid separating the surfaces, enable a positive pressure to be developed and exhibit a capacity to support a normal applied load. The magnitude of the pressure developed *is not* generally large enough to cause significant elastic deformation of the surfaces. The minimum film thickness in a hydrodynamically lubricated bearing is a function of applied load, speed, lubricant viscosity, and geometry. The relationship between the minimum film thickness h_{min} and the speed u and applied normal load F for conformal surfaces is given as

$$(h_{min})_{HL} \propto \left(\frac{u}{F}\right)^{1/2} \tag{1.1-1}$$

For more coverage of hydrodynamic lubrication see Section 2.

Many machine elements have contacting surfaces that *do not* conform to each other very well, as shown in figure 1.1-2 for a rolling-element bearing. The full burden of the load must then be carried by a very small contact area. In general, the contact areas between nonconformal surfaces enlarge considerably with increasing load, but they are still smaller than the contact areas between conformal surfaces. Some examples of nonconformal surfaces are mating gear teeth, cams and followers, and rolling-element bearings (fig. 1.1-2). The mode of lubrication normally found in these nonconformal contacts is elastohydrodynamic lubrication. The requirements necessary for hydrodynamic lubrication (converging surfaces, relative motion, and viscous fluid) are also required for elastohydrodynamic lubrication.

The relationship between the minimum film thickness and normal applied load and speed for an elastohydrodynamically lubricated contact is

$$(h_{min})_{EHL} \propto F^{-0.073} \tag{1.1-2}$$

$$(h_{min})_{EHL} \propto u^{0.68} \tag{1.1-3}$$

The results of equations (1.1-2) and (1.1-3) compare with that obtained for hydrodynamic lubrication expressed in equation (1.1-1) as follows:

(1) The exponent on the normal applied load is nearly seven times larger for hydrodynamic lubrication of conformal contacts than for elastohydrodynamic lubrication. This implies that in elastohydrodynamic lubrication the film thickness is only slightly affected by load while in hydrodynamic lubrication it is significantly affected by load.

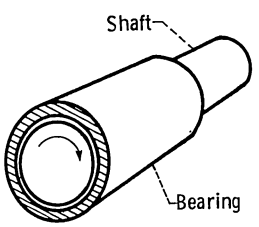

Figure 1.1-1.—Conformal surfaces. (From Hamrock and Anderson, 1983.)

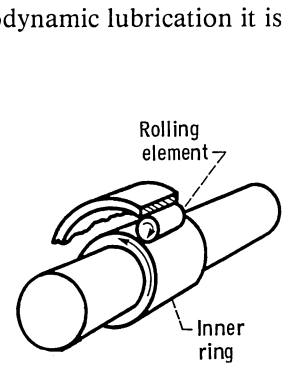

Figure 1.1-2.—Nonconformal surfaces. (From Hamrock and Anderson, 1983.)

(2) The exponent on mean velocity is slightly higher for elastohydrodynamic lubrication than for hydrodynamic lubrication.

For more discussion of elastohydrodynamic lubrication see Section 3.

The load per unit area in conformal bearings is relatively low, typically averaging only 1 MN/m^2 and seldom over 7 MN/m^2. By contrast, the load per unit area in nonconformal contacts will generally exceed 700 MN/m^2 even at modest applied loads. These high pressures result in elastic deformation of the bearing materials such that elliptical contact areas are formed for oil film generation and load support. The significance of the high contact pressures is that they result in a considerable increase in fluid viscosity. Inasmuch as viscosity is a measure of a fluid's resistance to flow, this increase greatly enhances the lubricant's ability to support load without being squeezed out of the contact zone. The high contact pressures in nonconforming surfaces therefore result in both an elastic deformation of the surfaces and large increases in the fluid's viscosity. The minimum film thickness is a function of the parameters found for hydrodynamic lubrication with the addition of an effective modulus-of-elasticity parameter for the bearing materials and a pressure-viscosity coefficient for the lubricant.

1.2 Bearing Selection

Ball bearings are used in many kinds of machines and devices with rotating parts. The designer is often confronted with decisions on whether a nonconformal bearing such as a rolling-element bearing or a conformal bearing such as a hydrodynamic bearing should be used in a particular application. The following characteristics make rolling-element bearings *more desirable* than hydrodynamic bearings in many situations:

(1) Low starting and operating friction
(2) The ability to support combined radial and thrust loads
(3) Less sensitivity to interruptions in lubrication
(4) No self-excited instabilities
(5) Good low-temperature starting

Within reasonable limits changes in load, speed, and operating temperature have but little effect on the satisfactory performance of rolling-element bearings.

The following characteristics make nonconformal bearings such as rolling-element bearings *less desirable* than conformal (hydrodynamic) bearings:

(1) Finite fatigue life subject to wide fluctuations
(2) Large space required in the radial direction
(3) Low damping capacity
(4) High noise level
(5) More severe alignment requirements
(6) Higher cost

Each type of bearing has its particular strong points, and care should be taken in choosing the most appropriate type of bearing for a given application.

The Engineering Sciences Data Unit documents (1965, 1967) provide an excellent guide to the selection of the type of journal or thrust bearing most likely to give the required performance when considering the load, speed, and geometry of the bearing. The following types of bearings were considered:

(1) Rubbing bearings, where the two bearing surfaces rub together (e.g., unlubricated bushings made from materials based on nylon, polytetrafluoroethylene, also known as PTFE, and carbon).
(2) Oil-impregnated porous metal bearings, where a porous metal bushing is impregnated with lubricant to give a self-lubricating effect (as in sintered-iron and sintered-bronze bearings).
(3) Rolling-element bearings, where relative motion is facilitated by interposing rolling elements between stationary and moving components (as in ball, roller, and needle bearings).
(4) Hydrodynamic film bearings, where the surfaces in relative motion are kept apart by pressures generated hydrodynamically in the lubricant film.

Figure 1.2-1, reproduced from the Engineering Sciences Data Unit publication (1965), gives a guide to the typical load that can be carried at various speeds, for a nominal life of 10 000 hr at room temperature, by journal bearings of various types on shafts of the diameters quoted. The heavy curves indicate the preferred type of journal bearing for a particular load, speed, and diameter and thus divide the graph into distinct regions. From figure 1.2-1 it is observed that rolling-element bearings are preferred at lower speeds and hydrodynamic oil film bearings are preferred at higher speeds. Rubbing bearings and oil-impregnated porous metal bearings are not preferred for any of the speeds, loads, or shaft diameters considered. Also, as the shaft diameter is increased, the transitional point at which hydrodynamic bearings are preferred over rolling-element bearings quite rapidly moves toward lower rotational frequency.

The applied load and speed are usually known, and this enables a preliminary assessment to be made of the type of journal bearing most likely to be suitable for a particular application. In many cases the shaft diameter will have been determined by other considerations, and figure 1.2-1 can be used to find the type of journal bearing that will give adequate load capacity at the required speed. These curves are based on good engineering practice and commercially available parts. Higher loads and speeds or smaller shaft diameters are possible with exceptionally high engineering standards or specially produced materials. Except for rolling-element bearings the curves are drawn for bearings with a width equal to

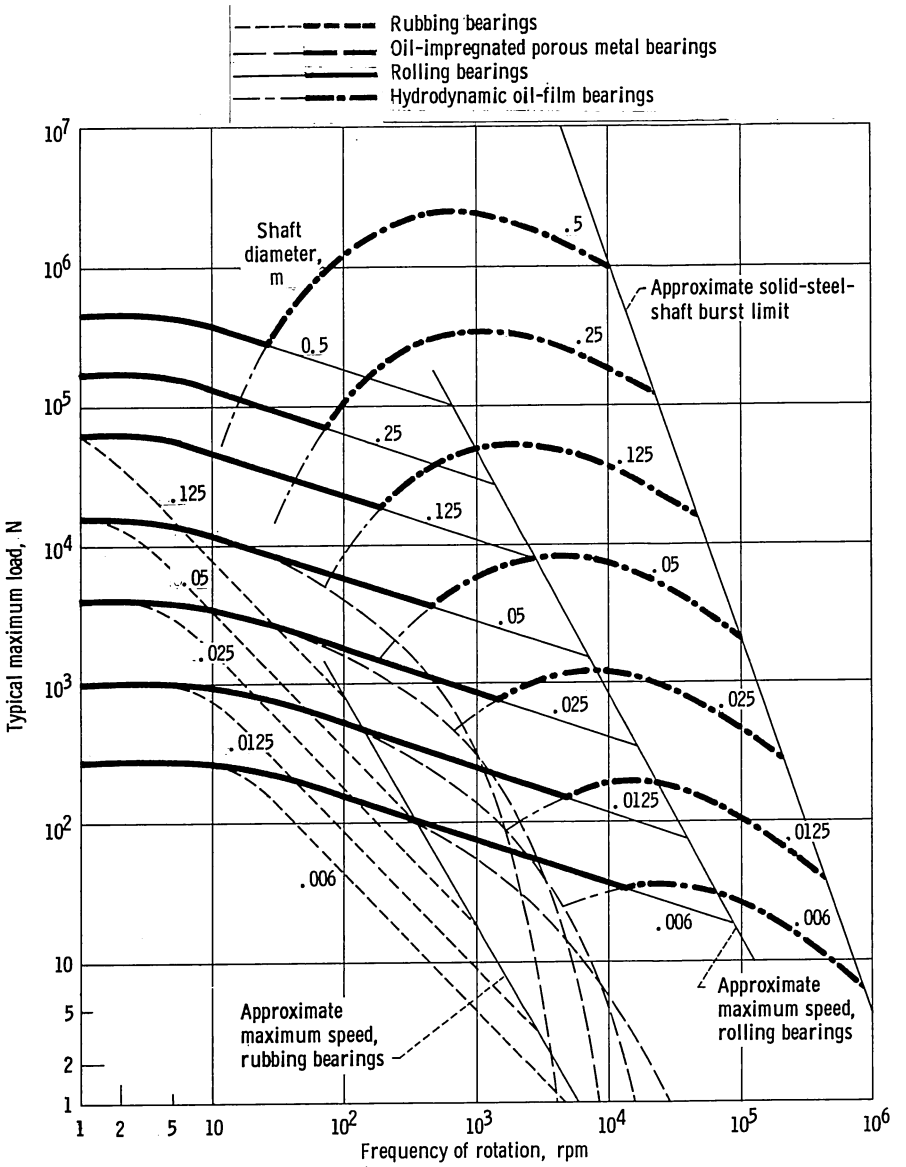

Figure 1.2-1.—General guide to journal bearing type. (Except for roller bearings, curves are drawn for bearings with width equal to diameter. A medium-viscosity mineral oil lubricant is assumed for hydrodynamic bearings.) (From Engineering Sciences Data Unit, 1965.)

the diameter. A medium-viscosity mineral oil lubricant is assumed for the hydrodynamic bearings.

Similarly, figure 1.2-2, reproduced from the Engineering Sciences Data Unit publication (1967), gives a guide to the typical maximum load that can be carried at various speeds for a nominal life of 10 000 hr at room temperature by thrust bearings of the various diameters quoted. The heavy curves again indicate the preferred type of bearing for a particular load, speed, and diameter and thus divide the graph into major regions. As with the journal bearing results (fig. 1.2-1) the hydrodynamic bearing is preferred at higher speeds. A difference between figures 1.2-1 and 1.2-2 is that at very low speeds there is a portion of the latter figure in which the rubbing bearing is preferred. As the shaft diameter is increased, the transitional point at which hydrodynamic bearings are preferred over rolling-element bearings again moves to the left. Oil-impregnated porous metal bearings are not preferred for any of the speeds, loads, or shaft diameters considered in this figure.

1.3 Lubricants

Both oils and greases are extensively used as lubricants for all types of machine elements over wide ranges of speeds, pressures, and operating temperatures. Frequently the choice is determined by considerations other than lubrication requirements. The requirements of the lubricant for successful operation of nonconformal contacts such as in rolling-element bearings and gears are

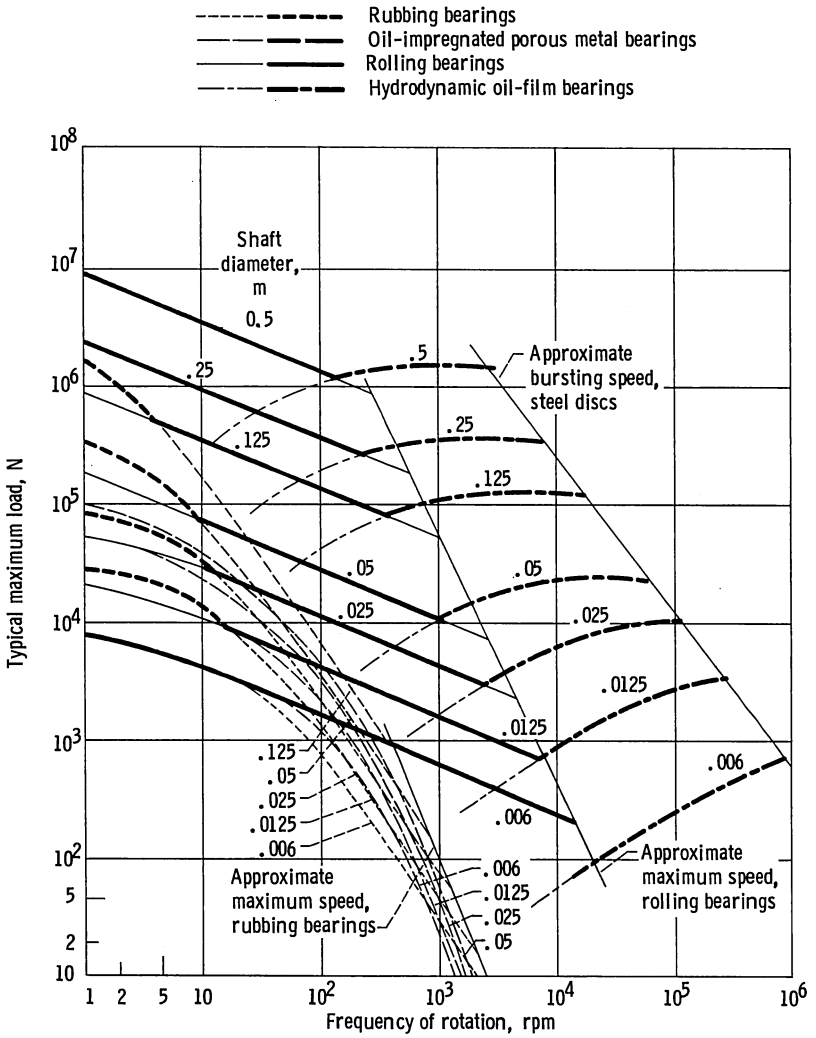

Figure 1.2-2.—General guide to thrust bearing type. (Except for roller bearings, curves are drawn for typical ratios of inside to outside diameter. A medium-viscosity mineral oil lubricant is assumed for hydrodynamic bearings.) (From Engineering Sciences Data Unit, 1967.)

considerably more stringent than those for conformal bearings and therefore will be the primary concern in this section.

Because of its fluidity oil has several advantages over grease: it can enter the loaded conjunction most readily to flush away contaminants, such as water and dirt, and particularly to transfer heat from heavily loaded machine elements. Grease, however, is extensively used because it permits simplified designs of housings and enclosures, which require less maintenance, and because it is more effective in sealing against dirt and contaminants.

1.3.1 Viscosity

In hydrodynamic and elastohydrodynamic lubrication the most important physical property of a lubricant is its viscosity. The viscosity of a fluid may be associated with its resistance to flow, that is, with the resistance arising from intermolecular forces and internal friction as the molecules move past each other. Thick fluids, like molasses, have relatively high viscosity; they do not flow easily. Thinner fluids, like water, have lower viscosity; they flow very easily.

The relationship for internal friction in a viscous fluid (as proposed by Newton, 1687) can be written as

$$\tau = \eta \frac{du}{dz} \tag{1.3-1}$$

where

τ internal shear stress in the fluid in the direction of motion

η coefficient of absolute or dynamic viscosity or coefficient of internal friction

du/dz velocity gradient perpendicular to the direction of motion (i.e., shear rate)

It follows from equation (1.3-1) that the unit of dynamic viscosity must be the unit of shear stress divided by the unit of shear rate. In the newton-meter-second system the unit of shear stress is the newton per square meter while that of shear rate is the inverse second. Hence the unit of dynamic viscosity will be newton per square meter multiplied by second, or N s/m^2. In the SI system the unit of pressure or stress (N/m^2) is known as pascal, abbreviated Pa, and it is becoming increasingly common to refer to the SI unit of viscosity as the pascal-second (Pa s). In the cgs system, where the dyne is the unit of force, dynamic viscosity is expressed as dyne-second per square centimeter. This unit is called the poise, with its submultiple the centipoise (1 cP = 10^2 P), of a more convenient magnitude for many lubricants, used in practice.

Conversion of dynamic viscosity from one system to another can be facilitated by table 1.3-1. To convert from a unit in the column on the left side of the table to a unit at the top of the table, multiply by the corresponding value given in the table. For example, $\eta = 0.04$ N s/m^2 $= 0.04 \times 1.45 \times 10^{-4}$ lbf s/in^2 $= 5.8 \times 10^{-6}$ lbf s/in^2. Three metric and one English system are presented—all based on force, length, and time. Metric units are the centipoise, the kilogram force-second per square meter, and the newton-second per square meter (or Pa s). The English unit is pound force-second per square inch, or reyn in honor of Osborne Reynolds.

In many situations it is convenient to use the *kinematic viscosity* rather than the dynamic viscosity. The kinematic viscosity η_k is equal to the dynamic viscosity η divided by the density ρ of the fluid ($\eta_k = \eta/\rho$). The ratio is literally kinematic, all trace of force or mass cancelling out. The unit of kinematic viscosity may be written in SI units as square meters per second, in English units as square inches per second, or in cgs units as square centimeters per second. The name stoke, in honor of Sir George Gabriel Stokes, was proposed for the cgs unit by Max Jakob in 1928. The centistoke, or one-hundredth part, is an everyday unit of more convenient size, corresponding to the centipoise.

The viscosity of a given lubricant varies within a given machine element as a result of the nonuniformity of pressure or temperature prevailing in the lubricant film. Indeed, many lubricated machine elements operate over ranges of pressure or temperature so extensive that the consequent substantial variations in the viscosity of the lubricant may dominate the operating characteristics of the machine element. Consequently an adequate knowledge of the viscosity-pressure and viscosity-pressure-temperature relationships of lubricants is thus indispensable.

1.3.2 Oil lubrication

Except for a few special requirements, petroleum oils satisfy most operating conditions in machine elements. High-quality products, free from adulterants that can have an abrasive or lapping action, are recommended. Animal or vegetable oils and even petroleum oils of poor quality tend to oxidize, to develop acids, or to form sludge or resinlike deposits on the bearing surfaces. They thus penalize bearing performance or endurance.

A composite of recommended lubricant kinematic viscosities at 38° C (100° F) is shown in figure 1.3-1. The ordinate of this figure is the speed factor, which is bearing bore size measured in millimeters multiplied by the speed in revolutions per minute. In many rolling-element bearing applications an oil equivalent to an SAE-10 motor oil (4×10^{-6} m^2/s, or 40 cS, at 38° C (100° F)) or a light turbine oil is the most frequent choice.

For a number of military applications where the operational requirements span the temperature range −54° to 204° C (−65° to 400° F), synthetic oils are used. Ester lubricants are most frequently employed in this temperature range. In applications where temperatures exceed 260° C (500° F), most synthetics will quickly break down, and either a solid lubricant (e.g., MoS_2) or a polyphenyl ether is recommended. For a more detailed discussion of synthetic lubricants, see Bisson and Anderson (1964).

1.3.3 Grease lubrication

The simplest method of lubricating a bearing is to apply grease because of its relatively nonfluid characteristics. Danger of leakage is reduced, and the housing and enclosure can be simpler and less costly than those

TABLE 1.3-1. - VISCOSITY CONVERSION

To convert from-	To-			
	cP	kgf s/m^2	N s/m^2	lbf s/in^2
	Multiply by-			
cP	1	1.02×10^{-4}	10^{-3}	1.45×10^{-7}
kgf s/m^2	9.807×10^3	1	9.807	1.422×10^{-3}
N s/m^2	10^3	1.02×10^{-1}	1	1.45×10^{-4}
lbf s/in^2	6.9×10^6	7.034×10^2	6.9×10^3	1

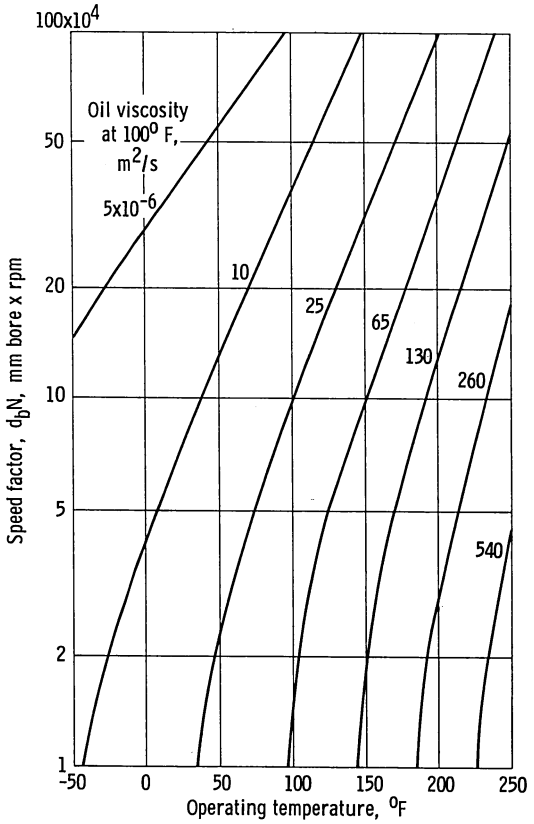

Figure 3.17 - Recommended lubricant viscosities for ball bearings.

Figure 1.3-1.—Recommended lubricant viscosities for ball bearings. (From Hamrock and Dowson, 1981.)

used with oil. Grease can be packed into bearings and retained with inexpensive enclosures, but packing should not be excessive and the manufacturer's recommendations should be closely adhered to.

The major limitation of grease lubrication is that it is not particularly useful in high-speed applications. In general, it is not employed for speed factors over 200 000, although selected greases have been used successfully for higher speed factors with special designs.

Greases vary widely in properties depending on both the type and the grade or consistency. For this reason few specific recommendations can be made. Greases used for most bearing operating conditions consist of petroleum, diester, polyester, or silicone oils thickened with sodium or lithium soaps or with more recently developed nonsoap thickeners. General characteristics of greases are as follows:

(1) Petroleum oil greases are best for general-purpose operation from −34° to 149° C (−30° to 300° F).

(2) Diester oil greases are designed for low-temperature service down to −54° C (−65° F).

(3) Ester-based greases are similar to diester oil greases but have better high-temperature characteristics, covering the range −73° to 177° C (−100° to 350° F).

(4) Silicone oil greases are used for both high- and low-temperature operation, over the widest temperature range of all greases (−73° to 232° C; −100° to 450° F), but have the disadvantage of low load-carrying capacity.

(5) Fluorosilicone oil greases have all of the desirable features of silicone oil greases plus good load capacity and resistance to fuels, solvents, and corrosive substances. Their very low volatility in vacuum down to 10^{-7} torr makes them useful in aerospace applications.

(6) Perfluorinated oil greases have a high degree of chemical inertness and are completely nonflammable. They have good load-carrying capacity and can operate at temperatures as high as 280° C (550° F) for long periods. This makes them useful in the chemical processing and aerospace industries, where high reliability justifies the additional cost.

Grease consistency is important since grease will slump badly and churn excessively when too soft and fail to lubricate when too hard. Either condition causes improper lubrication, excessive temperature rise, and poor performance and can shorten machine element life. A valuable guide to the estimation of the useful life of grease in rolling-element bearings has been published by the Engineering Sciences Data Unit (1978).

It has been demonstrated recently by Aihara and Dowson (1979) and by Wilson (1979) that the film thickness in grease-lubricated components can be calculated with adequate accuracy by using the viscosity of the base oil in the elastohydrodynamic equation (see Section 3). This enables the elastohydrodynamic lubrication film thickness formulas to be applied with confidence to grease-lubricated machine elements.

1.4 Lubrication Regimes

If a machine element is adequately designed and lubricated, the lubricated surfaces are separated by a lubricant film. Endurance testing of ball bearings, as reported by Tallian et al. (1965) has demonstrated that when the lubricant film is thick enough to separate the contacting bodies, fatigue life of the bearing is greatly extended. Conversely, when the film is not thick enough to provide full separation between the asperities in the contact zone, the life of the bearing is adversely affected by the high shear resulting from direct metal-to-metal contact.

To establish the effect of film thickness on the life of the machine element, we first introduce a relevant parameter Λ. The relationship between Λ and the minimum film thickness h_{min} is defined to be

$$\Lambda = \frac{h_{min}}{\left(\Delta_a^2 + \Delta_b^2\right)^{1/2}} \tag{1.4-1}$$

where

Δ_a rms surface finish of surface a

Δ_b rms surface finish of surface b

Hence Λ is just the minimum film thickness in units of the composite roughness of the two bearing surfaces.

1.4.1 Hydrodynamic lubrication regime

Hydrodynamic lubrication occurs when the lubricant film is sufficiently thick to prevent the opposing solids from coming into contact. This condition is often referred to as the ideal form of lubrication since it provides low friction and a high resistance to wear. The lubrication of the contact is governed by the bulk physical properties of the lubricant, notably viscosity, and the frictional characteristics arise purely from the shearing of the viscous lubricant. The pressure developed in the oil film of hydrodynamically lubricated bearings is due to two factors:

(1) The geometry of the moving surfaces produces a convergent film shape.

(2) The viscosity of the liquid results in a resistance to flow.

The lubricant films are normally many times thicker than the surface roughness so that the physical properties of the lubricant dictate contact behavior. The film thickness normally exceeds 10^{-6} m. For hydrodynamic lubrication the film parameter Λ, defined in equation (1.4-1), is in excess of 10 and may even rise to 100. Films of this thickness are clearly also insensitive to chemical action in surface layers of molecular proportions.

For normal load support to occur in bearings, positive pressure profiles must develop over the length of the bearing. Three different forms of hydrodynamic lubrication are presented in figure 1.4-1. For a positive load to be developed in a slider bearing (fig. 1.4-1(a)) the lubricant film thickness must be decreasing in the direction of sliding.

A squeeze film bearing (fig. 1.4-1(b)) is another mechanism of load support by hydrodynamic lubrication. The squeeze action is the normal approach of the bearing surfaces. The squeeze mechanism of pressure generation provides a valuable cushioning effect when the bearing surfaces tend to be pressed together. Positive pressures will be generated when the film thickness is diminishing.

An externally pressurized bearing is a mechanism of load support by hydrostatic lubrication, as illustrated in figure 1.4-1(c). The pressure drop across the bearing is used to support the load. The load capacity is independent of the motion of the bearing and the viscosity of the lubricant. There is no problem of contact at starting and stopping as with the other hydrodynamically lubricated bearings because pressure is applied before starting and maintained until after stopping.

Hydrodynamically and hydrostatically lubricated bearings are discussed further in Section 2.

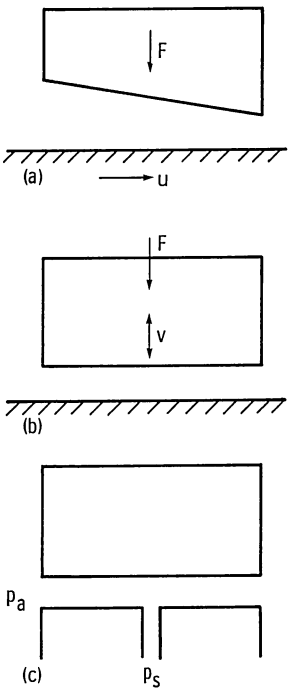

(a) Slider bearing.
(b) Squeeze film bearing.
(c) Externally pressurized bearing.

Figure 1.4-1.—Mechanisms of load support for hydrodynamic and hydrostatic lubrication.

1.4.2 Elastohydrodynamic lubrication regime

Elastohydrodynamic lubrication is a form of hydrodynamic lubrication where elastic deformation of the bearing surfaces becomes significant. It is usually associated with highly stressed machine components of low conformity. There are two distinct forms of elastohydrodynamic lubrication (EHL).

Hard EHL

Hard EHL relates to materials of *high* elastic modulus, such as metals. In this form of lubrication both the elastic deformation and the pressure-viscosity effects are equally important. Engineering applications in which elastohydrodynamic lubrication are important for high-elastic-modulus materials include gears and rolling-element bearings.

Soft EHL

Soft EHL relates to materials of *low* elastic modulus, such as rubber. For these materials the elastic distortions are large, even with light loads. Another feature of the elastohydrodynamics of low-elastic-modulus materials is the negligible effect of the relatively low pressures on the viscosity of the lubricating fluid. Engineering applications in which elastohydrodynamic lubrication are important for low-elastic-modulus materials include seals,

human joints, tires, and a number of lubricated machine elements of elastomeric material.

The common factors in hard and soft EHL are that the local elastic deformation of the solids provides coherent fluid films and that asperity interaction is largely prevented. Elastohydrodynamic lubrication normally occurs in contacts where the minimum film thickness is in the range $0.1\ \mu m < h_{min} \leq 10\ \mu m$ and the film parameter Λ is in the range $3 \leq \Lambda < 10$. Elastohydrodynamic lubrication is discussed further in Section 3.

1.4.3 Boundary lubrication regime

If in a lubricated contact the pressures become too high, the running speeds too low, or the surface roughness too great, penetration of the lubricant film will occur. Contact will take place between the asperities. The friction will rise and approach that encountered in dry friction between solids. More importantly, wear will take place. Adding a small quantity of certain organic compounds containing surface-active elements to the lubricating oil may, however, extend the life of the machine elements. These additives are present in small quantities (<1 percent) and function by forming low-shear-strength surface films strongly attached to the metal surfaces. Although they are sometimes only one or two molecules thick, such films are able to prevent metal-to-metal contact.

Some boundary lubricants are long-chain molecules with an active end group, typically an alcohol, an amine, or a fatty acid. When such a material, dissolved in a mineral oil, meets a metal or other solid surface, the active end group attaches itself to the solid and gradually builds up a surface layer. The surface films vary in thickness from 5×10^{-9} to 10^{-8} m depending on molecular size, and the film parameter Λ is less than unity ($\Lambda < 1$). Boundary lubrication is discussed further in Section 4.

Figure 1.4-2 illustrates the film conditions existing in hydrodynamic, elastohydrodynamic, and boundary lubrication. The surface slopes in this figure are greatly distorted for the purpose of illustration. To scale, real surfaces would appear as gently rolling hills rather than sharp peaks.

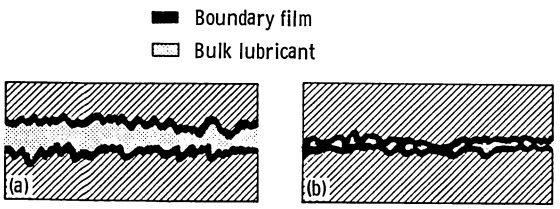

(a) Hydrodynamic and elastohydrodynamic lubrication – surfaces separated by bulk lubricant film.
(b) Boundary lubrication – performance essentially dependent on boundary film.

Figure 1.4-2.—Film conditions of lubrication regimes.

1.5 Relevant Equations

This section presents the equations frequently used in hydrodynamic and elastohydrodynamic lubrication theory. They are not relevant to boundary lubrication since in this lubrication regime bulk fluid effects are negligible. The differential equation governing the pressure distribution in hydrodynamically and elastohydrodynamically lubricated machine elements is known as the Reynolds equation. For steady-state hydrodynamic lubrication the Reynolds equation normally appears as

$$\frac{\partial}{\partial x}\left(h^3 \frac{\partial p}{\partial x}\right) + \frac{\partial}{\partial y}\left(h^3 \frac{\partial p}{\partial y}\right) = 12\,\eta u \frac{\partial h}{\partial x} \qquad (1.5\text{-}1)$$

where

h film thickness measured in the x-direction, m
p pressure, N/m^2
η lubricant viscosity, N s/m^2
u mean velocity, $(u_a + u_b)/2$, m/s

Solutions of equation (1.5-1) are rarely achieved analytically and approximate numerical solutions are sought.

For elastohydrodynamic lubrication the steady-state form of the Reynolds equation normally appears as

$$\frac{\partial}{\partial x}\left(\frac{\rho h^3}{\eta} \frac{\partial p}{\partial x}\right) + \frac{\partial}{\partial y}\left(\frac{\rho h^3}{\eta} \frac{\partial p}{\partial y}\right) = 12u \frac{\partial(\rho h)}{\partial x} \qquad (1.5\text{-}2)$$

where ρ is lubricant density in N s^2/m^4. The essential difference between equations (1.5-1) and (1.5-2) is that equation (1.5-2) allows for variation of viscosity and density in the x and y directions. Equations (1.5-1) and (1.5-2) allow for the bearing surfaces to be of finite length in the y-direction. Side leakage, or flow in the y-direction, is associated with the second term in equations (1.5-1) and (1.5-2). The solution of equation (1.5-2) is considerably more difficult than that of equation (1.5-1); therefore only numerical solutions are available.

The viscosity of a fluid may be associated with the resistance to flow arising from the intermolecular forces and internal friction as the molecules move past each other. Because of the much larger pressure variation in the lubricant conjunction the viscosity of the lubricant for elastohydrodynamic lubrication does not remain constant as is approximately true for hydrodynamic lubrication.

As long ago as 1893, Barus proposed the following formula for the isothermal viscosity-pressure dependence of liquids:

$$\eta = \eta_0 e^{\xi p} \qquad (1.5\text{-}3)$$

where

η_0 viscosity at atmospheric pressure

ξ pressure-viscosity coefficient of lubricant

The pressure-viscosity coefficient ξ characterizes the liquid considered and depends in most cases only on temperature, not on pressure.

Table 1.5-1 lists the absolute viscosities of 12 lubricants at atmospheric pressure and three temperatures as obtained from Jones et al. (1975). These values would correspond to η_0 to be used in equation (1.5-3) for the particular fluid and temperature to be used. The same 12 fluids with manufacturer and manufacturer's designation are shown in table 1.5-2. The pressure-viscosity coefficients ξ, expressed in square meters per newton, for these 12 fluids at three different temperatures are shown in table 1.5-3.

For a comparable change in pressure the relative density change is smaller than the viscosity change. However, the very high pressures in elastohydrodynamic films are such that the liquid should no longer be considered incompressible. From Dowson and Higginson (1966) the density of typical mineral oils can be written as

$$\rho = \rho_0\left(1 + \frac{0.6p}{1+1.7p}\right) \tag{1.5-4}$$

where p is given in gigapascals. This gives a maximum density increase of about 35 percent.

The film shape appearing in equation (1.5-2) can be written with sufficient accuracy as

$$h = h_0 + \frac{x^2}{2R_x} + \frac{y^2}{2R_y} + \delta(x,y) \tag{1.5-5}$$

where

h_0 film constant, m

$\delta(x,y)$ total elastic deformation, m

R_x effective radius in x-direction, m

R_y effective radius in y-direction, m

The coordinate origin here lies on the symmetry axis for the two bodies (see fig. 3.1-1). The elastic deformation can be written, from standard elasticity theory, in the form

$$\delta(x,y) = \frac{2}{\pi E'}\int\int_A \frac{p(x,y)\,dx_1 dy_1}{\left[(x-x_1)^2+(y-y_1)^2\right]^{1/2}} \tag{1.5-6}$$

where

$$E' = \frac{2}{\frac{1-\nu_a^2}{E_a} + \frac{1-\nu_b^2}{E_b}} \tag{1.5-7}$$

ν Poisson's ratio

E modulus of elasticity, N/m^2

TABLE 1.5-1. - ABSOLUTE VISCOSITIES OF TEST FLUIDS AT ATMOSPHERIC PRESSURE AND THREE TEMPERATURES

[From Jones et al. (1975).]

Test fluid	Temperature, °C		
	38	99	149
	Absolute viscosity, η, cP		
Advanced ester	25.3	4.75	2.06
Formulated advanced ester	27.6	4.96	2.15
Polyalkyl aromatic	25.5	4.08	1.80
Polyalkyl aromatic + 10 wt % heavy resin	32.2	4.97	2.03
Synthetic paraffinic oil (lot 3)	414	34.3	10.9
Synthetic paraffinic oil (lot 4)	375	34.7	10.1
Synthetic paraffinic oil (lot 4) + antiwear additive	375	34.7	10.1
Synthetic paraffinic oil (lot 2) + antiwear additive	370	32.0	9.93
C-ether	29.5	4.67	2.20
Superrefined naphthenic mineral oil	68.1	6.86	2.74
Synthetic hydrocarbon (traction fluid)	34.3	3.53	1.62
Fluorinated polyether	181	20.2	6.68

TABLE 1.5-2. - FLUIDS WITH MANUFACTURER AND MANUFACTURER'S DESIGNATION

[From Jones et al. (1975).]

Test fluid	Manufacturer	Designation
Advanced ester	Shell Oil Co.	Aeroshell® turbine oil 555 (base oil)
Formulated advanced ester	Shell Oil Co.	Aeroshell® turbine oil 555 (WRGL-358)
Polyalkyl aromatic	Continental Oil Co.	DN-600
Synthetic paraffinic oil (lot 3)	Mobil Oil Corp.	XRM 109F3
Synthetic paraffinic oil (lot 4)		XRM 109F4
Synthetic paraffinic oil + antiwear additive (lot 2)		XRM 177F2
Synthetic paraffinic oil + antiwear additive (lot 4)		XRM 177F4
C-ether	Monsanto Co.	MCS-418
Superrefined naphthenic mineral oil	Humble Oil and Refining Co.	FN 2961
Synthetic hydrocarbon (traction fluid)	Monsanto Co.	MCS-460
Fluorinated polyether	DuPont Co.	PR 143 AB (lot 10)

TABLE 1.5-3. - PRESSURE-VISCOSITY COEFFICIENTS FOR TEST FLUIDS AT THREE TEMPERATURES

[From Jones et al. (1975).]

Test fluid	Temperature, °C		
	38	99	149
	Pressure-viscosity coefficient, ξ, m^2/N		
Advanced ester	1.28×10^{-8}	0.987×10^{-8}	0.851×10^{-8}
Formulated advanced ester	1.37	1.00	.874
Polyalkyl aromatic	1.58	1.25	1.01
Polyalkyl aromatic + 10 wt % heavy resin	1.70	1.28	1.06
Synthetic paraffinic oil (lot 3)	1.77	1.51	1.09
Synthetic paraffinic oil (lot 4)	1.99	1.51	1.29
Synthetic paraffinic oil (lot 4) + antiwear additive	1.96	1.55	1.25
Synthetic paraffinic oil (lot 2) + antiwear additive	1.81	1.37	1.13
C-ether	1.80	.980	.795
Superrefined naphthenic mineral oil	2.51	1.54	1.27
Synthetic hydrocarbon (traction fluid)	3.12	1.71	.939
Fluorinated polyether	4.17	3.24	3.02

Equation (1.5-1) is normally involved in hydrodynamic lubrication situations; equations (1.5-2) to (1.5-6) are normally involved in elastohydrodynamic lubrication situations.

2 Hydrodynamic and Hydrostatic Lubrication

Surfaces lubricated hydrodynamically are normally conformal, as pointed out in Section 1.1. The conformal nature of the surfaces can take its form either as a thrust bearing or as a journal bearing, both of which will be considered in this section. Three features must exist for hydrodynamic lubrication to occur:

(1) A viscous fluid must separate the lubricated surfaces.

(2) There must be relative motion between the surfaces.

(3) The geometry of the film shape must be larger in the inlet than at the outlet so that a convergent wedge of lubricant is formed.

If feature (2) is absent, lubrication can still be achieved by establishing relative motion between the fluid and the surfaces through external pressurization. This is discussed further in Section 2.3.

In hydrodynamic lubrication the entire friction arises from the shearing of the lubricant film so that it is determined by the viscosity of the oil: the thinner (or less viscous) the oil, the lower the friction. The great advantages of hydrodynamic lubrication are that the friction can be very low ($\mu \simeq 0.001$) and, in the ideal case, there is no wear of the moving parts. The main problems in hydrodynamic lubrication are associated with starting or stopping since the oil film thickness theoretically is zero when the speed is zero.

The emphasis in this section is on hydrodynamic and hydrostatic lubrication. This section is not intended to be all inclusive but rather to typify the situations existing in hydrodynamic and hydrostatic lubrication. For additional information the reader is recommended to investigate Gross et al. (1980), Reiger (1967), Pinkus and Sternlicht (1961), and Rippel (1963).

2.1 Liquid-Lubricated Hydrodynamic Journal Bearings

Journal bearings, as shown in figure 2.1-1, are used to support shafts and to carry radial loads with minimum power loss and minimum wear. The bearing can be represented by a plain cylindrical bushing wrapped around the shaft, but practical bearings can adopt a variety of forms. The lubricant is supplied at some convenient point through a hole or a groove. If the bearing extends around the full 360° of the shaft, the bearing is described as a "full journal bearing." If the angle of wrap is less than 360°, the term "partial journal bearing" is employed.

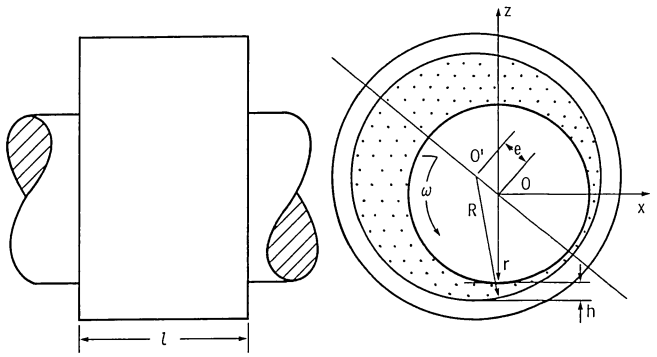

Figure 2.1-1.—Journal bearing.

2.1.1 Plain configuration

Journal bearings rely on the motion of the shaft to generate the load-supporting pressures in the lubricant film. The shaft does not normally run concentric with the bearing center. The distance between the shaft center and the bearing center is known as the eccentricity. This eccentric position within the bearing clearance is influenced by the load that it carries. The amount of eccentricity adjusts itself until the load is balanced by the pressure generated in the converging portion of the bearing. The pressure generated, and therefore the load capacity of the bearing, depends on the shaft eccentricity e, the frequency of rotation N, and the effective viscosity of the lubricant η in the converging film as well as the bearing dimensions l and d and the clearance c. The three dimensionless groupings normally used for journal bearings are

(1) The eccentricity ratio, $\epsilon = e/c$

(2) The length-to-diameter ratio, $\lambda = l/d$

(3) The Sommerfeld number, $\mathrm{Sm} = \eta N d^3 l / 4 F c^2$

When designing a journal bearing the first requirement to be met is that it should operate with an adequate minimum film thickness, which is directly related to the eccentricity ($h_{\min} = c - e$). Figures 2.1-2, 2.1-3, and 2.1-4 show the eccentricity ratio, the dimensionless minimum film thickness, and the dimensionless Sommerfeld number for, respectively, a full journal bearing and partial journal bearings of 180° and 120°. In these figures a recommended operating eccentricity ratio is indicated as well as a preferred operational area. The left boundary of the shaded zone defines the optimum eccentricity ratio for minimum coefficient of friction, and the right boundary is the optimum eccentricity ratio for maximum load. In these figures it can be observed that the shaded area is significantly reduced for the partial bearings as compared with the full journal bearing. These plots were adapted from results given in Raimondi and Boyd (1958).

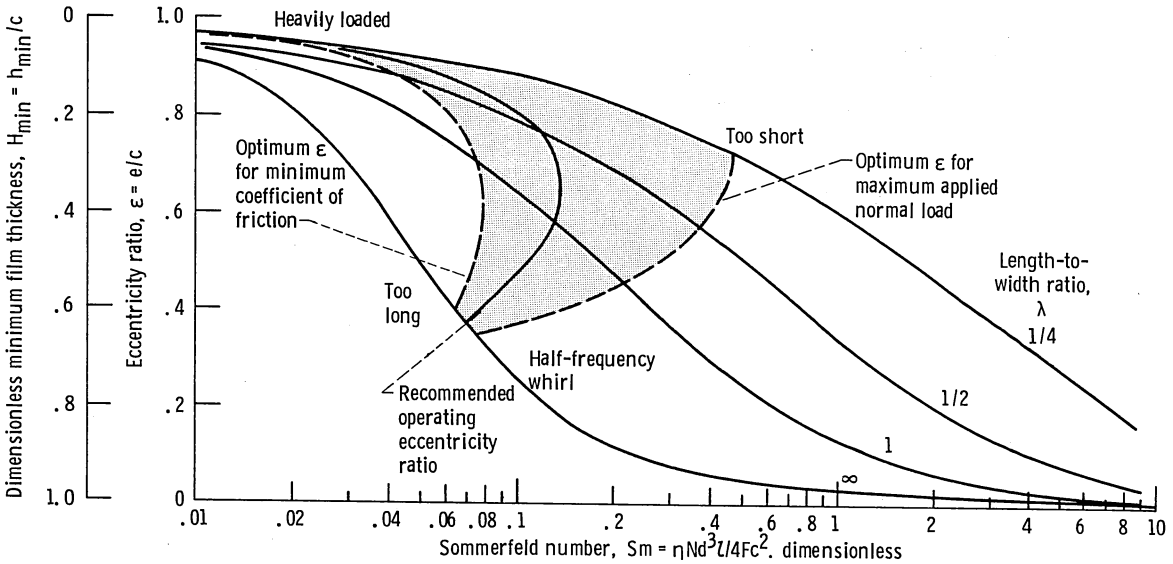

Figure 2.1-2.—Design figure showing eccentricity ratio, dimensionless minimum film thickness, and Sommerfeld number for full journal bearings. (Adapted from Raimondi and Boyd, 1958.)

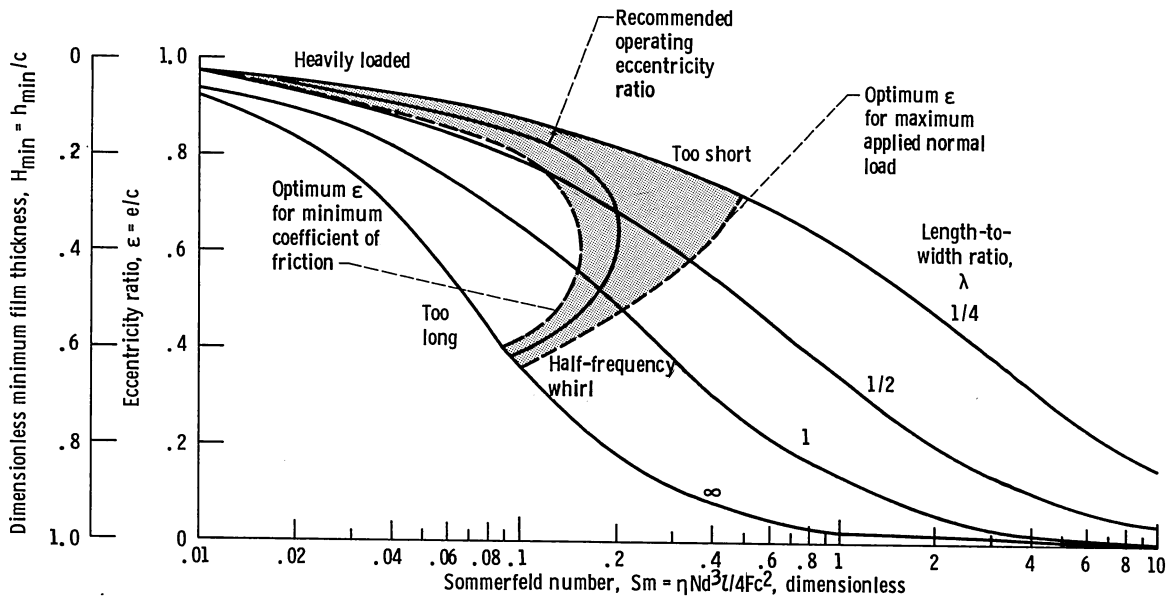

Figure 2.1-3.—Design figure showing eccentricity ratio, dimensionless minimum film thickness, and Sommerfeld number for 180° partial journal bearings, centrally loaded. (Adapted from Raimondi and Boyd, 1958.)

Figures 2.1-5, 2.1-6, and 2.1-7 show a plot of attitude angle φ (angle between the direction of the load and a line drawn through the centers of the bearing and the journal) and the bearing characteristic number for various length-to-diameter ratios for, respectively, a full journal bearing and partial journal bearings of 180° and 120°. This angle establishes where the minimum and maximum film thicknesses are located within the bearing. These plots were also adapted from results given in Raimondi and Boyd (1958), where additional information about the coefficient of friction, the flow variable, the temperature rise, and the maximum film pressure ratio for a complete range of length-to-diameter ratios as well as for full or partial journal bearings can be found.

2.1.2 Nonplain configuration

As applications have demanded higher speeds, vibration problems due to critical speeds, unbalance, and instability have created a need for journal bearing geometries other than plain journal bearings. These geometries have various patterns of variable clearance so as to create pad film thicknesses that have more strongly converging and diverging regions. Figure 2.1-8 shows elliptical, offset half, three-lobe, and four-lobe

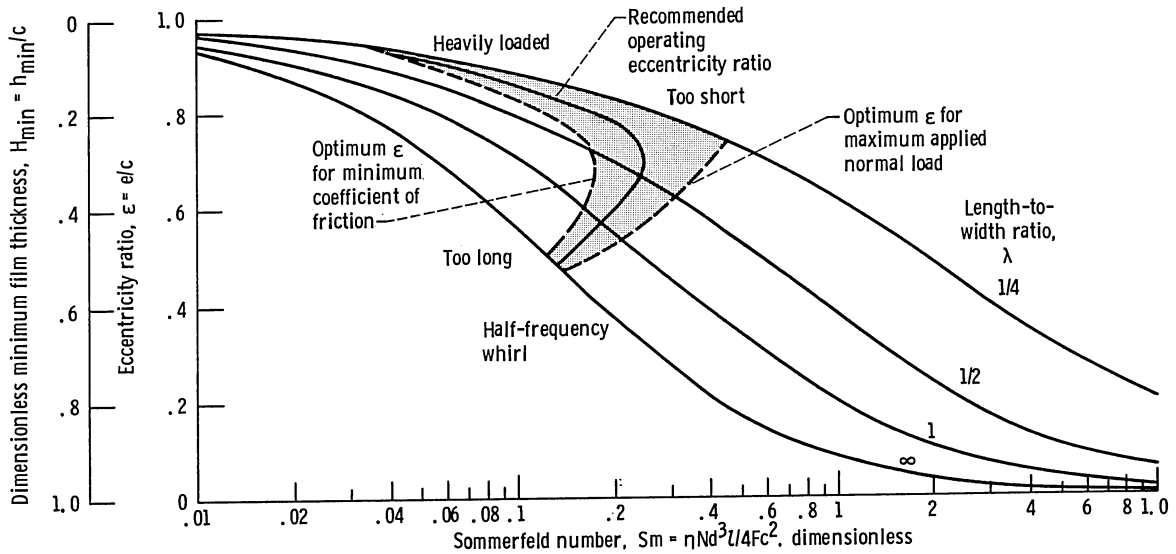

Figure 2.1-4.—Design figure showing eccentricity ratio, dimensionless minimum film thickness, and Sommerfeld number for 120° partial journal bearings, centrally loaded. (Adapted from Raimondi and Boyd, 1958.)

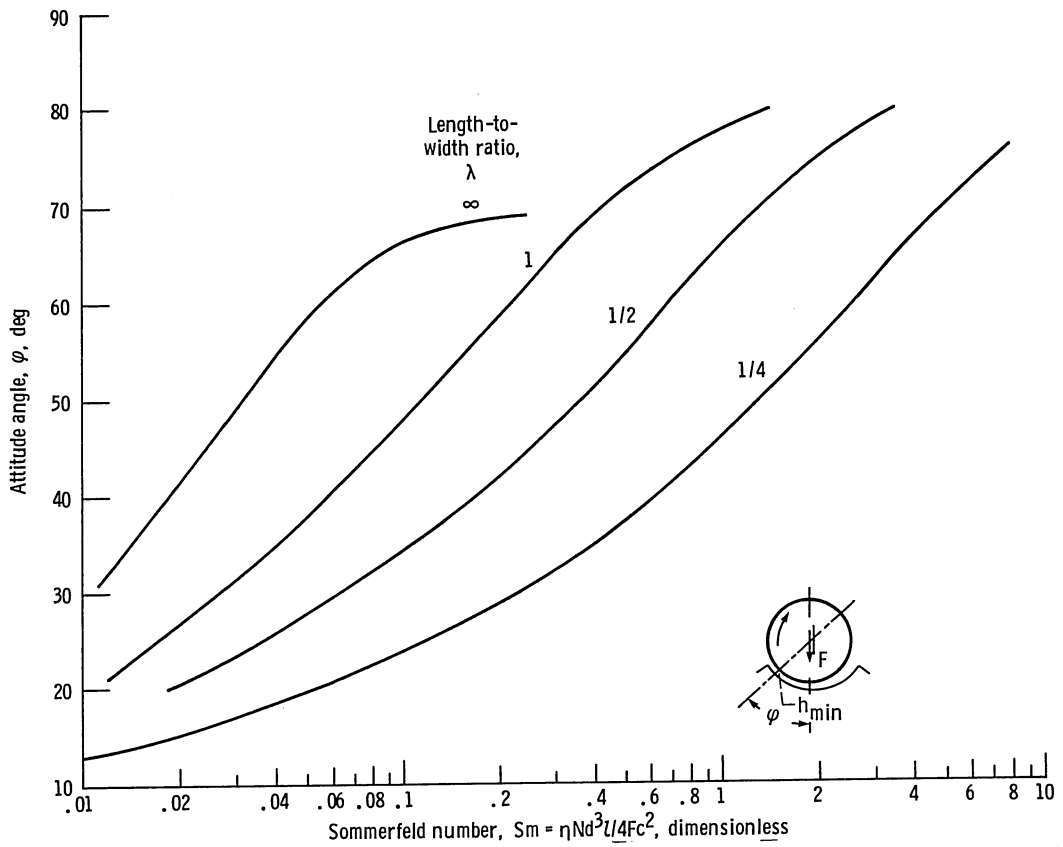

Figure 2.1-5.—Design figure showing attitude angle (position of minimum film thickness) and Sommerfeld number for full journal bearings, centrally loaded. (Adapted from Raimondi and Boyd, 1958.)

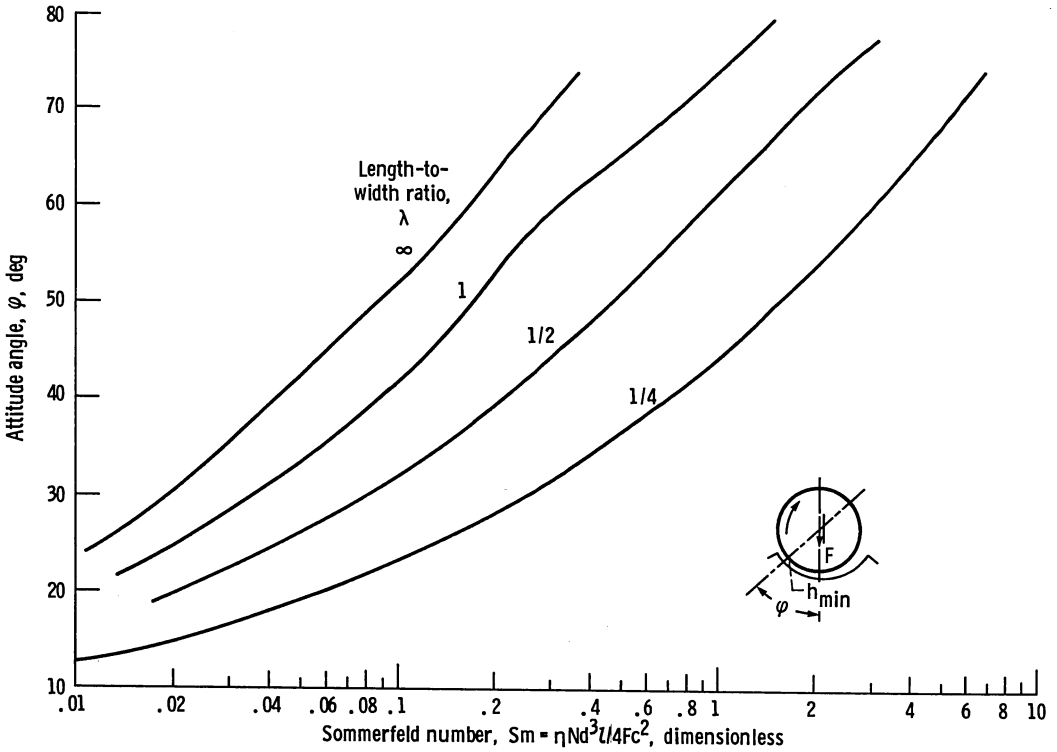

Figure 2.1-6.—Design figure showing attitude angle (position of minimum film thickness) and Sommerfeld number for 180° partial journal bearings, centrally loaded. (Adapted from Raimondi and Boyd, 1958.)

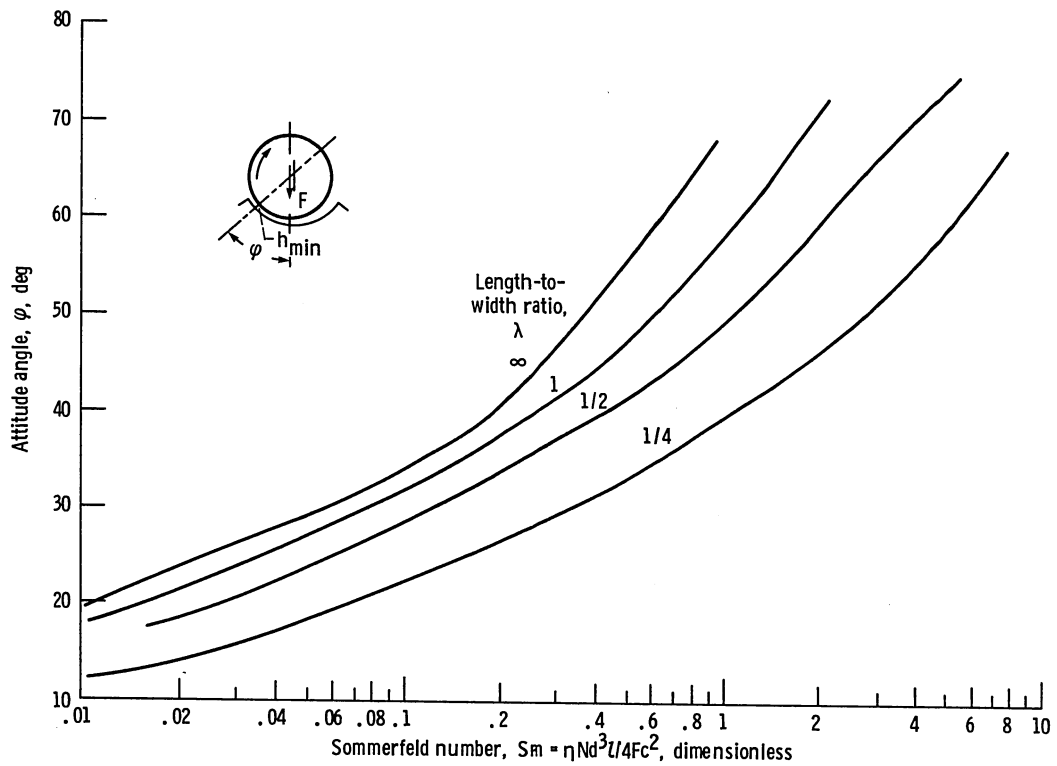

Figure 2.1-7.—Design figure showing attitude angle (position of minimum film thickness) and Sommerfeld number for 120° partial journal bearings, centrally loaded. (Adapted from Raimondi and Boyd, 1958.)

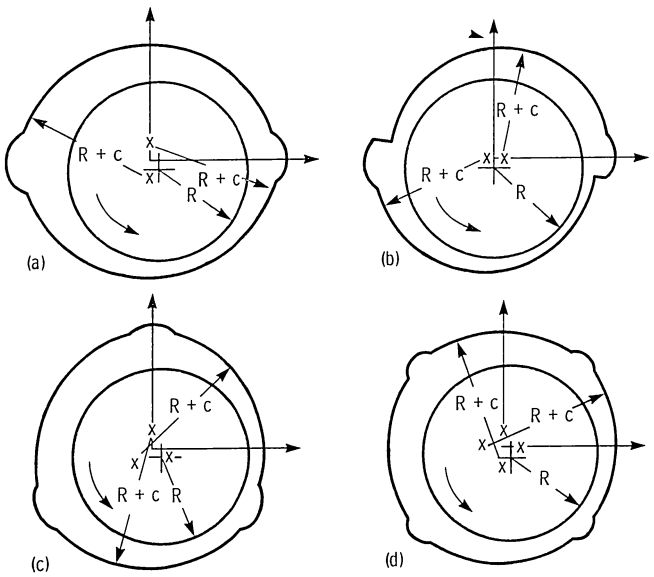

(a) Elliptical bore bearing ($\alpha_a = 0.5$, $m_p = 0.4$).
(b) Offset half bearing ($\alpha_a = 1.125$, $m_p = 0.4$).
(c) Three-lobe bearing ($\alpha_a = 0.5$, $m_p = 0.4$).
(d) Four-lobe bearing ($\alpha_a = 0.5$, $m_p = 0.4$).

Figure 2.1-8.—Types of fixed-incline-pad preloaded journal bearings. (From Allaire and Flack, 1980.)

bearings—bearings different from the plain journal bearing. An excellent discussion of the performance of these bearings is provided in Allaire and Flack (1980), and some of their conclusions are presented here. In figure 2.1-8, each pad is moved in toward the center of the bearing some fraction of the pad clearance in order to make the fluid-film thickness more converging and diverging than that which occurs in a plain journal bearing. The pad center of curvature is indicated by a cross. Generally, these bearings give good suppression of instabilities in the system but can be subject to subsynchronous vibration at high speeds. Accurate manufacturing of these bearings is not always easy to obtain.

A key parameter used in describing these bearings is the fraction of length in which the film thickness is converging to the full pad length, called the offset factor and defined as

$$\alpha_a = \frac{\text{Length of pad with converging film thickness}}{\text{Full pad length}}$$

The elliptical bearing (fig. 2.1-8(a)) indicates that the two pad centers of curvature are moved along the y-axis. This creates a pad with one-half of the film shape converging and the other half diverging (if the shaft were centered), corresponding to an offset factor of $\alpha_a = 0.5$. The offset half bearing (fig. 2.1-8(b)) consists of a two-axial-groove bearing that is split by moving the top half horizontally. This results in low vertical stiffness. Generally, the vibration characteristics of this bearing are such as to avoid oil whirl, which can drive a machine unstable. The offset half bearing has a purely converging film thickness with a converged pad arc length of 160° and the point opposite the center of curvature at 180°. Both the three-lobe and four-lobe bearings (figs. 2.1-8(c) and (d)) have an offset factor of $\alpha_a = 0.5$.

The fractional reduction of the film clearance when the pads are brought in is called the preload factor m_p. Let the bearing clearance at the pad minimum film thickness (with the shaft center) be denoted by c_b. Figure 2.1-9(a) shows that the largest shaft that can be placed in the bearing has a radius $R + c_b$, thereby establishing the definition of c_b. The preload factor m_p is given by

$$m_p = \frac{c - c_b}{c}$$

A preload factor of zero corresponds to having all of the pad centers of curvature coinciding at the center of the bearing; a preload factor of 1.0 corresponds to having all of the pads touching the shaft. Figures 2.1-9(b) and (c) illustrate these extreme situations. Values of the preload factor are indicated in the various types of fixed journal bearings shown in figure 2.1-8.

Figure 2.1-10 shows the variation of the whirl ratio with Sommerfeld number for the four bearing types shown in figure 2.1-8 at the threshold of instability. It is evident that a definite relationship exists between the stability and whirl ratio such that the more stable bearing distinctly whirls at a lower speed ratio. With the excep-

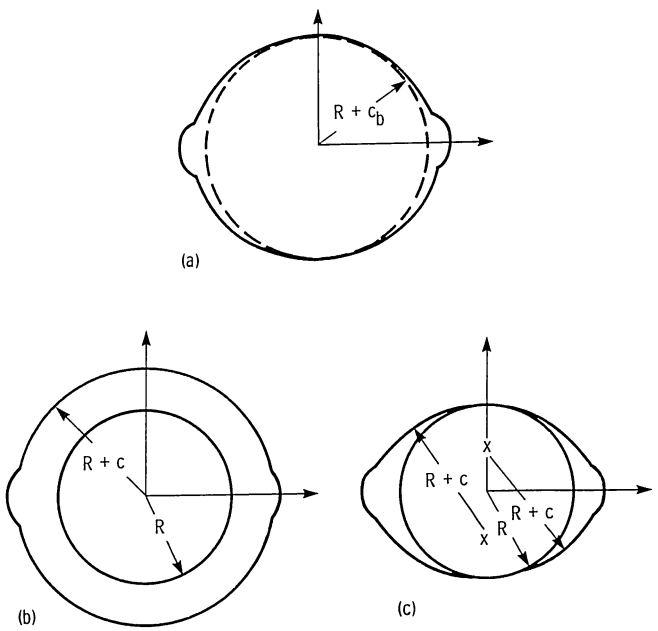

(a) Largest shaft that fits in bearing.
(b) $m = 0$, largest shaft $= R + c$, bearing clearance $c_b = c$.
(c) $m = 1.0$, largest shaft $= R$, bearing clearance $c_b = 0$.

Figure 2.1-9.—Effect of preload on two-lobe bearings. (From Allaire and Flack, 1980.)

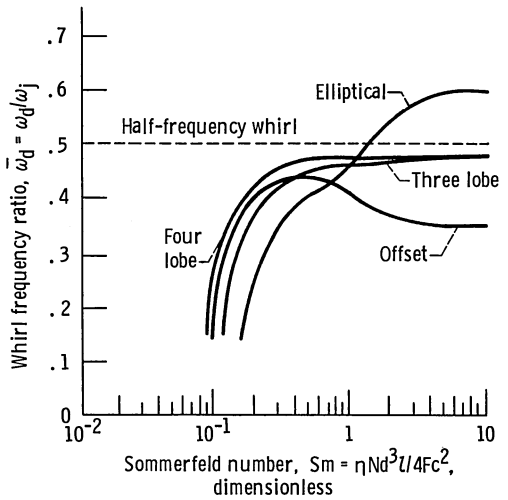

Figure 2.1-10.—Chart for determining whirl frequency ratio. (From Allaire and Flack, 1980.)

tion of the elliptical bearing, all bearings whirl at speeds less than 0.48 of the rotor speed. The offset bearing attains a maximum whirl ratio of 0.44 at a Sommerfeld number of about 0.4 and decreases to a steady value of 0.35 at higher Sommerfeld numbers. This observation corresponds to the superior stability with the offset bearing at high speed and light load.

The whirl ratios with the three-lobe and four-lobe bearings share similar characteristics. They both rise sharply at low Sommerfeld numbers and remain fairly constant for most portions of the curves. Asymptotic whirl ratios of 0.47 and 0.48, respectively, are reached at high Sommerfeld numbers. In comparison with the four-lobe bearing, the three-lobe bearing always has the lower whirl ratio.

The elliptical bearing is the least desirable for large Sommerfeld numbers. At $Sm > 1.3$ the ratio exceeds 0.5.

2.2 Liquid-Lubricated Hydrodynamic Thrust Bearings

In a thrust bearing a thrust plate attached to, or forming part of, the rotating shaft is separated from the sector-shaped bearing pads by a film of lubricant. The load capacity of the bearing arises entirely from the pressure generated by the motion of the thrust plate over the bearing pads. This action is achieved only if the clearance space between the stationary and moving components is convergent in the direction of motion. The pressure generated in, and therefore the load capacity of, the bearing, depends on the velocity of the moving slider $u = (R_1 + R_2)\omega/2 = \pi(R_1 + R_2)N$, the effective viscosity, the length of the pad l, the width of the pad b, the normal applied load F, the inlet film thickness h_i, and the outlet film thickness h_o. For thrust bearings three dimensionless parameters are used

(1) $\lambda = l/b$, pad length-to-width ratio

(2) $Sm_t = \eta u b l^2/Fh_o^2$, Sommerfeld number for thrust bearings

(3) $\bar{h}_i = h_i/h_o$, film thickness ratio

It is important to recognize that the total thrust load F is equal to nF, where n is the number of pads in a thrust bearing. In this section three different thrust bearings will be investigated. Two fixed-pad types, a fixed incline and a step sector, and a pivoted-pad type will be discussed.

2.2.1 Fixed-incline pad

The simplest form of fixed-pad thrust bearing provides only straight-line motion and consists of a flat surface sliding over a fixed pad or land having a profile similar to that shown in figure 2.2-1. The fixed-pad bearing depends for its operation on the lubricant being drawn into a wedge-shaped space and thus producing pressure that counteracts the load and prevents contact between the sliding parts. Since the wedge action only takes place when the sliding surface moves in the direction in which the lubricant film converges, the fixed-incline bearing (fig. 2.2-1) can only carry load for this direction of operation. If reversibility is desired, a combination of two or more pads with their surfaces sloped in opposite direction is required. Fixed-incline pads are used in multiples as in the thrust bearing shown in figure 2.2-2.

The following procedure assists in the design of a fixed-incline-pad thrust bearing:

(1) Choose a pad width-to-length ratio. A square pad ($\lambda = 1$) is generally felt to give good performance. From figure 2.2-3, if it is known whether maximum load or minimum power loss is most important in the particular

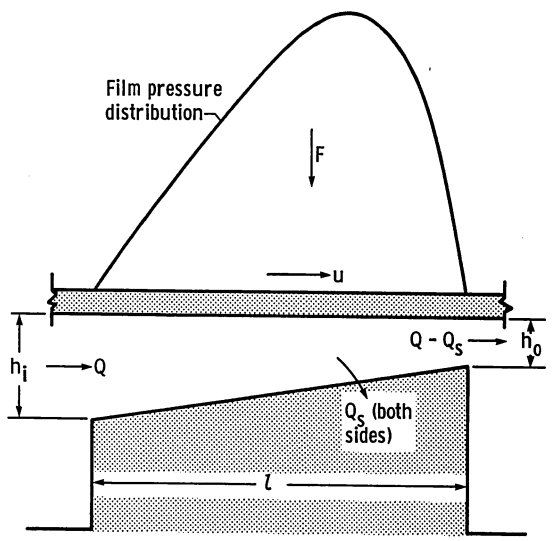

Figure 2.2-1.—Configuration of fixed-incline pad bearing. (From Raimondi and Boyd, 1955.)

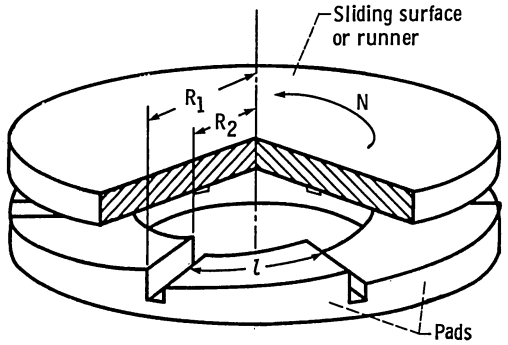

Figure 2.2-2.—Configuration of fixed-incline-pad thrust bearing. (From Raimondi and Boyd, 1955.)

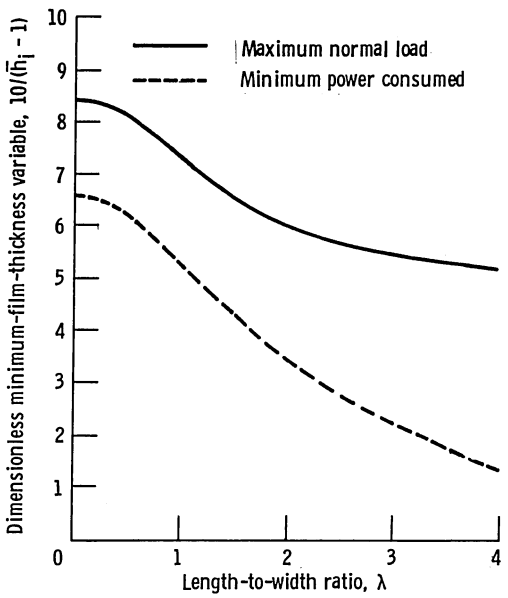

Figure 2.2-3.—Chart for determining minimum film thickness corresponding to maximum load or minimum power loss for various pad proportions—fixed-incline-pad bearings. (From Raimondi and Boyd, 1955.)

application, a value of the minimum film thickness ratio can be determined.

(2) Within the terms in the Sommerfeld number the term least likely to be preassigned is the outlet film thickness. Therefore determine h_o from figure 2.2-4. Since $\bar{h}_i$ is known from figure 2.2-3, h_i can be determined $(h_i = \bar{h}_i h_o)$.

(3) Check table 2.2-1 to see if minimum (outlet) film thickness is sufficient for the preassigned surface finish. If not,

(a) Increase the fluid viscosity or speed of the bearing

(b) Decrease the load or the surface finish

Upon making this change return to step 1.

(4) Once an adequate minimum film thickness has been determined, use figures 2.2-5 to 2.2-7 to obtain, respectively, the coefficient of friction, the power consumed, and the flow.

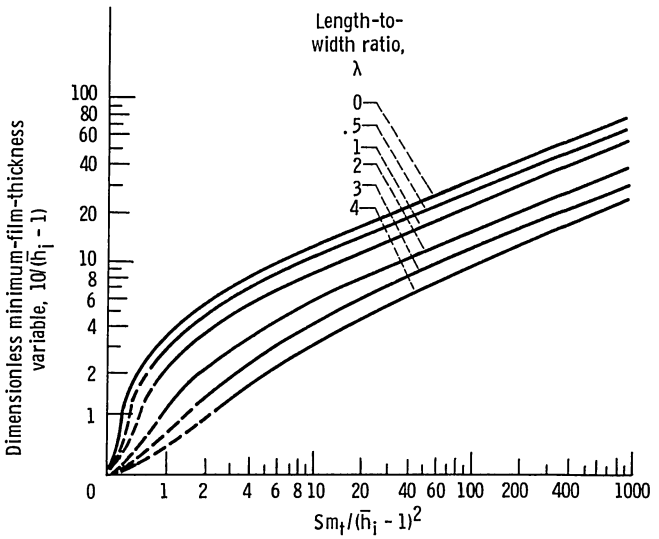

Figure 2.2-4.—Chart for determining minimum film thickness for fixed-incline-pad thrust bearings. (From Raimondi and Boyd, 1955.)

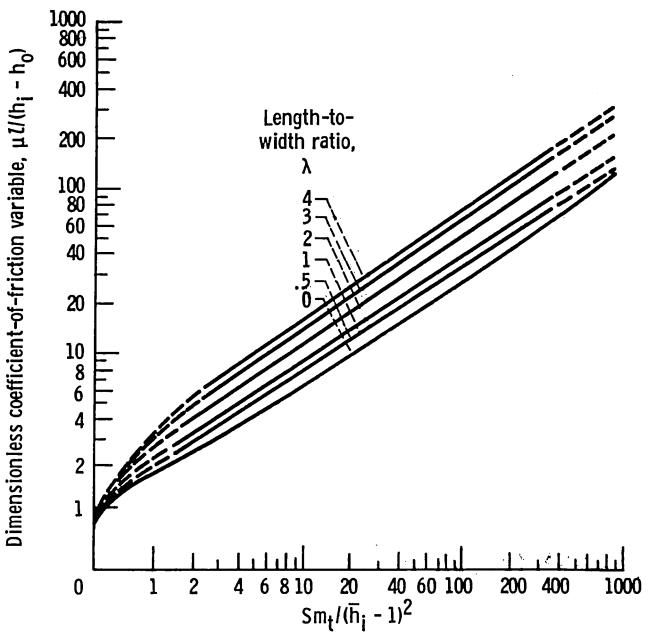

Figure 2.2-5.—Chart for determining coefficient of friction for fixed-incline-pad thrust bearings. (From Raimondi and Boyd, 1955.)

2.2.2 Pivoted pad

The simplest form of pivoted-pad bearing provides only for straight-line motion and consists of a flat surface sliding over a pivoted pad as shown in figure 2.2-8. If the pad is assumed to be in equilibrium under a given set of operating conditions, any change in these conditions, such as a change in load, speed, or viscosity, will alter the pressure distribution and thus momentarily shift the center of pressure, creating a moment that causes the pad to change its inclination. In equilibrium, however, it can be shown that (for an incompressible lubricant) the ratio

TABLE 2.2-1. - ALLOWABLE MINIMUM OUTLET FILM THICKNESS FOR A GIVEN SURFACE FINISH

[From Engineering Sciences Data Unit (1967).]

Surface finish		Description of surface	Examples of manufacturing methods	Approximate relative costs	Allowable minimum outlet film thickness[a], h_o	
Familiar British units, μin. CLA[b]	SI units, μm[c] CLA				Familiar British units, in.	SI units, m
4-8	0.1 - 0.2	Mirror-like surface without toolmarks, close tolerances	Grind, lap, and superfinish	17-20	0.00010	0.0000025
8-16	0.2 - 0.4	Smooth surface without scratches, close tolerances	Grind and lap	17-20	.00025	.0000062
16-32	0.4 - 0.8	Smooth surface, close tolerances	Grind, file, and lap	10	.00050	.0000125
32-63	0.8 - 1.6	Accurate bearing surface without toolmarks	Grind, precision mill, and file	7	.00100	.000025
63-125	1.6 - 3.2	Smooth surface without objectionable toolmarks, moderate tolerances	Shape, mill, grind, and turn	5	.00200	.000050

[a]The values of film thickness are given only for guidance. They indicate the film thickness required to avoid metal-to-metal contact under clean oil conditions with no misalignment. It may be necessary to take a larger film thickness than that indicated (e.g., to obtain an acceptable temperature rise). It has been assumed that the average surface finish of the pads is the same as that of the runner.

[b]CLA = centerline average.

[c]μm = micrometer; 40 μin. (microinch) = 1 μm.

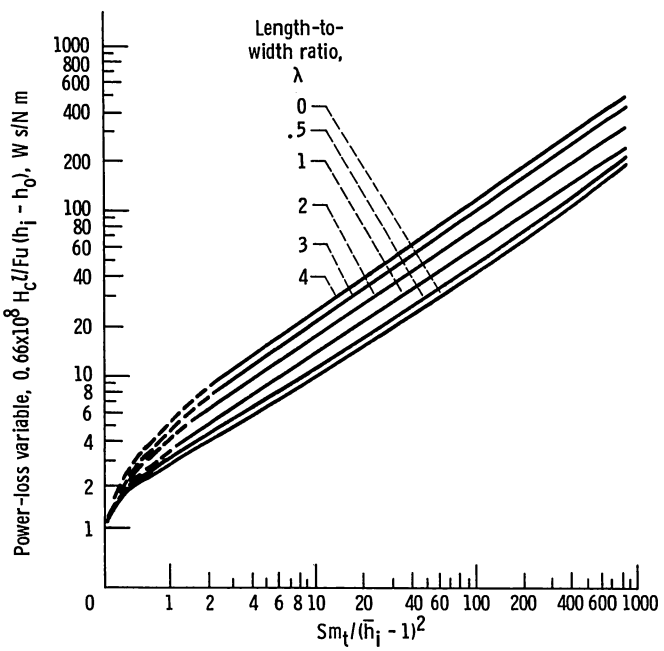

Figure 2.2-6.—Chart for determining power loss for fixed-incline-pad thrust bearings. (From Raimondi and Boyd, 1955.)

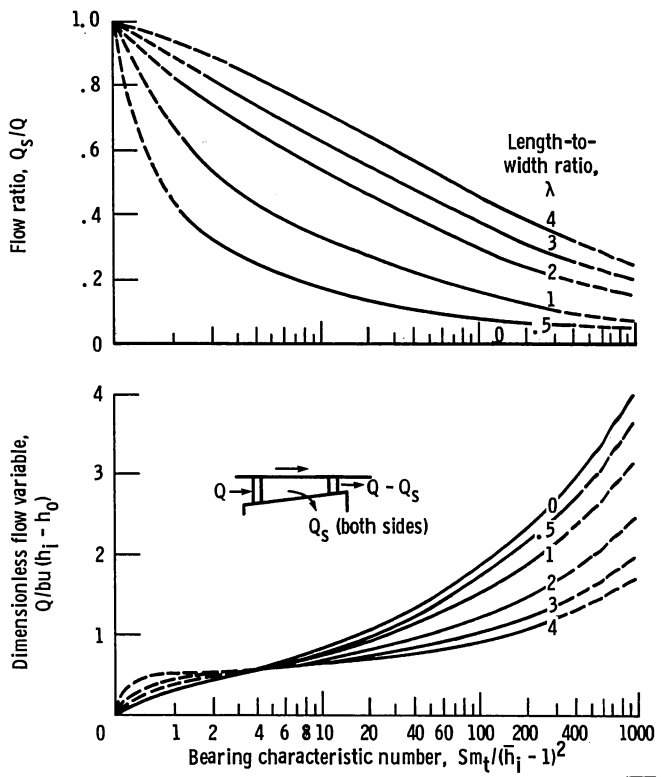

Figure 2.2-7.—Charts for determining lubricant flow for fixed-incline-pad thrust bearings. (From Raimondi and Boyd, 1955.)

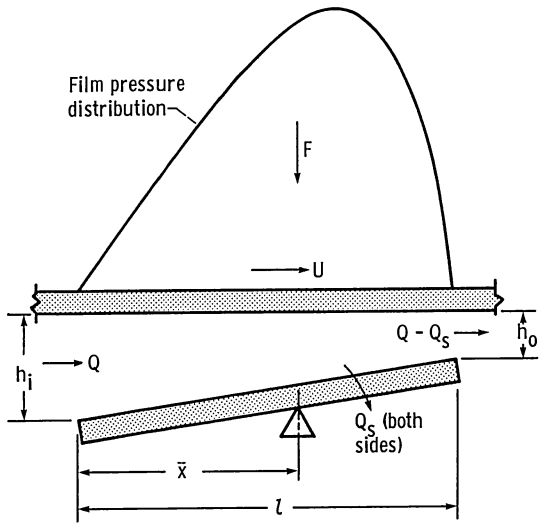

Figure 2.2-8.—Configuration of pivoted-pad bearings. (From Raimondi and Boyd, 1955.)

of the inlet film thickness to the outlet film thickness h_i/h_o is fixed and is independent of load, speed, and viscosity by the pivot position x given in the ratio $\bar{x}/l$. Thus the pad will automatically return to its original inclination under the new steady operating conditions.

Pivoted-pads are sometimes used in multiples as pivoted-pad thrust bearings, shown in figure 2.2-9. Calculations are carried through for a single pad, and the properties for the complete bearing are found by combining these calculations in the proper manner.

Normally, a pivoted pad will only carry load if the pivot is placed somewhere between the center of the pad and the outlet edge ($0.5 < \bar{x}/l \leq 1.0$). With the pivot so placed, the pad therefore can only carry load for one direction of rotation.

The following procedure helps in the design of pivoted-pad thrust bearings:

(1) Having established if minimum power or maximum load is more critical in the particular application and chosen a pad length-to-width ratio, establish the pivot position from figure 2.2-10.

(2) In the Sommerfeld number for thrust bearings the unknown parameter is usually the outlet or minimum film thickness. Therefore establish the value of h_o from figure 2.2-11.

(3) Check table 2.2-1 to see if the outlet film thickness is sufficient for the preassigned surface finish. If sufficient, go on to step 4. If not, consider

(a) Increasing the fluid viscosity

(b) Increasing the speed of the bearing

(c) Decreasing the load of the bearing

(d) Decreasing the surface finish of the bearing lubrication surfaces. Upon making this change return to step 1.

(4) Once an adequate outlet film thickness is established, determine the film thickness ratio, power loss, coefficient of friction, and flow from figures 2.2-12 to 2.2-15.

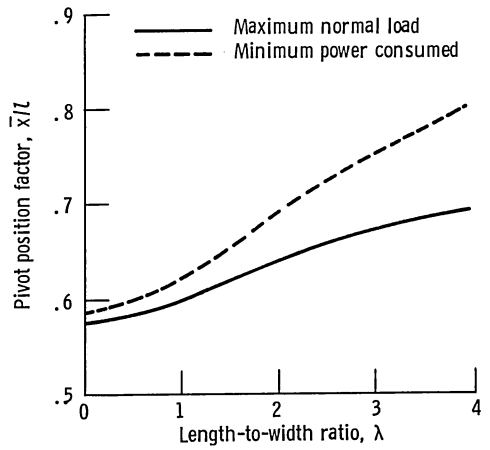

Figure 2.2-10.—Chart for determining pivot position corresponding to maximum load or minimum power loss for various pad proportions—pivoted-pad bearings. (From Raimondi and Boyd, 1955.)

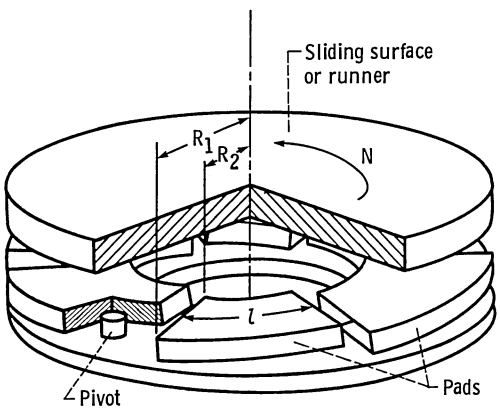

Figure 2.2-9.—Configuration of pivoted-pad thrust bearings. (From Raimondi and Boyd, 1955.)

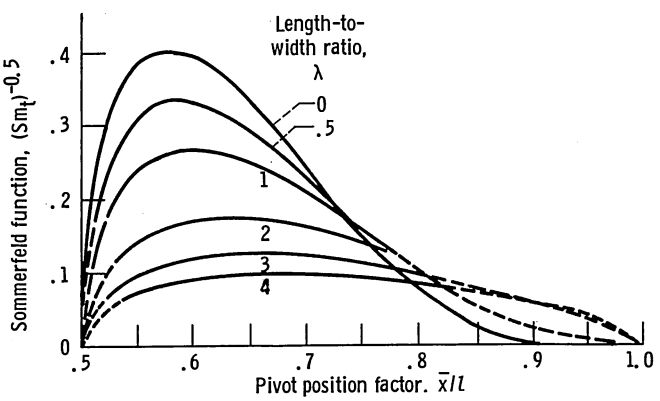

Figure 2.2-11.—Chart for determining outlet film thickness for pivoted-pad thrust bearings. (From Raimondi and Boyd, 1955.)

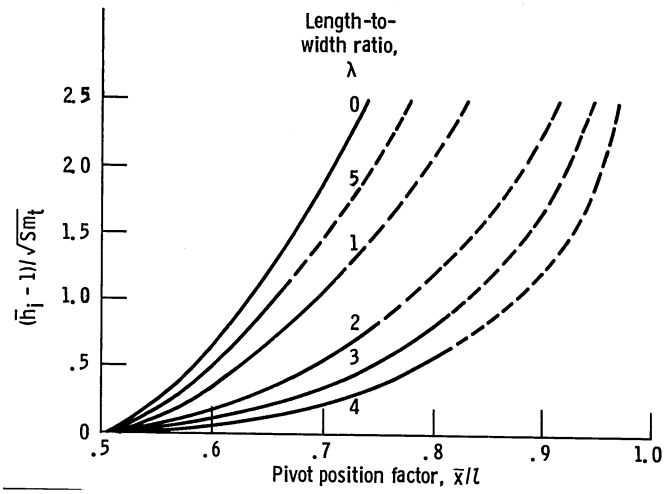

Figure 2.2-12.—Chart for determining film thickness ratio $\bar{h}_i$ for pivoted-pad thrust bearings. (From Raimondi and Boyd, 1955.)

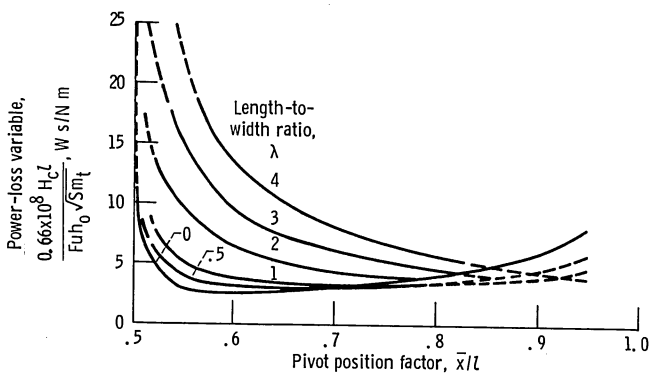

Figure 2.2-13.—Chart for determining power loss for pivoted-pad thrust bearings. (From Raimondi and Boyd, 1955.)

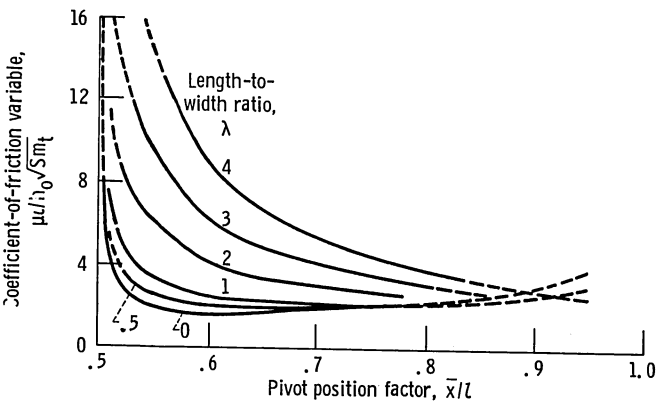

Figure 2.2-14.—Chart for determining coefficient of friction for pivot-pad thrust bearings. (From Raimondi and Boyd, 1955.)

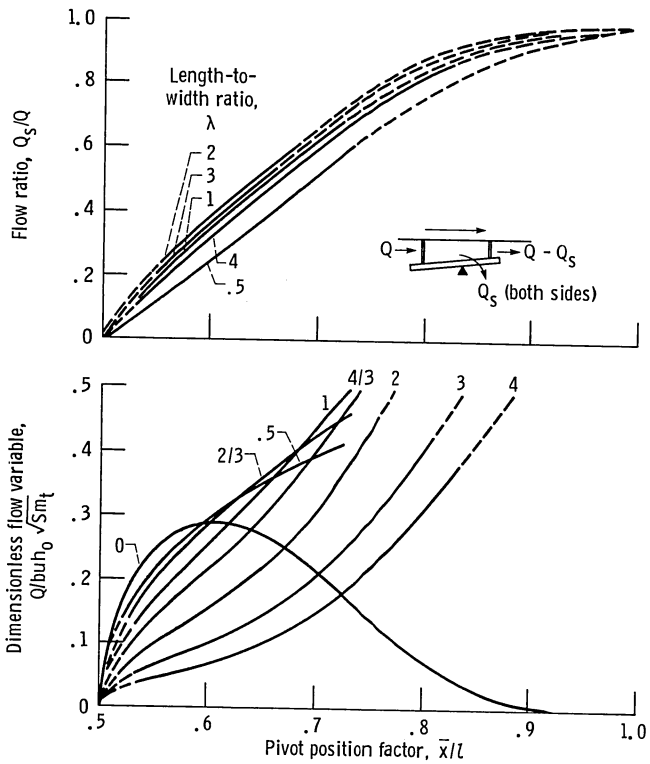

Figure 2.2-15.—Chart for determining lubricant flow for pivot-pad thrust bearings. (From Raimondi and Boyd, 1955.)

2.2.3 *Step sector*

The configuration of a step-sector thrust bearing is shown in figure 2.2-16. The parameters used to define the dimensionless load and stiffness are

(1) $\bar{h}_i = h_i/h_o$, film thickness ratio
(2) $\bar{\theta} = \theta_i/(\theta_i + \theta_o)$, dimensionless step location
(3) n, number of sectors
(4) $\alpha_r = R_2/R_1$, radius ratio
(5) θ_g, angular extent of lubrication feed groove

Note that the first four parameters are dimensionless and the fifth is dimensional and expressed in radians.

For *maximum load capacity* the optimum parallel step-sector bearing for a given α_r and θ_g is

$$\bar{\theta}_{opt} = 0.558, \quad (\bar{h}_i)_{opt} = 1.668, \quad \text{and} \quad n_{opt} = \frac{2\pi}{\theta_g + \dfrac{2.24(1-\alpha_r)}{1+\alpha_r}}$$

where n_{opt} is rounded off to the nearest integer and its minimum value is 3. For *maximum stiffness,* results are identical to the above with the exception that $(\bar{h}_i)_{opt} = 1.467$. These results were obtained from Hamrock (1983).

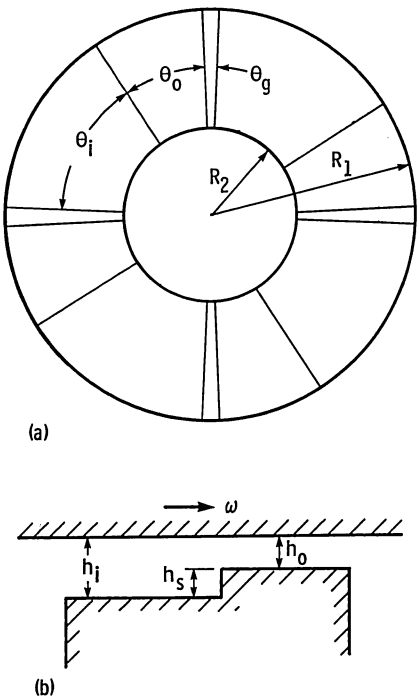

(a) Top view.
(b) Section through a sector.

Figure 2.2-16.—Configuration of step-sector thrust bearing. (From Hamrock, 1983.)

2.3 Hydrostatic Bearings

In Sections 2.1 and 2.2 the load-supporting fluid pressure is generated by relative motion between the bearing surfaces. Thus the bearing's load capacity depends on the relative speeds of the surfaces. When the relative speeds of the bearing are low or the loads are high, liquid-lubricated journal and thrust bearings may not be adequate. If full-film lubrication with no metal-to-metal contact is desired under such conditions, another technique, called hydrostatic or externally pressurized lubrication, may be used.

The salient features that distinguish hydrostatic from hydrodynamic bearings are that the fluid is pressurized externally to the hydrostatic bearings and the pressure drop across the bearing is used to support the load. The load capacity is independent of the motion of bearing surfaces or the fluid viscosity. There is no problem of contact of the surfaces at starting and stopping as with conventional hydrodynamically lubricated bearings because pressure is applied before starting and maintained until after stopping. Hydrostatic bearings can be very useful under conditions of little or no relative motion and under extreme conditions of temperature or corrosivity, where it may be necessary to use bearing materials with poor boundary lubricating properties. Surface contact can be avoided completely, so material properties are much less important than in hydrodynamic bearings. The load capacity of a hydrostatic bearing is proportional to the available pressure.

Hydrostatic bearings do, however, require an external source of pressurization such as a pump. This represents an additional system complication and cost.

The chief advantage of hydrostatic bearings is their ability to support extremely heavy loads at slow speeds with a minimum of driving force. For this reason they have been successfully applied in rolling mills, machine tools, radio and optical telescopes, large radar antennas, and other heavily loaded, slowly moving equipment.

The formation of a fluid film in a hydrostatic bearing system is shown in figure 2.3-1. A simple bearing system with the pressure source at zero pressure is shown in figure 2.3-1(a). The runner under the influence of a load F is seated on the bearing pad. As the source pressure builds up (fig. 2.3-1(b)) the pressure in the pad recess also increases. The pressure in the recess is built up to a point (fig. 2.3-1(c)) where the pressure on the runner over an area equal to the pad recess area is just sufficient to lift the load. This is commonly called the lift pressure. Just after the runner separates from the bearing pad (fig. 2.3-1(d)) the pressure in the recess is less than that required to lift the bearing runner ($p_r < p_l$). After lift, flow commences through the system. Therefore a pressure drop exists between the pressure source and the bearing (across the restrictor) and from the recess to the exit of the bearing.

If more load is added to the bearing (fig. 2.3-1(e)), the film thickness will decrease and the recess pressure will rise until pressure within both the bearing clearance and the recess is sufficient to carry the increased load. If the load is now decreased to less than the original (fig. 2.3-1(f)), the film thickness will increase to some higher value and the recess pressure will decrease accordingly. The maximum load that can be supported by the pad will be reached, theoretically, when the pressure in the recess is equal to the pressure at the source. If a load greater than this is applied, the bearing will seat and remain seated until the load is reduced and can again be supported by the supply pressure.

2.3.1 Pad coefficients

To find the load-carrying capacity and flow requirements of any given hydrostatic bearing pad, it is necessary to determine certain pad coefficients. Since the selection of pad and recess geometries is up to the designer, the major design problem is the determination of particular bearing coefficients for particular geometries.

The load-carrying capacity of a bearing pad, regardless of its shape or size can be expressed as

$$F = a_f A_p p_r \tag{2.3-1}$$

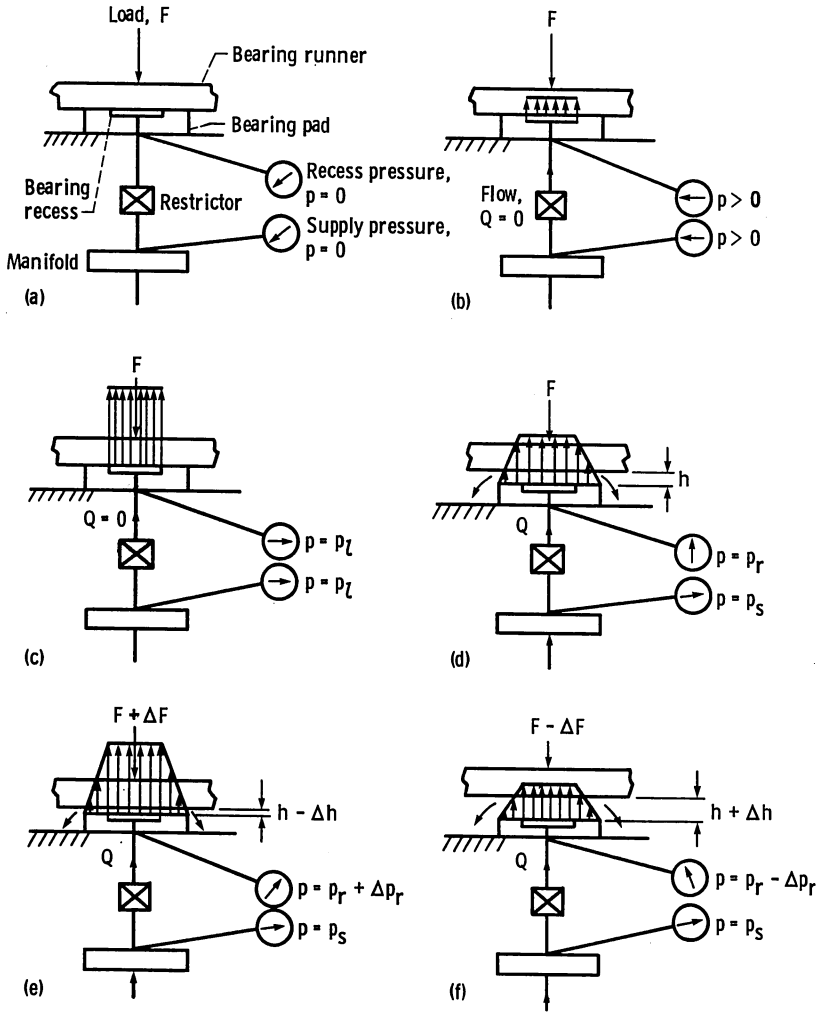

(a) Pump off.
(b) Pressure building up.
(c) Pressure x recess area = F.
(d) Bearing operating.
(e) Increased load.
(f) Decreased load.

Figure 2.3-1.—Formation of fluid film in hydrostatic bearing system. (From Rippel, 1963.)

where

a_f bearing pad load coefficient
A_p total projected pad area, m^2
p_r recess pressure, N/m^2

The amount of lubricant flow across a pad and through the bearing clearance is

$$Q=q_f\frac{F}{A_p}\frac{h^3}{\eta} \tag{2.3-2}$$

where

q_f pad flow coefficient
h film thickness, m
η lubricant absolute viscosity, $N\ s/m^2$

The pumping power required by the hydrostatic pad can be evaluated by determining the product of recess pressure and flow:

$$H_b=p_rQ=H_f\left(\frac{F}{A_p}\right)^2\frac{h^3}{\eta} \tag{2.3-3}$$

where $H_f=q_f/a_f$ is the bearing pad power coefficient. Therefore in designing hydrostatic bearings the designer is primarily concerned with the three bearing coefficients (a_f, q_f, and H_f) expressed in equations (2.3-1) to (2.3-3). Values of any two of these coefficients suffice to determine the third.

Bearing coefficients are dimensionless quantities that relate performance characteristics of load, flow, and power to physical parameters. The bearing coefficients

for two types of bearing pad will be considered, both of which exhibit pure radial flow and are flat, thrust-loaded types of bearings. For other types of hydrostatic bearings see Rippel (1963).

Circular step bearing pad

The bearing coefficients for this type of pad are expressed as

$$a_f = \frac{1}{2}\left[\frac{1-(R_o/R)^2}{\log_e(R/R_o)}\right] \tag{2.3-4}$$

$$q_f = \frac{\pi}{3}\left[\frac{1}{1-(R_o/R)^2}\right] \tag{2.3-5}$$

$$H_f = \frac{2\pi \log_e(R/R_o)}{3\left[1-(R_o/R)^2\right]^2} \tag{2.3-6}$$

For this type of pad the total projected bearing pad area A_p is equal to πR^2.

Figure 2.3-2 shows the three bearing pad coefficients for various ratios of recess radius to bearing radius for a circular step thrust bearing. The bearing pad load coefficient a_f varies from zero for extremely small recesses to unity for bearings having large recesses with respect to pad dimensions. In a sense, a_f is a measure of how efficiently the bearing uses the recess pressure to support the applied load.

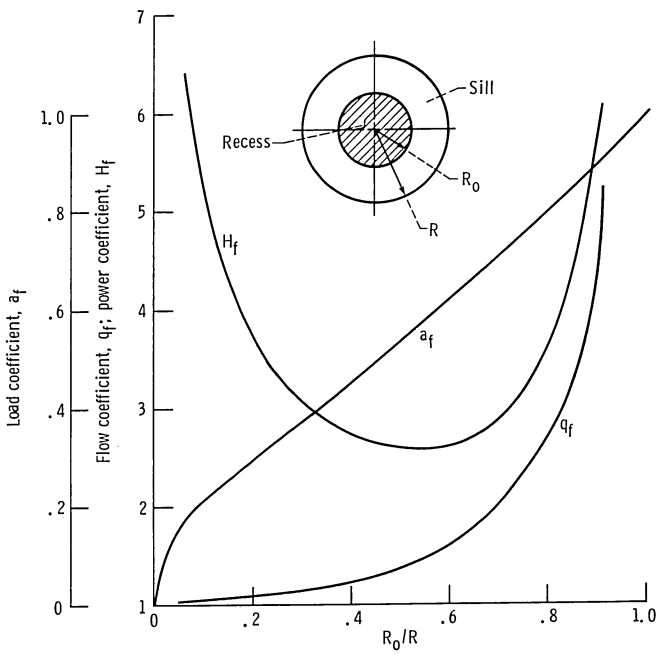

Figure 2.3-2.—Chart for determining bearing pad coefficients for circular step thrust bearing. (From Rippel, 1963.)

In figure 2.3-2 we see that the pad flow coefficient q_f varies from unity for pads with relatively small recesses to a value approaching infinity for bearings with extremely large recesses. Physically, as the recess becomes larger with respect to the bearing, the hydraulic resistance to fluid flow decreases, and thus flow increases.

From figure 2.3-2, the power coefficient H_f approaches infinity for very small recesses, decreases to a minimum value as the recess size increases, and approaches infinity again for very large recesses. For this particular bearing the minimum value of H_f occurs at a ratio of recess radius to bearing radius R_o/R of 0.53. For all bearing-pad configurations the ratio of recess length to bearing length at which the minimum value of H_f is reached lies between 0.4 and 0.6.

Annular thrust bearing

Figure 2.3-3 shows an annular thrust pad bearing. In this bearing the lubricant flows from the annular recess over the inner and outer sills. For this type of bearing the pad coefficients are

$$a_f = \frac{1}{2\left(R_4^2-R_3^2\right)}\left[\frac{R_4^2-R_3^2}{\log_e(R_4/R_3)} - \frac{R_2^2-R_1^2}{\log_e(R_2/R_1)}\right] \tag{2.3-7}$$

$$q_f = \frac{\pi}{6a_f}\left[\frac{1}{\log_e(R_4/R_3)} - \frac{1}{\log_e(R_2/R_1)}\right] \tag{2.3-8}$$

$$H_f = \frac{q_f}{a_f} \tag{2.3-9}$$

For this bearing the total projected bearing pad area is

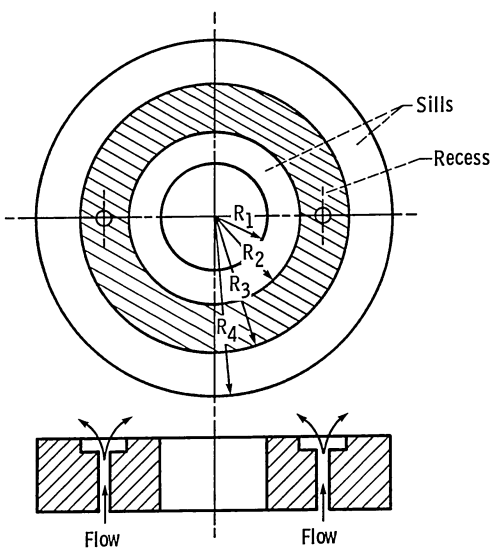

Figure 2.3-3.—Configuration of annular thrust pad bearing. (From Rippel, 1963.)

$$A_p = \pi\left(R_4^2 - R_1^2\right) \tag{2.3-10}$$

Figure 2.3-4 shows the bearing pad load coefficient for an annular thrust pad bearing as obtained from equations (2.3-7) to (2.3-9). For this figure it is assumed that the annular recess is centrally located within the bearing width; this therefore implies that $R_1 + R_4 = R_2 + R_3$. The curve for a_f applies for all R_1/R_4 ratios.

The hydrostatic bearings considered in this section have been limited to flat thrust-loaded bearings. Design information about other pad configurations can be obtained from Rippel (1963). The approach used for the simple, flat, thrust-loaded pad configuration is helpful in considering the more complex geometries covered by Rippel (1963).

2.3.2 *Compensating elements*

As compared with common bearing types, hydrostatic bearings are relatively complex systems. In addition to the bearing pad the system includes a pump and a compensating element or restrictor. Three common types of compensating element for hydrostatic bearings are the capillary tube, the sharp-edged orifice, and constant-flow-valve compensation.

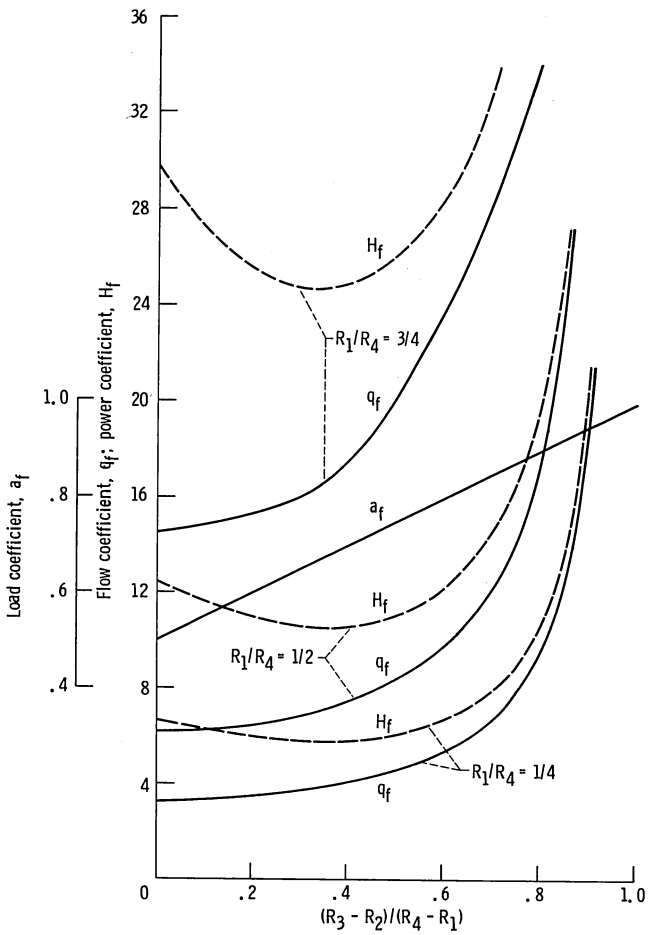

Figure 2.3-4.—Chart for determining bearing pad coefficients for annular thrust pad bearings. (From Rippel, 1963.)

Capillary compensation

Figure 2.3-5 shows a capillary-compensated hydrostatic bearing as obtained from Rippel (1963). The small diameter of the capillary tube provides restriction and resultant pressure drop in the bearing pad. The characteristic feature of capillary compensation is a long tube of relatively small diameter ($l_c > 20\ d_c$). The laminar flow of fluid through such a tube while neglecting entrance and exit effects and viscosity changes due to temperature and pressure can be expressed as

$$Q_c = \frac{k_c(p_s - p_r)}{\eta} \tag{2.3-11}$$

where

$$k_c = \frac{\pi d_c^4}{128\, l_c} \tag{2.3-12}$$

For a given capillary tube, k_c is a constant expressed in cubic meters. Thus from equation (2.3-11) the flow through a capillary tube is related linearly to the pressure drop across it. In a hydrostatic bearing with capillary compensation and a fixed supply pressure, the flow through the bearing will decrease with increasing load since the pocket pressure p_r is proportional to the load. To satisfy the assumption of laminar flow, Reynolds number must be less than 2000 when expressed as

$$N_R = \frac{4\rho Q_c}{\pi d_c \eta} < 2000 \tag{2.3-13}$$

where ρ is the mass density of the lubricant in N s^2/m^4.

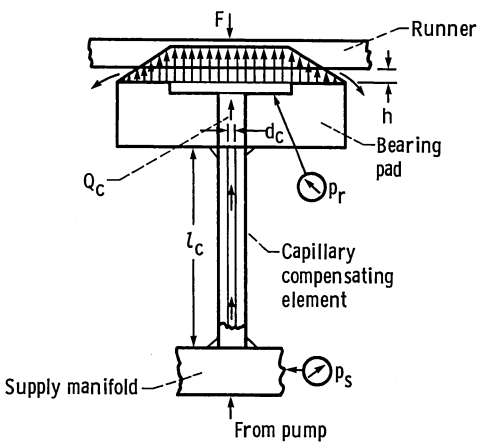

Figure 2.3-5.—Capillary-compensated hydrostatic bearing. (From Rippel, 1963.)

Hypodermic needle tubing serves quite well as capillary tubing for hydrostatic bearings. Very small diameter tubing is available, but diameters less than 6×10^{-4} m should not be used because of the tendency to clog.

Orifice compensation

Orifice compensation is illustrated in figure 2.3-6. The flow of an incompressible fluid through a sharp-edged orifice can be expressed as

$$Q_o=k_o(p_s-p_r)^{1/2} \tag{2.3-14}$$

where

$$k_o=\frac{\pi c_d d_o^2}{\sqrt{8\rho}}$$

and c_d is the orifice discharge coefficient. For a given orifice size and given lubricant, k_o is a constant expressed in $m^4/s\ N^{1/2}$. Thus from equation (2.3-14) flow through an orifice is proportional to the square root of the pressure difference across the orifice.

The discharge coefficient c_d is a function of Reynolds number. For an orifice the Reynolds number is

$$N_R=\frac{d_o}{\eta}[2\rho\ (p_s-p_r)]^{1/2} \tag{2.3-15}$$

For a Reynolds number greater than approximately 15, which is the usual case in orifice-compensated hydrostatic bearings, c_d is about 0.6 for $d_o/D<0.1$. For a Reynolds number less than 15 the discharge coefficient is approximately

$$c_d=0.20\sqrt{N_R} \tag{2.3-16}$$

The pipe diameter D at the orifice should be at least 10 times the orifice diameter d_o. Sharp-edge orifices, depending on their diameters, have a tendency to clog, therefore orifice diameters d_o less than 5×10^{-4} m should be avoided.

Constant-flow-valve compensation

Constant-flow-valve compensation is illustrated in figure 2.3-7. This type of restrictor has a constant flow regardless of the pressure difference across the valve. Hence the flow is independent of recess pressure.

The relative ranking of the three types of compensating elements with regard to a number of considerations is given in table 2.3-1. A rating of 1 in this table indicates best or most desirable. This table should help in deciding which type of compensation is most desirable in a particular application.

Basically, any type of compensating element can be designed into a hydrostatic bearing system if loads on the bearing never change. But if stiffness, load, or flow varies, the choice of the proper compensating element becomes more difficult and the reader is again referred to Rippel (1963).

2.4 Gas-Lubricated Hydrodynamic Bearings

A relatively recent (within the last 30 years) extension of hydrodynamic lubrication that is of growing importance is gas lubrication. It consists of using air or some other gas as a lubricant rather than a mineral oil. The viscosity of air is 1000 times smaller than that of very thin mineral oils. Consequently, the viscous resistance is very much less. However, the distance of nearest approach (i.e., the closest distance between the shaft and the bearing) is also correspondingly smaller, so that special precautions must be taken. To obtain full benefits from gas lubrication, the following should be observed:

(1) Surfaces must have a very fine finish.
(2) Alignment must be very good.
(3) Dimensions and clearances must be very accurate.
(4) Speeds must be high.
(5) Loading must be relatively low.

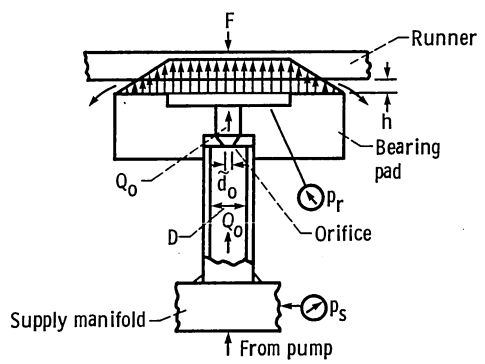

Figure 2.3-6.—Orifice-compensated hydrostatic bearing. (From Rippel, 1963.)

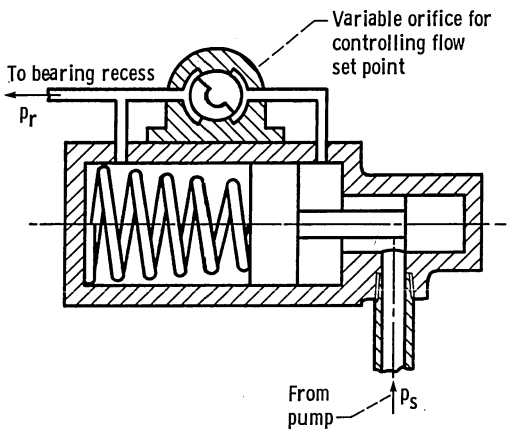

Figure 2.3-7.—Constant-flow-valve compensation in hydrostatic bearing. (From Rippel, 1963.)

TABLE 2.3-1. - COMPENSATING-ELEMENT CONSIDERATIONS[a]

[From Rippel (1963).]

Consideration	Compensating element		
	Capillary	Orifice	Constant-flow valve
Initial cost	2	1	3
Cost to fabricate and install	2	3	1
Space required	2	1	3
Reliability	1	2	3
Useful life	1	2	3
Commercial availability	2	3	1
Tendency to clog	1	2	3
Serviceability	2	1	3
Adjustability	3	2	1

[a]Rating of 1 is best or most desirable.

Another main difference between the behavior of similar gas and liquid films besides viscosity is the compressibility of the gas. At low relative speeds it is reasonable to expect the gas-film density to remain nearly constant and the film therefore to behave as if it were incompressible. At high speeds, however, the density change is likely to become of primary importance so that such gas-film properties must differ appreciably from those of similar liquid films.

Gas-lubricated bearings can also operate at very high temperatures since the lubricant will not chemically degrade. Furthermore, if air is used as the lubricant, it costs nothing. Gas bearings are finding increasing usage in gas-cycle machinery where the cycle gas is used in the bearings, thus eliminating the need for a conventional lubrication system; in gyros, where precision and constancy of torque are critical; and in food and textile processing machinery, where cleanliness and absence of contaminants are critical; also in the magnetic recording tape industry.

2.4.1 Journal bearings

Plain gas-lubricated journal bearings are of little interest because of their poor stability characteristics. Lightly loaded bearings that operate at low eccentricity ratios are subjected to fractional frequency whirl, which can result in bearing destruction. Two types of nonplain gas-lubricated journal bearings find widespread use, namely, the pivoted pad and the herringbone groove.

Pivoted-pad journal bearings

Pivoted-pad journal bearings are most frequently used as shaft supports in gas-bearing machinery because of their excellent stability characteristics. An individual pivot pad and shaft assembly is shown in figure 2.4-1, and a three-pad pivoted-pad bearing assembly is shown in figure 2.4-2. Generally, each pad provides pad rotational degrees of freedom about three orthogonal axes (pitch, roll, and yaw). Pivoted-pad bearings are complex because of the many geometric variables involved in their design. Some of these variables are

(1) Number of pads
(2) Angular extent of pad, α_p
(3) Aspect ratio of pad, R/l
(4) Pivot location, φ_p/α_p
(5) Machined-in clearance ratio, c/R

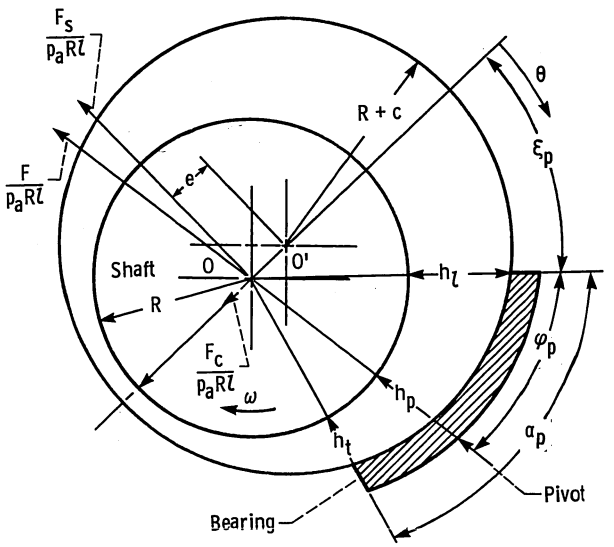

Figure 2.4-1.—Geometry of individual shoe-shaft bearing. (From Gunter et al., 1964.)

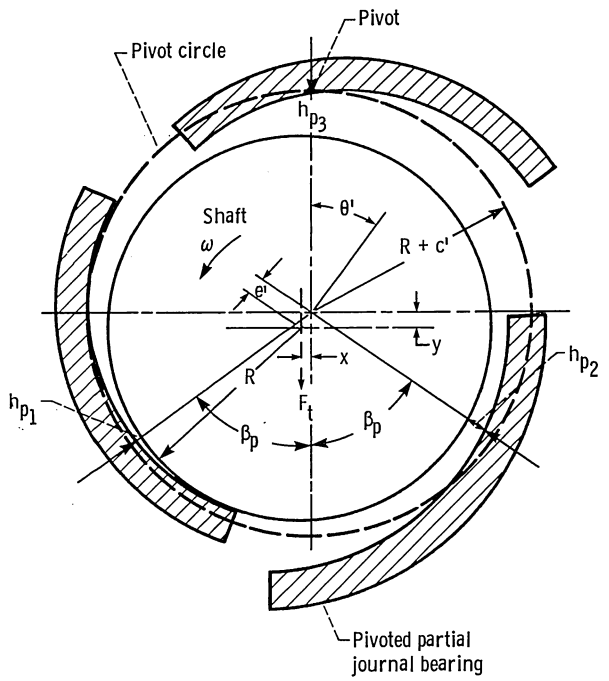

Figure 2.4-2.—Geometry of pivoted-pad journal bearing with three shoes. (From Gunter et al., 1964.)

(6) Pivot circle clearance ratio, c'/R

(7) Angle between line of centers and pad leading edge, ξ_p

Analysis is accomplished by first determining the characteristics of an individual pad. Both geometric and operating parameters influence the design of a pivoted pad. The operating parameter of importance is the dimensionless bearing number Λ_j, where

$$\Lambda_j = \frac{6\eta\omega R^2}{p_a c^2}$$

The results of computer solutions obtained from Gunter et al. (1964) for the performance of a single pad are shown in figures 2.4-3 to 2.4-5. These figures illustrate load coefficient, pivot film thickness, and trailing-edge film thickness as functions of pivot location and eccentricity ratio. These field maps apply for a pad with a radius-to-width ratio of 0.606, a circumferential extent of 9.45° (an aspect ratio of 1), and $\Lambda_j = 3.5$. For other geometries and Λ_j values similar maps must be generated. Additional maps are given in Gunter et al. (1964).

Figures 2.4-6 to 2.4-8 show load coefficient and stiffness coefficient for a range of Λ_j values up to 4. These plots are for a pivot position of 2/3.

When the individual pad characteristics are known, the characteristics of the multipad bearing can be determined by using a trial-and-error approach. With the arrangement shown in figure 2.4-2, the load is directed between the two lower pivots. For this case the load carried by each of the lower pads is initially assumed to be $F \cos \beta$. The pivot film thicknesses h_{p_1} and h_{p_2} are then calculated. The upper-pad pivot film thickness h_{p_3}, eccentricity ratio ϵ, and load coefficient C_{l_3} can be determined. The additional load on the shaft due to the reaction of pad 3 is added to the system load. Calculations are repeated until the desired accuracy is achieved.

Pivoted-pad journal bearings are usually assembled with a pivot circle clearance c' somewhat less than the machined-in clearance c. When $c'/c < 1$, the bearing is said to be preloaded. Preload is usually given in terms of a preload coefficient, which is equal to $(c - c')/c$. Preloading is used to increase bearing stiffness and to prevent complete unloading of one or more pads. The latter condition can lead to pad flutter and possible contact of the pad leading edge and the shaft, which, in turn, can result in bearing failure.

Herringbone-groove journal bearings

A fixed-geometry bearing that has demonstrated good stability characteristics and thus promise for use in high-speed gas bearings is the herringbone bearing. It consists of a circular journal and bearing sleeve with shallow, herringbone-shaped grooves cut into either member. Figure 2.4-9 illustrates a partially grooved herringbone journal bearing. In this figure the groove and bearing parameters are also indicated. Figures 2.4-10 to 2.4-14 were obtained from Hamrock and Fleming (1971) and are design charts that present curves for optimizing the design parameters for herringbone journal bearings for maximum radial load. The (a) portion of these figures is for the grooved member rotating and the (b) portion is for the smooth member rotating. The only groove parameter not represented in these figures in the number of grooves to be used. From Hamrock and Fleming (1971) it was found that the *minimum* number of grooves to be placed around the journal can be represented by $n \geq \Lambda_j/5$.

More than any other factors, self-excited whirl instability and low load capacity limit the usefulness of gas-lubricated journal bearings. The whirl problem is the tendency of the journal center to orbit the bearing center at an angular speed less than or equal to half that of the journal about its own center. In many cases the whirl amplitude is large enough to cause destructive contact of the bearing surfaces.

Figure 2.4-15, obtained from Fleming and Hamrock (1974), shows the stability attained by the optimized herringbone bearings. In this figure the stability parameter $\bar{M}$ is introduced, where

$$\bar{M} = \frac{\bar{m} p_a h_r^5}{2R^5 l \eta^2}$$

and $\bar{m}$ is the mass supported by the bearing.

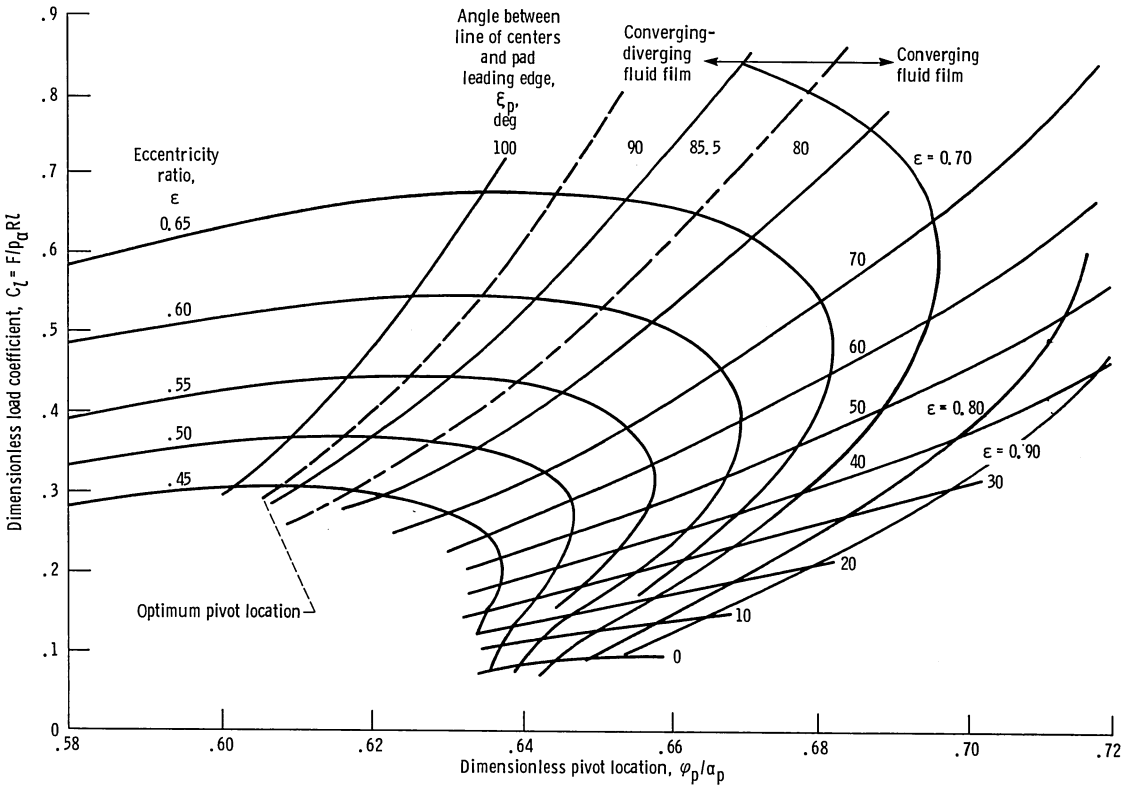

Figure 2.4-3.—Chart for determining load coefficient. Bearing radius-to-length ratio, R/l, 0.6061; angular extent of pad, α_p, 94.5°; dimensionless bearing number, Λ_j, 3.5. (From Gunter et al., 1964.)

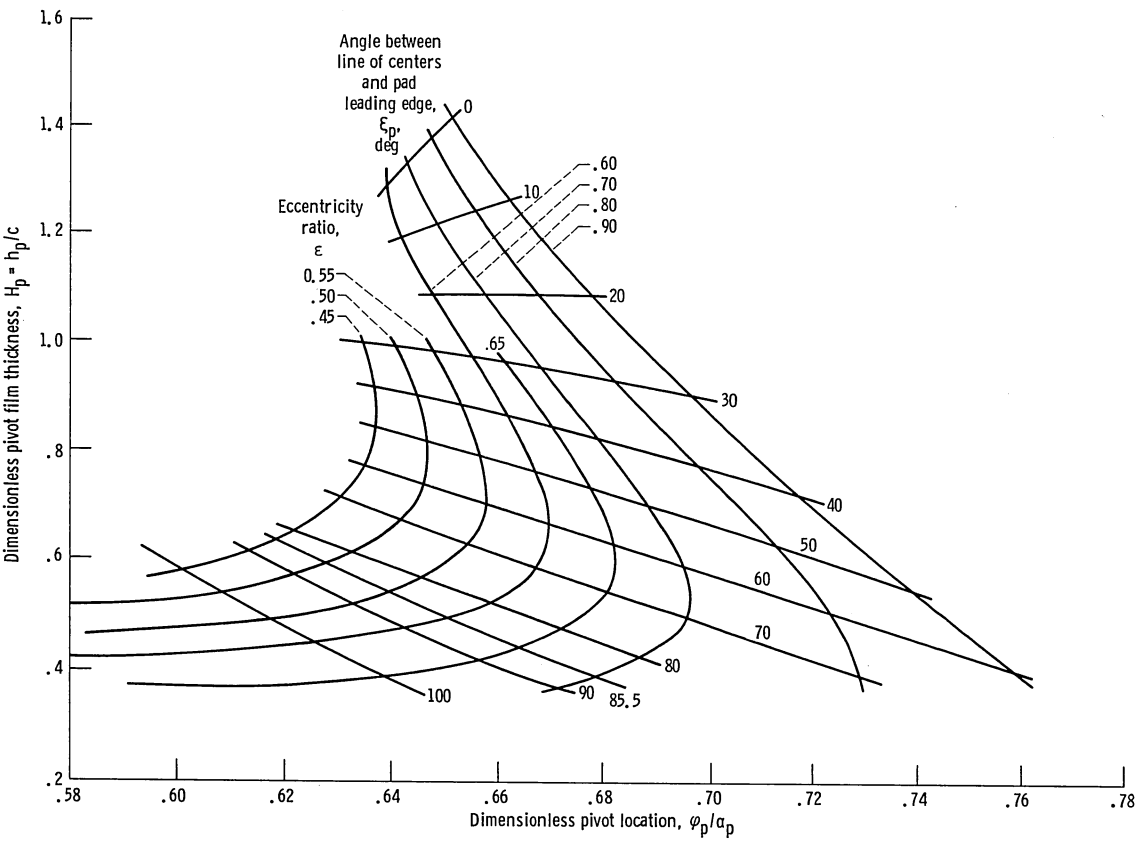

Figure 2.4-4.—Chart for determining pivot film thickness. Bearing radius-to-length ratio, R/l, 0.6061; angular extent of pad, α_p, 94.5°; dimensionless bearing number, Λ_j, 3.5. (From Gunter et al., 1964.)

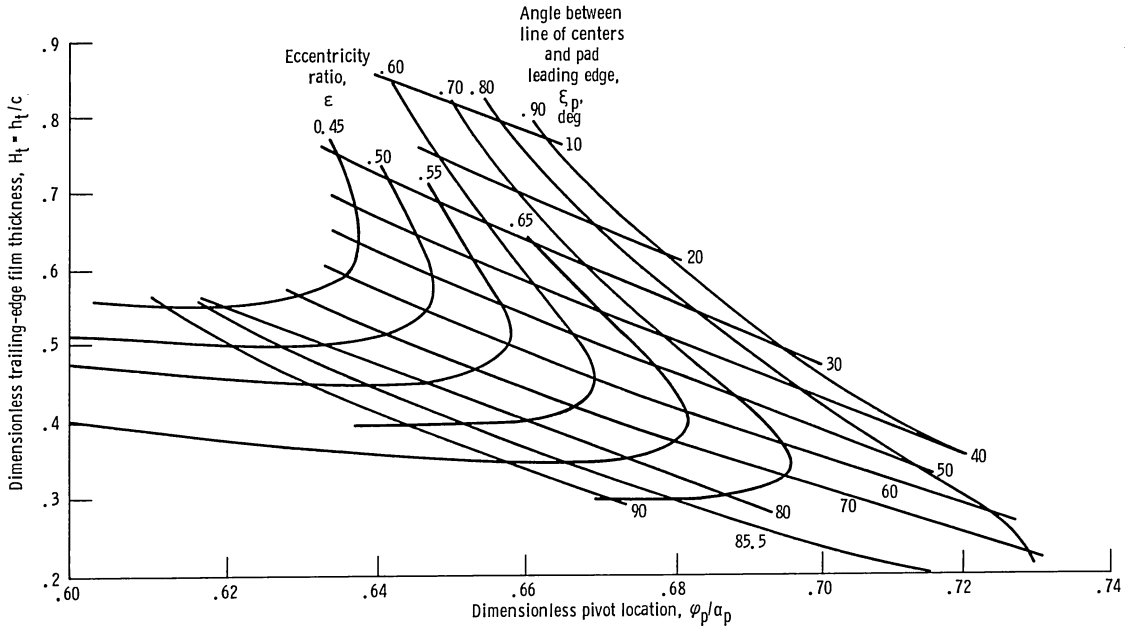

Figure 2.4-5.—Chart for determining trailing-edge film thickness. Bearing radius-to-length ratio, R/l, 0.6061; angular extent of pad, α_p, 94.5°, dimensionless bearing number, Λ_j,3.5. (From Gunter et al., 1964.)

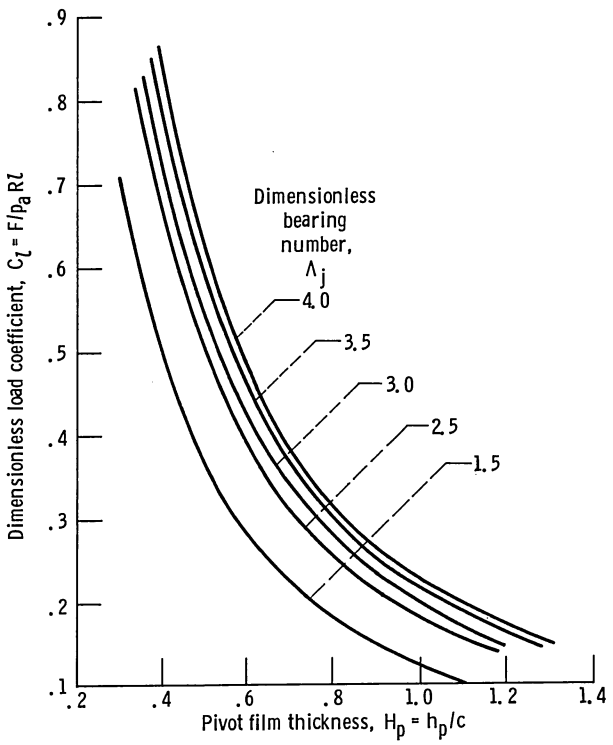

Figure 2.4-6.—Chart for determining load coefficient. Angular extent of pad, α_p, 94.5°; ratio of angle between pad leading edge and pivot to α_p, φ_p/α_p, 2/3; length-to-width ratio, λ, 1.0. (From Gunter et al., 1964.)

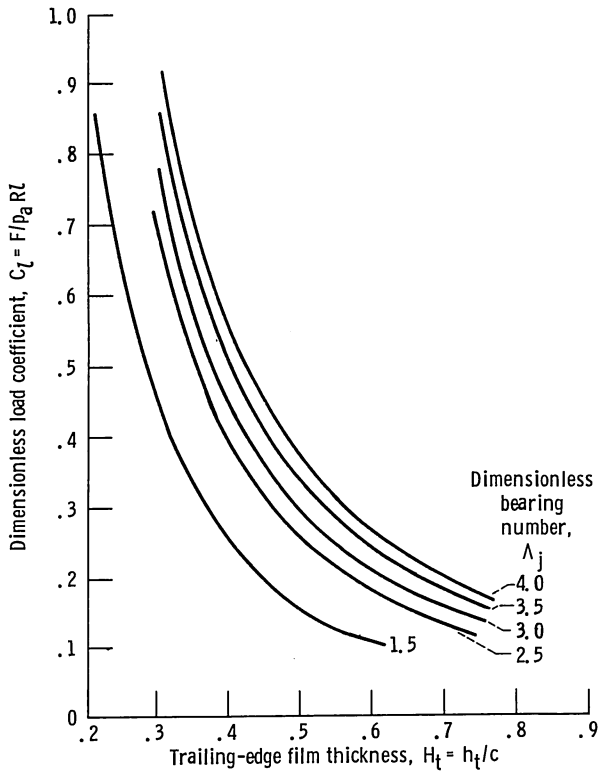

Figure 2.4-7.—Chart for determining load coefficient. Angular extent of pad, α_p, 94.5°; ratio of angle between pad loading edge and pivot to α_p, φ_p/α_p, 2/3; length-to-width ratio, λ, 1.0. (From Gunter et al., 1964.)

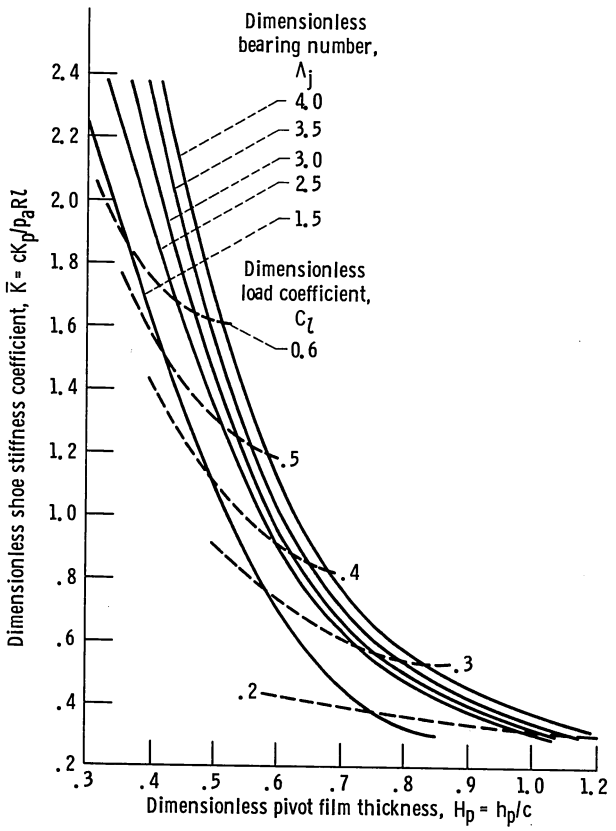

Figure 2.4-8.—Chart for determining shoe stiffness coefficient. (From Gunter et al., 1964.)

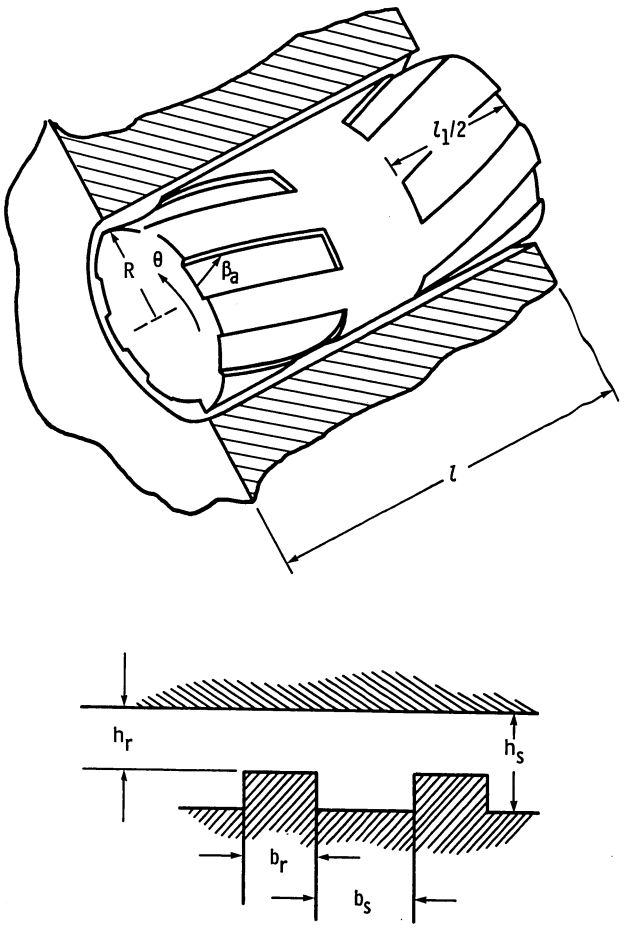

Figure 2.4-9.—Configuration of concentric herringbone-groove journal bearing. Bearing parameters: $\lambda = l/2R$; $\Lambda_j = 6\mu UR/p_a h_r^2$. Groove parameters: $H_a = h_s/h_r$; $\alpha_b = b_s/(b_r + b_s)$; β_a; $\gamma = l_1/l$; n. (From Hamrock and Fleming, 1971.)

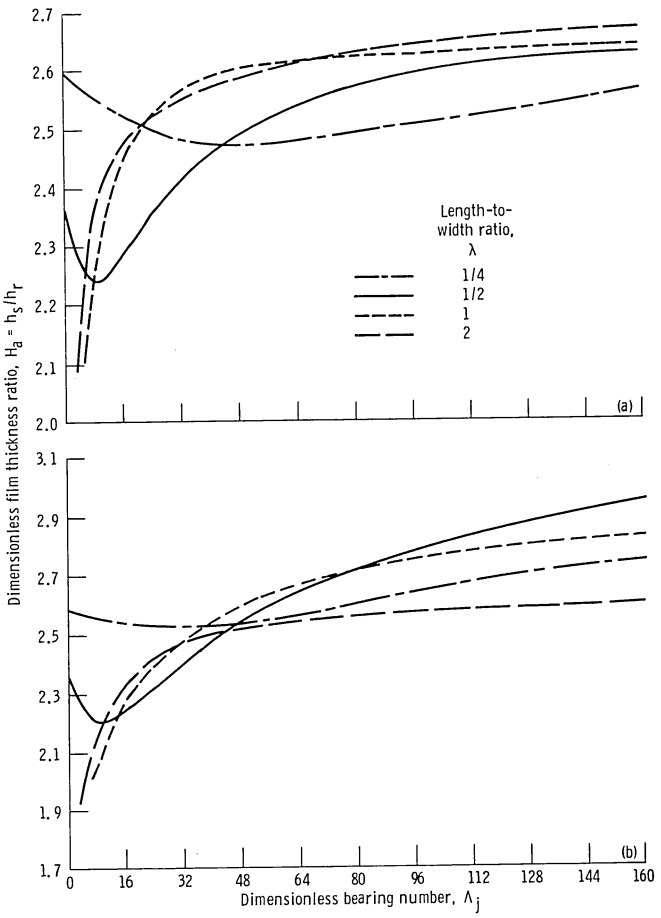

(a) Grooved member rotating.
(b) Smooth member rotating.

Figure 2.4-10.—Chart for determining optimal film thickness. (From Hamrock and Fleming, 1971.)

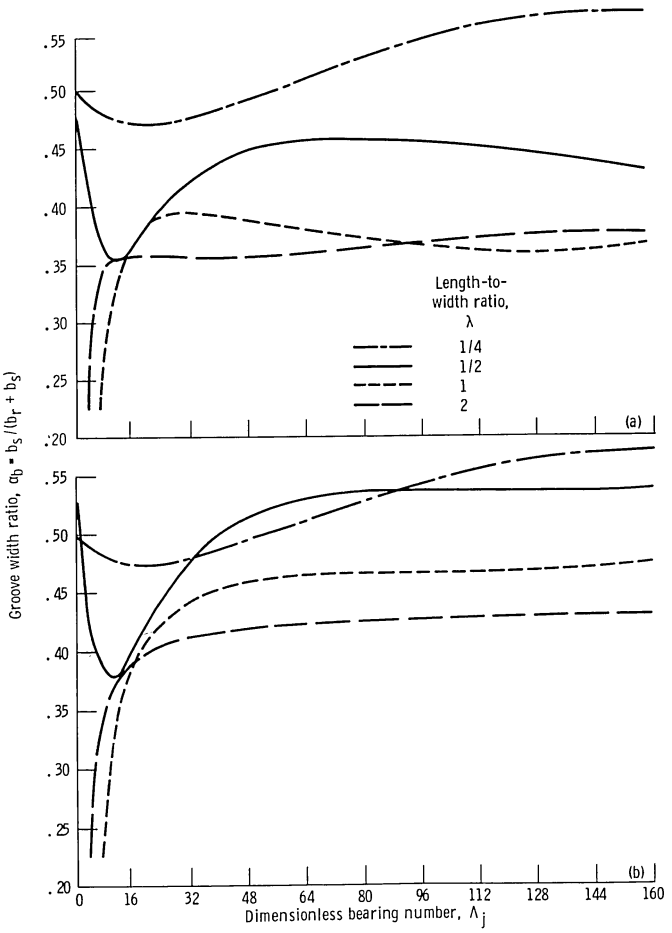

(a) Grooved member rotating.
(b) Smooth member rotating.

Figure 2.4-11.—Chart for determining optimal groove width ratio. (From Hamrock and Fleming, 1971.)

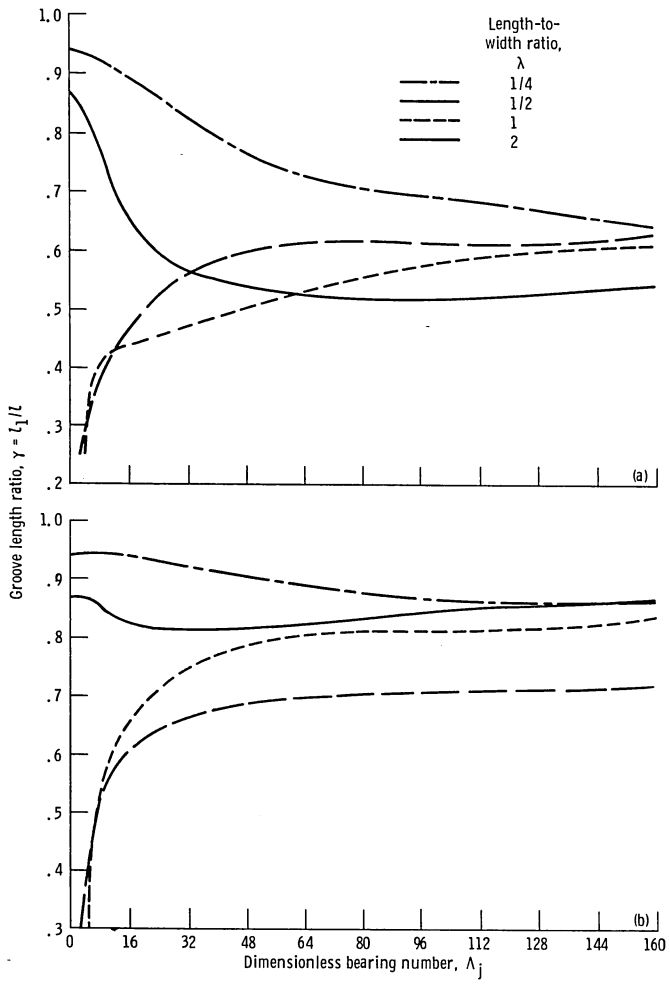

(a) Grooved member rotating.
(b) Smooth member rotating.

Figure 2.4-12.—Chart for determining optimal groove length ratio. (From Hamrock and Fleming, 1971.)

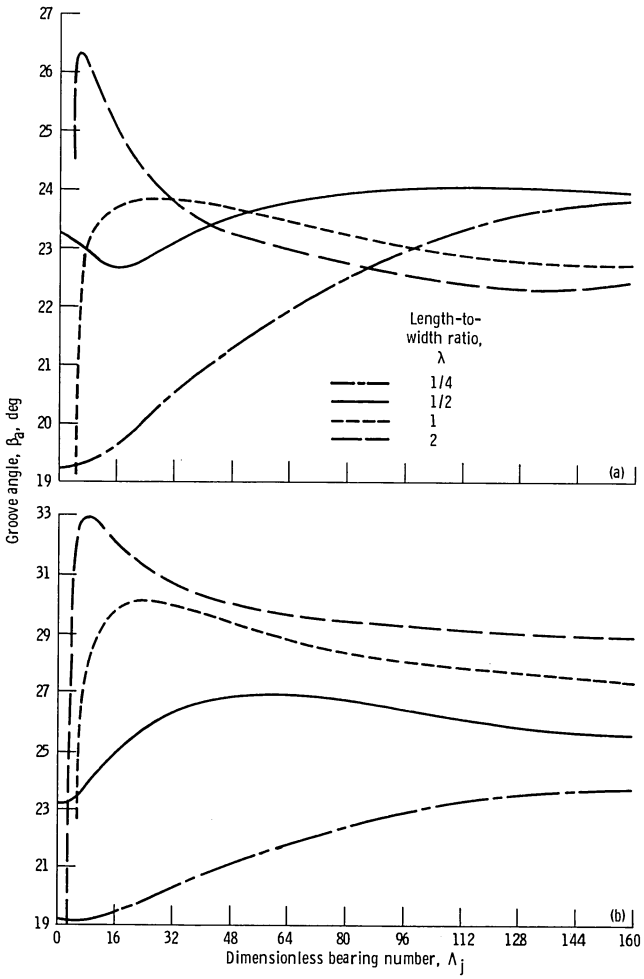

(a) Grooved member rotating.
(b) Smooth member rotating.

Figure 2.4-13.—Chart for determining optimal groove angle. (From Hamrock and Fleming, 1971.)

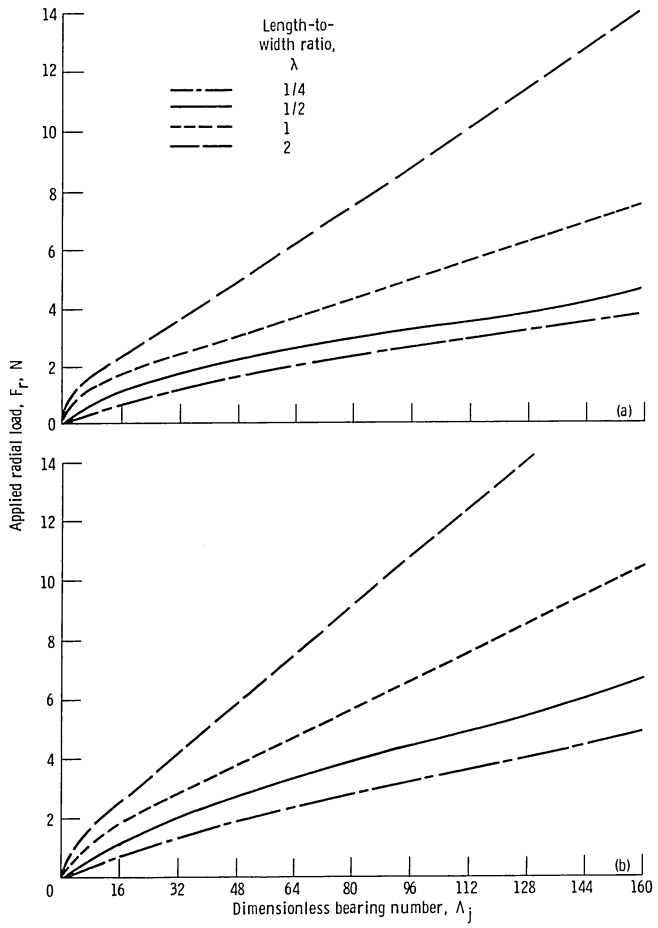

(a) Grooved member rotating.
(b) Smooth member rotating.

Figure 2.4-14.—Chart for determining maximum radial load capacity. (From Hamrock and Fleming, 1971.)

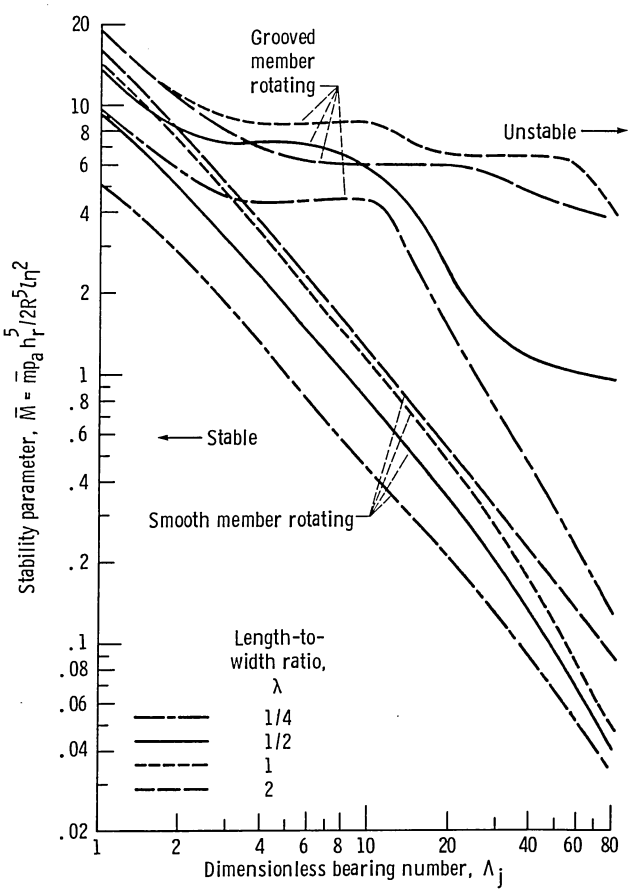

Figure 2.4-15.—Chart for determining maximum stability of herringbone-groove bearings. (From Fleming and Hamrock, 1974.)

In figure 2.4-15 the bearings with the grooved member rotating are substantially more stable than those with the smooth member rotating, especially at high compressibility numbers.

2.4.2 Thrust bearings

Two types of gas-lubricated thrust bearing have found the widest use in practical applications. These are the Rayleigh step and the spiral- or herringbone-groove bearings.

Rayleigh step bearing

Figure 2.4-16 shows a Rayleigh step thrust bearing. In this figure the ridge region is where the film thickness is h_r and the step region is where the film thickness is h_s. The feed groove is the deep groove separating the end of the ridge region and the beginning of the next step region. Although not shown in the figure, the feed groove is orders of magnitude deeper than the film thickness h_r. A pad is defined as the section that includes ridge, step, and

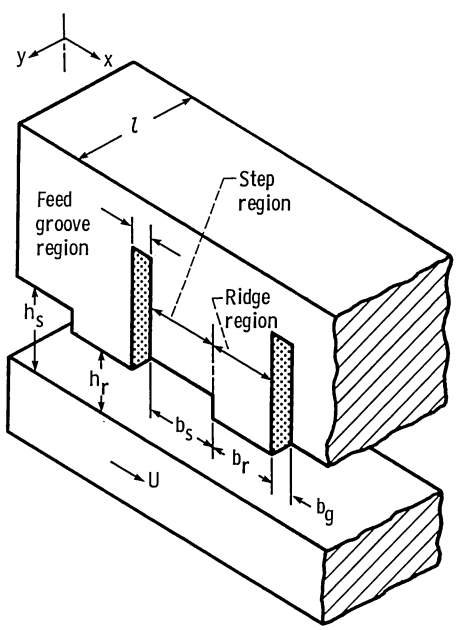

Figure 2.4-16.—Configuration of rectangular step thrust bearing. (From Hamrock, 1972.)

feed groove regions. The length of the feed groove is small relative to the length of the pad. Note that each pad acts independently since the pressure profile is broken at the lubrication feed groove.

The load capacity and stiffness of a Rayleigh step thrust bearing are functions of the following parameters:

(1) $\Lambda_t = 6\eta u l / p_a h_r^2$, dimensionless bearing number
(2) $\lambda_a = (b_r + b_s + b_g)/l$, length ratio
(3) $H_a = h_s/h_r$, film thickness ratio
(4) $\psi_s = b_s/(b_s + b_r + b_g)$, step location parameter

Figure 2.4-17(a) shows the effect of Λ_t on λ_a, H_a, and ψ_s for the *maximum-load-capacity condition*. The optimal step parameters λ_a, H_a, and ψ_s approach an asymptote as the dimensionless bearing number Λ_t becomes small. This asymptotic condition corresponds to the incompressible solution or $\lambda_a = 0.918$, $\psi_s = 0.555$, $H_a = 1.693$. For $\Lambda_t > 1$ it is observed that there is a different optimum value of λ_a, H_a and ψ_s for each value of Λ_t.

Figure 2.4-17(b) shows the effect of Λ_t on λ_a, H_a, and ψ_s for the *maximum-stiffness condition*. As in figure 2.4-17(a) the optimal step parameters approach asymptotes as the incompressible solution is reached. The asymptotes are $\lambda_a = 0.915$, $\psi_s = 0.557$, and $H_a = 1.470$. Note that there is a difference in the asymptote for the film thickness ratio but virtually no change in λ_a and ψ_s when compared with the results obtained for maximum-load-capacity condition.

Figure 2.4-18 shows the effect of dimensionless bearing number Λ_t on dimensionless load capacity and stiffness. The difference in these figures is that the optimal step parameters are obtained in figure 2.4-18(a) for maximum load capacity and in figure 2.4-18(b) for maximum stiffness.

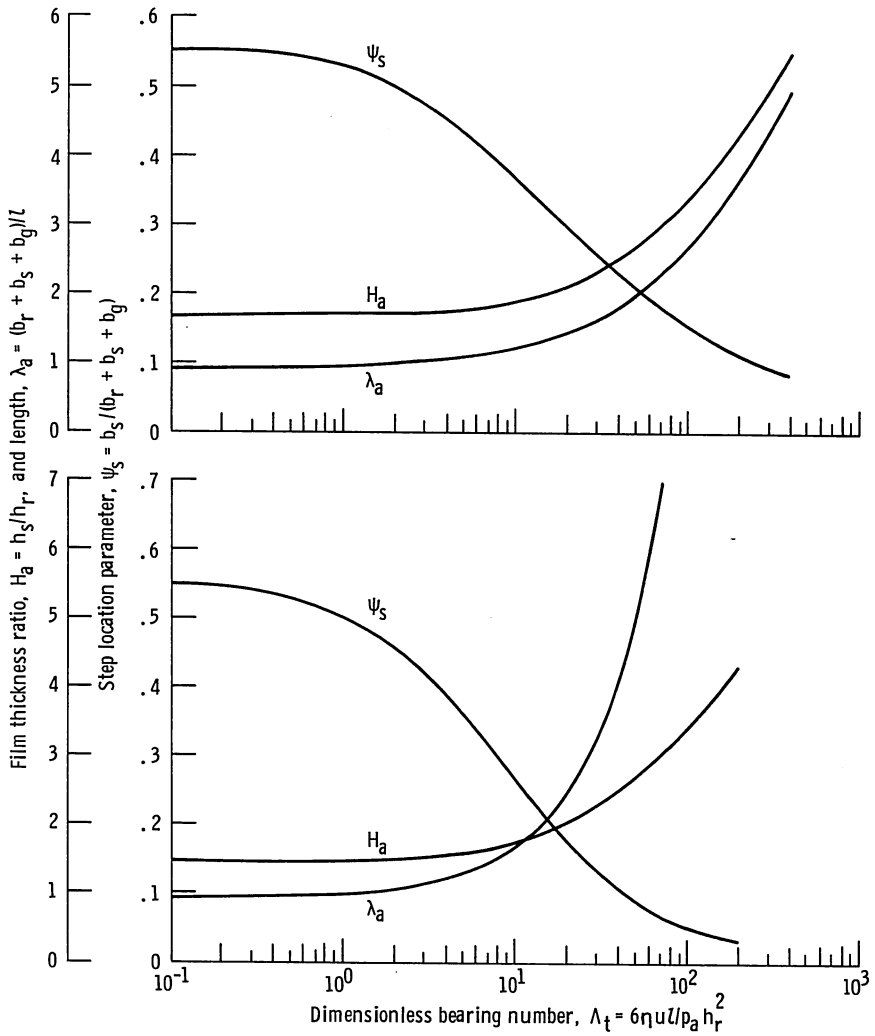

(a) Maximum dimensionless load capacity.
(b) Maximum dimensionless stiffness.

Figure 2.4-17.—Chart for determining optimal step parameters. (From Hamrock, 1972.)

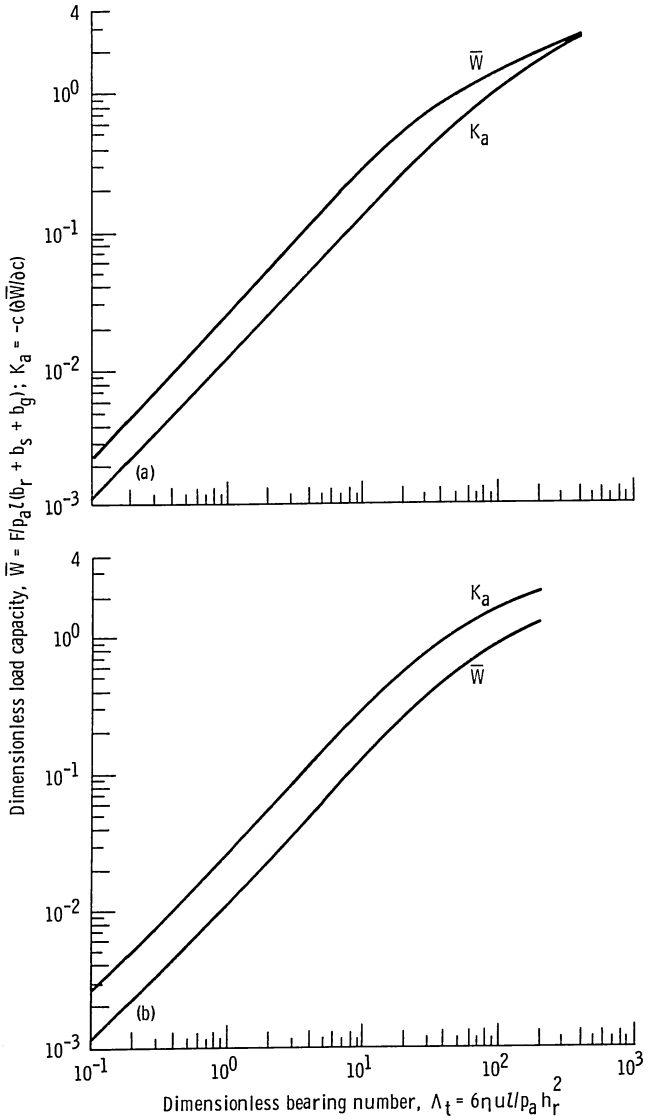

(a) Maximum dimensionless load capacity.
(b) Maximum dimensionless stiffness.

Figure 2.4–18.—Chart for determining dimensionless load capacity and stiffness. (From Hamrock, 1972.)

For optimization of a step-sector thrust bearing, parameters for the sector must be found that are analogous to those for the rectangular step bearing. The following substitutions accomplish this transformation:

$$l \rightarrow R_1 - R_2$$

$$n(b_s + b_r + b_g) \rightarrow \pi(R_1 + R_2)$$

$$u \rightarrow \frac{\omega}{2}(R_1 + R_2)$$

where n is the number of pads placed in the step sector.

By making use of these equations, the dimensionless bearing number can be rewritten as

$$\Lambda_c = \frac{3\eta\omega(R_1^2 - R_2^2)}{p_a h_r^2}$$

The optimal number of pads to be placed in the sector is obtained from the following formula:

$$n = \frac{\pi(R_1 + R_2)}{(\lambda_a)_{opt}(R_1 - R_2)}$$

where $(\lambda_a)_{opt}$ is obtained from figure 2.4–17(a) or (b) for a given dimensionless bearing number Λ_t. Since n will not normally be an integer, rounding it to the nearest integer is required. Therefore, through the parameter transformation discussed above, the results presented in figures 2.4–17 and 2.4–18 can be used directly in designing optimal step-sector gas-lubricated thrust bearings.

Spiral-groove thrust bearings

An inward-pumping spiral-groove thrust bearing is shown in figure 2.4–19. An inward-pumping thrust bearing is somewhat more efficient than an outward-pumping thrust bearing and therefore is the only type considered here.

The dimensionless parameters normally associated with a spiral-groove thrust bearing are

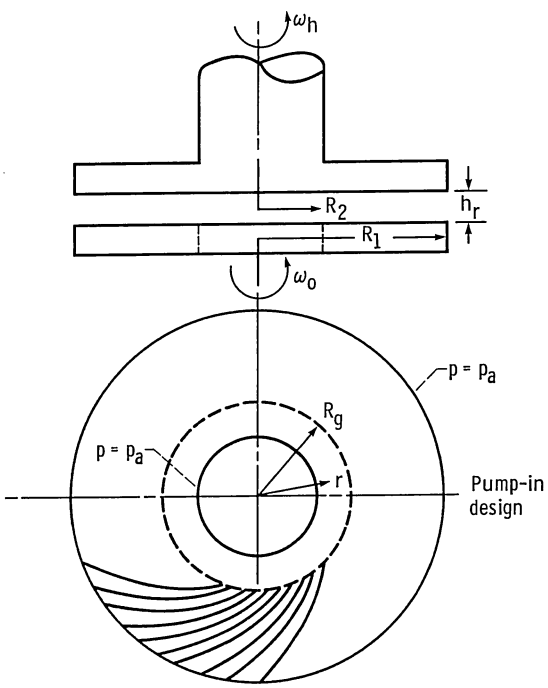

Figure 2.4–19.—Configuration of spiral-groove thrust bearing. (From Reiger, 1967.)

(1) Angle of inclination, β_a
(2) Width ratio, $\bar{b}=b_s/b_r$
(3) Film ratio, $H_a=h_s/h_r$
(4) Radius ratio, $\alpha_r=R_2/R_1$
(5) Groove length fraction, $\bar{R}=(R_1-R_g)/(R_1-R_2)$
(6) Number of grooves, n
(7) Dimensionless bearing number, $\Lambda_c=3\eta\omega\left(R_1^2-R_2^2\right)/p_a h_r^2$

The first six parameters are geometrical parameters and the last parameter is an operating parameter.

The performance of spiral-groove thrust bearings is represented by the following dimensionless parameters:

(1) Load

$$\bar{W}_\infty=\frac{1.5\,G_f F}{\pi p_a\left(R_1^2-R_2^2\right)} \tag{2.4-1}$$

(2) Stiffness

$$\bar{K}_\infty=\frac{1.5\,h_r G_f K_p}{\pi p_a\left(R_1^2-R_2^2\right)} \tag{2.4-2}$$

(3) Flow

$$\bar{Q}=\frac{3\eta Q}{\pi p_a h_r^3} \tag{2.4-3}$$

(4) Torque

$$\bar{T}=\frac{6T_r}{\pi p_a\left(R_1^2+R_2^2\right)h_r\Lambda_c} \tag{2.4-4}$$

When the geometrical and operating parameters are specified, the load, stiffness, flow, and torque can be obtained.

The design charts of Reiger (1967) are reproduced as figures 2.4–20 to 2.4–26. Figure 2.4–20 shows the dimensionless load for various radius ratios as a function of dimensionless bearing number Λ_c. This figure can be used to calculate the dimensionless load for a finite number of grooves; figure 2.4–21 can be used to determine the value of the groove factor. Figure 2.4–22 shows curves of dimensionless stiffness; figure 2.4–23, curves of dimensionless flow; and figure 2.4–24, curves of dimensionless torque. Optimized groove geometry parameters can be obtained from figure 2.4–25. Finally figure 2.4–26 is used to calculate groove radius R_g (shown in fig. 2.4–19). Figure 2.4–26 shows the required groove length fraction $\bar{R}=(R_1-R_g)/(R_1-R_2)$ to ensure stability from self-excited oscillations.

In a typical design problem the given factors are load, speed, bearing envelope, gas viscosity, ambient pressure, and an allowable radius-to-clearance ratio. The maximum value of the radius-to-clearance ratio is usually

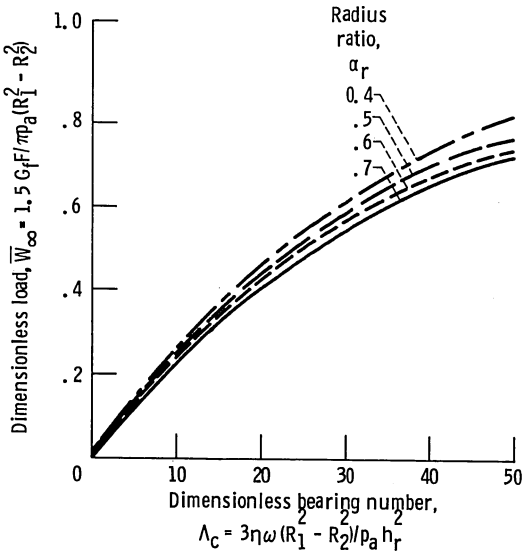

Figure 2.4–20.—Chart for determining load for spiral-groove thrust bearings. (From Reiger, 1967.)

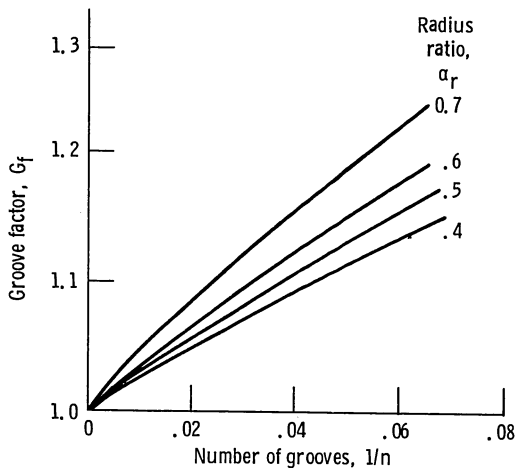

Figure 2.4–21.—Chart for determining groove factor for spiral-groove thrust bearings. (From Reiger, 1967.)

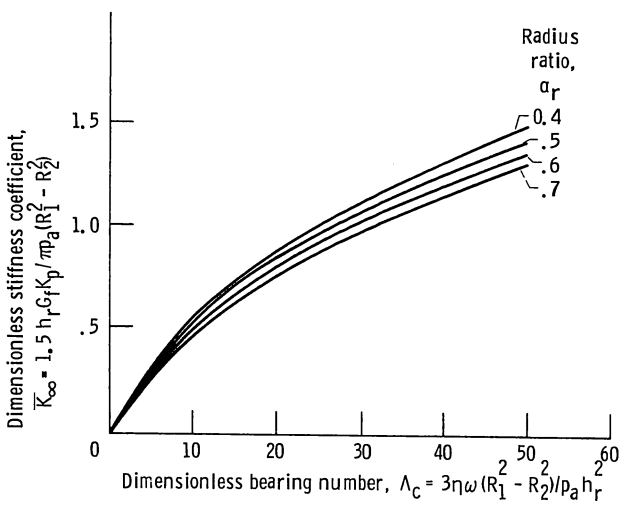

Figure 2.4–22.—Chart for determining stiffness for spiral-groove thrust bearings. (From Reiger, 1967.)

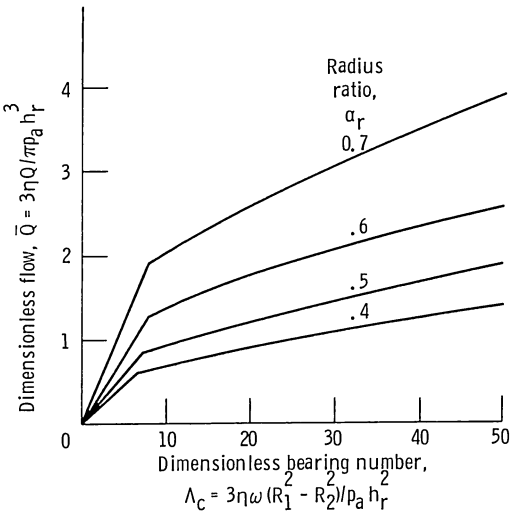

Figure 2.4-23.—Chart for determining flow for spiral-groove thrust bearings. (From Reiger, 1967.)

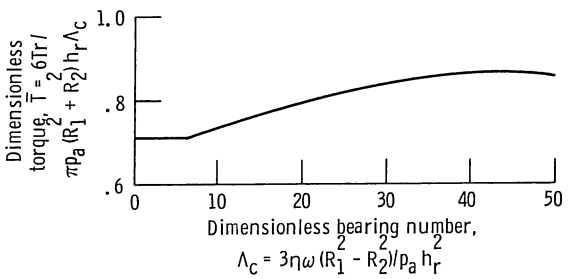

Figure 2.4-24.—Chart for determining torque for spiral-groove thrust bearings. (Curve is for all radius ratios. From Reiger, 1967.)

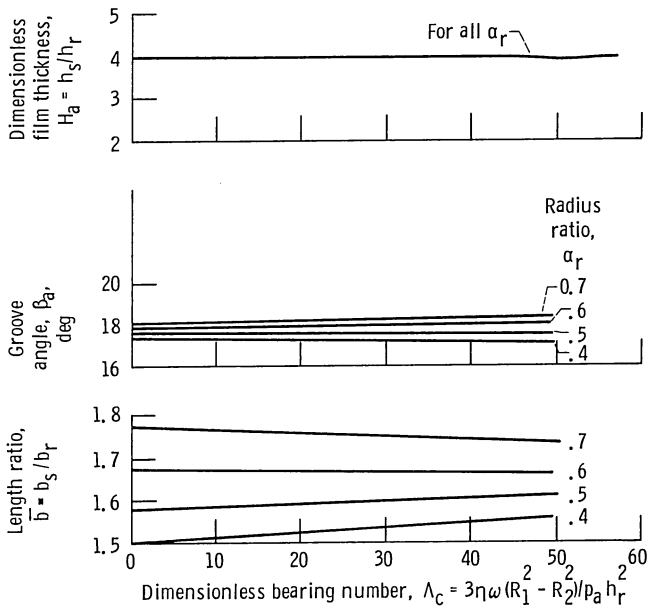

Figure 2.4-25.—Chart for determining optimal groove geometry for spiral-groove thrust bearings. (From Reiger, 1967.)

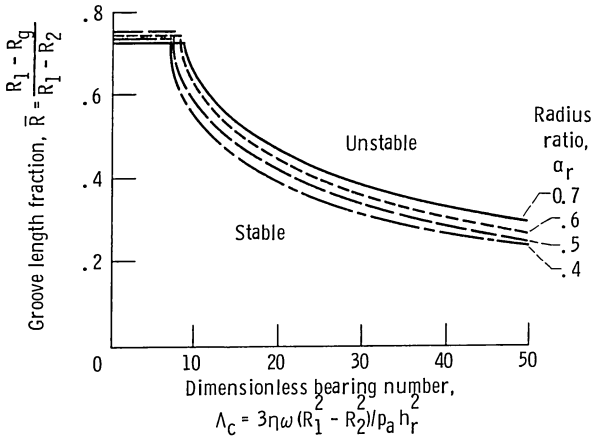

Figure 2.4-26.—Chart for determining groove length fraction for spiral-groove thrust bearings. (From Reiger, 1967.)

dictated by the distortion likely to occur to the bearing surfaces. Typical values are 5000 to 10 000. The procedure normally followed in designing a spiral-groove thrust bearing while using the design curves given in figures 2.4-20 to 2.4-26 is as follows:

(1) Select the number of grooves n.

(2) From figure 2.4-21 determine the groove factor G_f for given $\alpha_r = R_2/R_1$ and n.

(3) Calculate $\bar{W}_\infty = 1.5\, G_f F/\pi p_a (R_1^2 - R_2^2)$.

(4) If $\bar{W}_\infty > 0.8$, R_1 must be increased. Return to step 2.

(5) From figure 2.4-20, given W_∞ and α_r establish Λ_c.

(6) Calculate $\dfrac{R_1}{h_r} = \left\{ \dfrac{\Lambda_c p_a}{3\eta\omega\left[1 - (R_2/R_1)^2\right]} \right\}^{1/2}$

If $R_1/h_r > 10\,000$ (or whatever preassigned radius-to-clearance ratio), a larger bearing or higher speed is required. Return to step 2. If these changes cannot be made, an externally pressurized bearing must be used.

(7) Having established what α_r and Λ_c should be, obtain values of $\bar{K}_\infty$, $\bar{Q}$, and $\bar{T}$ from figures 2.4-22, 2.4-23, and 2.4-24, respectively. From equations (2.4-2), (2.4-3), and (2.4-4) calculate K_p, Q, and T_r.

(8) From figure 2.4-25 obtain groove geometry ($\bar{b}$, β_a, and H_a) and from figure 2.4-26 obtain R_g.

3 Elastohydrodynamic Lubrication

Dowson (1965) defines elastohydrodynamic lubrication (EHL) as "the study of situations in which elastic deformation of the surrounding solids plays a significant role in the hydrodynamic lubrication process." Elastohydrodynamic lubrication implies complete fluid-film lubrication and no asperity interaction of the surfaces. There are two distinct forms of elastohydrodynamic lubrication:

(1) *Hard EHL*—relating to materials of high elastic modulus, such as metals. In this form of lubrication not

only are the elastic deformation effects important, but the pressure-viscosity effects are equally so. Engineering applications in which this form of lubrication is dominant include gears and rolling-element bearings.

(2) *Soft EHL*—relating to materials of low elastic modulus, such as rubber. For these materials the elastic distortions are large, even with light loads. Another feature is the negligible pressure-viscosity effect on the lubricating film. Engineering applications in which soft EHL is important include seals, human joints, tires, and a number of lubricated elastomeric material machine elements.

The recognition and understanding of elastohydrodynamic lubrication represents one of the major developments in the field of tribology in this century. The revelation of a previously unsuspected regime of lubrication is clearly an event of importance in tribology. Elastohydrodynamic lubrication not only explained the remarkable physical action responsible for the effective lubrication of many machine elements, but it also brought order to the understanding of the complete spectrum of lubrication regimes, ranging from boundary to hydrodynamic.

A way of coming to an understanding of elastohydrodynamic lubrication is to compare it with hydrodynamic lubrication. The major developments that have led to our present understanding of hydrodynamic lubrication (Tower, 1883, and Reynolds, 1886) predate the major developments of elastohydrodynamic lubrication (Grubin, 1949, and Petrusevich, 1951) by 65 years. Both hydrodynamic and elastohydrodynamic lubrication are considered as fluid-film lubrication in that the lubricant film is sufficiently thick to prevent any significant degree of asperity contact between the opposing solids. Fluid-film lubrication is often referred to as the ideal form of lubrication since it provides low friction and high resistance to wear.

This section highlights some of the important aspects of elastohydrodynamic lubrication while illustrating its use in a number of applications. It is not intended to be exhaustive but rather to point out the significant features of this important regime of lubrication. For more details the reader is referred to Hamrock and Dowson (1981).

3.1 Contact Stresses and Deformations

As pointed out in Section 1.1, elastohydrodynamic lubrication is the mode of lubrication normally found in nonconformal contacts such as rolling-element bearings. A load-deflection relationship for nonconformal contacts is developed in this section. The deformation within the contact is calculated from, among other things, the ellipticity parameter and the elliptic integrals of the first and second kinds. Simplified expressions that allow quick calculations of the stresses and deformations to be made easily from a knowledge of the applied load, the material properties, and the geometry of the contacting elements are presented in this section.

3.1.1 Elliptical contacts

The undeformed geometry of contacting solids in a nonconformal contact can be represented by two ellipsoids. The two solids with different radii of curvature in a pair of principal planes (x and y) passing through the contact between the solids make contact at a single point under the condition of zero applied load. Such a condition is called point contact and is shown in figure 3.1-1, where the radii of curvature are denoted by r's. It is assumed that convex surfaces (fig. 3.1-1) exhibit positive curvature and concave surfaces, negative curvature. Therefore if the center of curvature lies within the solids, the radius of curvature is positive; if the center of curvature lies outside the solids, the radius of curvature is negative. It is important to note that if coordinates x and y are chosen such that

$$\frac{1}{r_{ax}} + \frac{1}{r_{bx}} > \frac{1}{r_{ay}} + \frac{1}{r_{by}} \tag{3.1-1}$$

coordinate x then determines the direction of the semiminor axis of the contact area when a load is applied and y, the direction of the semimajor axis. The direction of motion is always considered to be along the x-axis so that a and b must actually be ellipsoids of revolution about their own y-axis.

The curvature sum and difference, which are quantities of some importance in the analysis of contact stresses and deformations, are

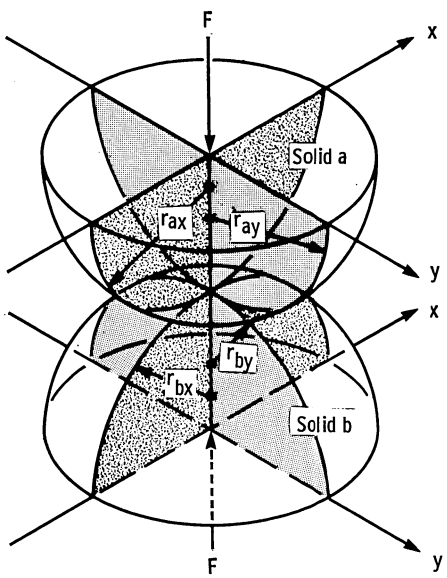

Figure 3.1-1.—Geometry of contacting elastic solids. (From Hamrock and Dowson, 1981.)

$$\frac{1}{R} = \frac{1}{R_x} + \frac{1}{R_y} \tag{3.1-2}$$

$$\Gamma = R\left(\frac{1}{R_x} - \frac{1}{R_y}\right) \tag{3.1-3}$$

where

$$\frac{1}{R_x} = \frac{1}{r_{ax}} + \frac{1}{r_{bx}} \tag{3.1-4}$$

$$\frac{1}{R_y} = \frac{1}{r_{ay}} + \frac{1}{r_{by}} \tag{3.1-5}$$

$$\alpha = \frac{R_y}{R_x} \tag{3.1-6}$$

Equations (3.1-4) and (3.1-5) effectively redefine the problem of two ellipsoidal solids approaching one another in terms of an equivalent ellipsoidal solid of radii R_x and R_y approaching a plane.

The ellipticity parameter k is defined as the elliptical-contact diameter in the y-direction (transverse direction) divided by the elliptical-contact diameter in the x-direction (direction of motion) or $k = D_y/D_x$. It is determined by the radius ratio α and is independent of applied load. If equation (3.1-1) is satisfied and $\alpha \geq 1$, the contact ellipse will be oriented so that its major diameter will be transverse to the direction of motion, and consequently $k \geq 1$. Otherwise, the major diameter would lie along the direction of motion with both $\alpha \leq 1$ and $k \leq 1$. Figure 3.1-2 shows the ellipticity parameter and the elliptic integrals of the first and second kinds for a range of curvature ratios ($\alpha = R_y/R_x$) usually encountered in concentrated contacts.

Simplified solutions for $\alpha > 1$

The classical Hertzian solution requires the calculation of the ellipticity parameter k from the complete elliptic integrals of the first and second kinds $\mathfrak{F}$ and $\mathfrak{E}$. This entails finding a solution to a transcendental equation relating k, $\mathfrak{F}$, and $\mathfrak{E}$ to the geometry of the contacting solids. Possible approaches include an iterative numerical procedure, as described for example by Hamrock and Anderson (1973), or the use of charts, as shown by Jones (1946). Hamrock and Brewe (1983) provide a shortcut to the classical Hertzian solution for the local stress and deformation of two elastic bodies in contact. The shortcut is accomplished by using simplified forms of the ellipticity parameter and the complete elliptic integrals, expressing them as functions of the geometry. The results of Hamrock and Brewe's (1983) work are summarized here.

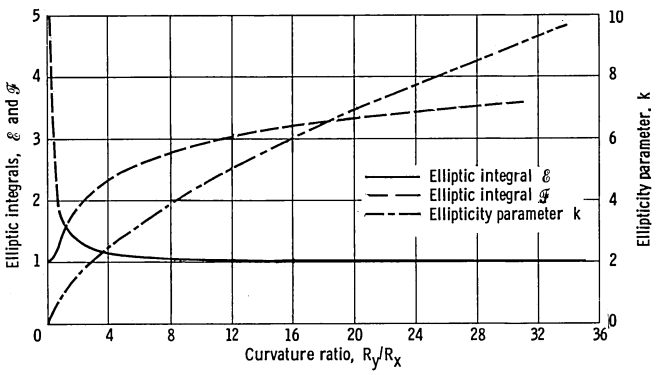

Figure 3.1-2.—Chart for determining ellipticity parameter and elliptic integrals of first and second kinds. (From Hamrock and Brewe, 1983.)

A power fit using linear regression by the method of least squares resulted in the following expression for the ellipticity parameter:

$$k = \alpha^{2/\pi} \qquad \text{for } \alpha \geq 1 \tag{3.1-7}$$

The asymptotic behavior of $\mathfrak{E}$ and $\mathfrak{F}$ ($\alpha \to 1$ implies $\mathfrak{E} \to \mathfrak{F} \to \pi/2$, and $\alpha \to \infty$ implies $\mathfrak{F} \to \infty$ and $\mathfrak{E} \to 1$) was suggestive of the type of functional dependence that $\mathfrak{E}$ and $\mathfrak{F}$ might follow. As a result, an inverse and logarithmic fit were tried for $\mathfrak{E}$ and $\mathfrak{F}$, respectively. The following expressions provided excellent curve fit:

$$\mathfrak{E} = 1 + \frac{q}{\alpha} \qquad \text{for } \alpha \geq 1 \tag{3.1-8}$$

$$\mathfrak{F} = \frac{\pi}{2} + q \ln \alpha \qquad \text{for } \alpha \geq 1 \tag{3.1-9}$$

where

$$q = \frac{\pi}{2} - 1 \tag{3.1-10}$$

When the ellipticity parameter k (eq. (3.1-7)), the elliptic integrals of the first and second kinds (eqs. (3.1-8) and (3.1-9)), the normal applied load F, Poisson's ratio ν, and the modulus of elasticity E of the contacting solids are known, we can write the major and minor axes of the contact ellipse and the maximum deformation at the center of the contact, from the analysis of Hertz (1881), as

$$D_y = 2\left(\frac{6k^2\mathfrak{E}FR}{\pi E'}\right)^{1/3} \tag{3.1-11}$$

$$D_x = 2\left(\frac{6\mathfrak{E}FR}{\pi k E'}\right)^{1/3} \tag{3.1-12}$$

$$\delta = \mathfrak{F}\left[\left(\frac{9}{2\mathfrak{E}R}\right)\left(\frac{F}{\pi k E'}\right)^2\right]^{1/3} \tag{3.1-13}$$

where (as in eq. (1.5-7))

$$E' = \frac{2}{\frac{1-\nu_a^2}{E_a} + \frac{1-\nu_b^2}{E_b}} \tag{3.1-14}$$

In these equations D_y and D_x are proportional to $F^{1/3}$ and δ is proportional to $F^{2/3}$.

The maximum Hertzian stress at the center of the contact can also be determined by using equations (3.1-11) and (3.1-12)

$$\sigma_{max} = \frac{6F}{\pi D_x D_y} \tag{3.1-15}$$

Simplified solutions for $\alpha < 1$

Table 3.1-1 gives the simplified equations for $\alpha < 1$ as well as for $\alpha \geq 1$. Recall that $\alpha \geq 1$ implies $k \geq 1$ and equation (3.1-1) is satisfied, and $\alpha < 1$ implies $k < 1$ and equation (3.1-1) is not satisfied. It is important to make the proper evaluation of α since it has a great significance in the outcome of the simplified equations.

Figure 3.1-3 shows these diverse situations in which the simplified equations can be usefully applied. The locomotive wheel on a rail (fig. 3.1-3(a)) illustrates an example in which the ellipticity parameter k and the radius ratio α are less than 1. The ball rolling against a flat plate (fig. 3.1-3(b)) provides pure circular contact (i.e., $\alpha = k = 1.0$). Figure 3.1-3(c) shows how the contact ellipse is formed in the ball – outer-ring contact of a ball bearing. Here the semimajor axis is normal to the direction of rolling and consequently α and k are greater than 1. Table 3.1-2 shows how the degree of conformity affects the contact parameters for the various cases illustrated in figure 3.1-3.

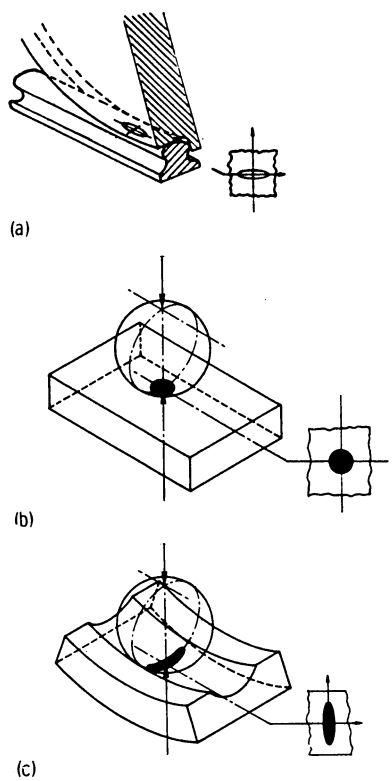

(a) Wheel on rail.
(b) Ball on plane.
(c) Ball – outer-race contact.

Figure 3.1-3.—Three degrees of conformity. (From Hamrock and Brewe, 1983.)

TABLE 3.1-1. - SIMPLIFIED EQUATIONS

[From Hamrock and Anderson (1983).]

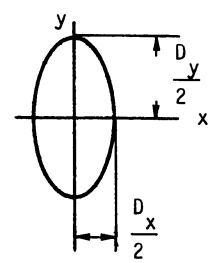	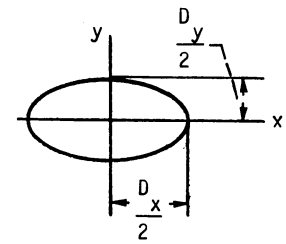
$\alpha \geq 1$	$\alpha < 1$
$k = \alpha^{2/\pi}$	$k = \alpha^{2/\pi}$
$\mathscr{F} = \frac{\pi}{2} + q \ln \alpha$	$\mathscr{F} = \frac{\pi}{2} + q \ln \alpha$
where $q = \frac{\pi}{2} - 1$	where $q = \frac{\pi}{2} - 1$
$\mathscr{E} = 1 + \frac{q}{\alpha}$	$\mathscr{E} = 1 + q\alpha$
$D_y = 2\left(\frac{6k^2 \mathscr{E} FR}{\pi E'}\right)^{1/3}$	$D_y = 2\left(\frac{6k \mathscr{E} FR}{\pi E'}\right)^{1/3}$
where $R^{-1} = R_x^{-1} + R_y^{-1}$	where $R^{-1} = R_x^{-1} + R_y^{-1}$
$D_x = 2\left(\frac{6 \mathscr{E} FR}{\pi k E'}\right)^{1/3}$	$D_x = 2\left(\frac{6 \mathscr{E} FR}{\pi E' k^2}\right)^{1/3}$
$\delta = \mathscr{F}\left[\left(\frac{4.5}{\mathscr{E} R}\right)\left(\frac{F}{\pi k E'}\right)^2\right]^{1/3}$	$\delta = \mathscr{F}\left[\left(\frac{4.5}{\mathscr{E} R}\right)\left(\frac{Fk}{\pi E'}\right)^2\right]^{1/3}$

TABLE 3.1-2. - PRACTICAL APPLICATIONS FOR DIFFERING CONFORMITIES

[From Hamrock and Brewe (1983). $E' = 2.197 \times 10^7$ N/cm^2.]

Contact parameters	Wheel on rail	Ball on plane	Ball - outer-race contact
F	1.00×10^5 N	222.4111 N	222.4111 N
r_{ax}	50.1900 cm	0.6350 cm	0.6350 cm
r_{ay}	∞	0.6350 cm	0.6350 cm
r_{bx}	∞	∞	-3.8900 cm
r_{by}	30.0000 cm	∞	-0.6600 cm
u	0.5977	1.0000	22.0905
k	0.7206	1.0000	7.1738
$\mathscr{E}$	1.3412	1.5708	1.0258
$\mathscr{F}$	1.8645	1.5708	3.3375
D_y	1.0807 cm	0.0426 cm	0.1810 cm
D_x	1.4997 cm	0.0426 cm	0.0252 cm
δ	0.0108 cm	7.13×10^{-4} cm	3.57×10^{-4} cm
σ_{max}	1.1784×10^5 N/cm^2	2.34×10^5 N/cm^2	9.30×10^4 N/cm^2

3.1.2 Rectangular contacts

For this situation the contact ellipse discussed in the preceding section is of infinite length in the transverse direction ($D_y \to \infty$). This type of contact is exemplified by a cylinder loaded against a plate, a groove, or another parallel cylinder or by a roller loaded against an inner or outer ring. In these situations the contact semiwidth is given by

$$b = R_x \left(\frac{8W}{\pi} \right)^{1/2} \tag{3.1-16}$$

where

$$W = \frac{F'}{E' R_x} \tag{3.1-17}$$

and F' is the load per unit length along the contact.

The maximum deformation given by the approach of centers of two cylinders can be written as (ESDU, 1978)

$$\delta = \frac{2WR_x}{\pi} \left[\frac{2}{3} + \ln\left(\frac{2r_{ax}}{b} \right) + \ln\left(\frac{2r_{bx}}{b} \right) \right] \tag{3.1-18}$$

The maximum Hertzian stress in a rectangular contact can be written as

$$\sigma_{max} = E' \left(\frac{W}{2\pi} \right)^{1/2} \tag{3.1-19}$$

3.2 Dimensionless Grouping

The variables appearing in elastohydrodynamic lubrication theory are

E' effective elastic modulus, N/m^2
F normal applied load, N
h film thickness, m
R_x effective radius in x (motion) direction, m
R_y effective radius in y (transverse) direction, m
u mean surface velocity in x-direction, m/s
ξ pressure-viscosity coefficient of fluid, m^2/N
η_0 atmospheric viscosity, N s/m^2

From these variables the following five dimensionless groupings can be established:

Dimensionless film thickness

$$H = \frac{h}{R_x} \tag{3.2-1}$$

Ellipticity parameter

$$k = \frac{D_y}{D_x} = \left(\frac{R_y}{R_x} \right)^{2/\pi} \tag{3.2-2}$$

Dimensionless load parameter

$$W = \frac{F}{E' R_x^2} \tag{3.2-3}$$

Dimensionless speed parameter

$$U=\frac{\eta_0 u}{E' R_x} \tag{3.2-4}$$

Dimensionless materials parameter

$$G=\xi E' \tag{3.2-5}$$

The dimensionless minimum film thickness can now be written as a function of the other parameters involved:

$$H=f(k,\ U,\ W,\ G)$$

The most important practical aspect of elastohydrodynamic lubrication theory becomes the determination of this function f for the case of the minimum film thickness within a conjunction. Maintaining a fluid-film thickness of adequate magnitude is clearly vital to the efficient operation of machine elements.

3.3 Hard-EHL Results

By using the numerical procedures outlined in Hamrock and Dowson (1976), the influence of the ellipticity parameter and the dimensionless speed, load, and materials parameters on minimum film thickness was investigated by Hamrock and Dowson (1977). The ellipticity parameter k was varied from 1 (a ball-on-plate configuration) to 8 (a configuration approaching a rectangular contact). The dimensionless speed parameter U was varied over a range of nearly two orders of magnitude, and the dimensionless load parameter W over a range of one order of magnitude. Situations equivalent to using materials of bronze, steel, and silicon nitride and lubricants of paraffinic and naphthenic oils were considered in the investigation of the role of the dimensionless materials parameter G. Thirty-four cases were used in generating the minimum-film-thickness formula for hard EHL given here.

$$\boxed{H_{\min}=3.63\ U^{0.68}G^{0.49}W^{-0.073}\left(1-e^{-0.68k}\right)} \tag{3.3-1}$$

In this equation the dominant exponent occurs on the speed parameter, while the exponent on the load parameter is very small and negative. The materials parameter also carries a significant exponent, although the range of this variable in engineering situations is limited.

In addition to the minimum-film-thickness formula, contour plots of pressure and film thickness throughout the entire conjunction can be obtained from the numerical results. A representative contour plot of dimensionless pressure is shown in figure 3.3-1 for $k=1.25$, $U=0.168\times10^{-11}$, and $G=4522$. In this figure and in figure 3.3-2, the + symbol indicates the center of the Hertzian contact zone. The dimensionless representation of the X and Y coordinates causes the actual Hertzian contact ellipse to be a circle regardless of the value of the ellipticity parameter. The Hertzian contact circle is shown by asterisks. On this figure is a key showing the contour labels and each corresponding value of dimensionless pressure. The inlet region is to the left and the exit region is to the right. The pressure gradient at the exit end of the conjunction is much larger than that in the inlet region. In figure 3.3-1 a pressure spike is visible at the exit of the contact.

Contour plots of the film thickness are shown in figure 3.3-2 for the same case as figure 3.3-1. In this figure two

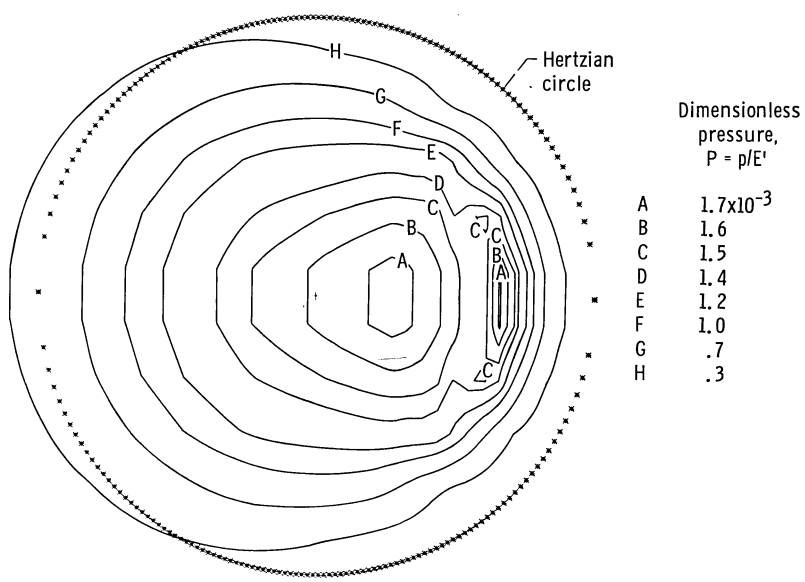

Figure 3.3-1.—Contour plot of dimensionless pressure. $k=1.25$; $U=0.168\times10^{11}$; $W=0.111\times10^{-6}$; $G=4522$. (From Hamrock and Dowson, 1977.)

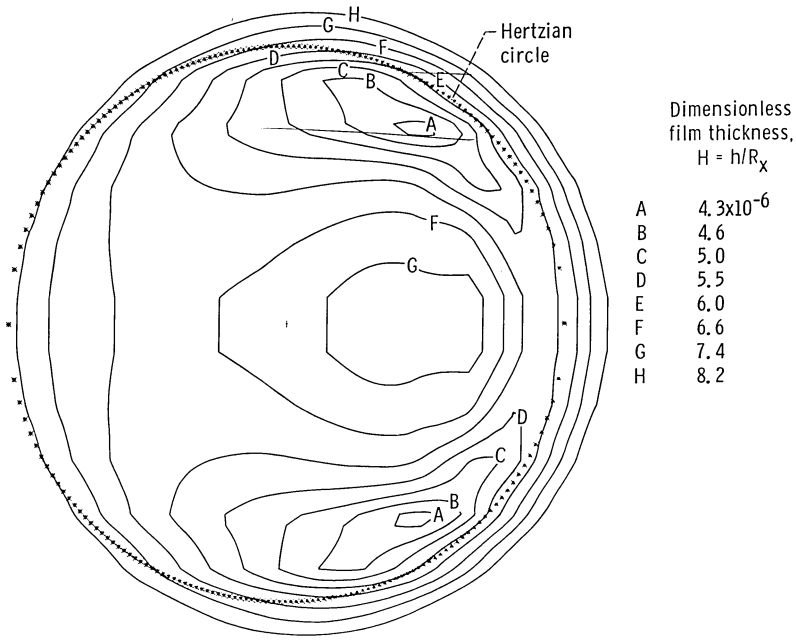

Figure 3.3-2.—Contour plot of dimensionless film thickness. $k = 1.25$; $U = 0.168 \times 10^{11}$; $W = 0.111 \times 10^{-6}$; $G = 4522$. (From Hamrock and Dowson, 1977.)

minimum regions occur in well-defined lobes that follow, and are close to, the edge of the Hertzian contact circle. These results contain all of the essential features of available experimental observations based on optical interferometry (Cameron and Gohar, 1966).

3.4 Soft-EHL Results

In a similar manner, Hamrock and Dowson (1978) investigated the behavior of soft EHL contacts. The ellipticity parameter was varied from 1 (a circular configuration) to 12 (a configuration approaching a rectangular contact), while U and W were varied by one order of magnitude and there were two different dimensionless materials parameters. Seventeen cases were considered in obtaining the dimensionless minimum-film-thickness equation for soft EHL

$$\boxed{H_{\min} = 7.43\, U^{0.65} W^{-0.21} (1 - 0.85\, e^{-0.31k})} \qquad (3.4\text{-}1)$$

The powers of U in equations (3.3-1) and (3.4-1) are quite similar, but the power of W is much more significant for soft-EHL results. The expression showing the effect of the ellipticity parameter is of exponential form in both equations, but with quite different constants.

A major difference between equations (3.3-1) and (3.4-1) is the absence of the materials parameter in the expression for soft EHL. There are two reasons for this: the negligible effect of the relatively low pressures on the viscosity of the lubricating fluid, and the way in which the role of elasticity is automatically incorporated into the prediction of conjunction behavior through the parameters U and W. Apparently the chief effect of elasticity is to allow the Hertzian contact zone to grow in response to increases in load.

3.5 Film Thickness for Different Regimes of Fluid-Film Lubrication

The types of lubrication that exist within nonconformal contacts like that shown in figure 3.1-1 are influenced by two major physical effects: the elastic deformation of the solids under an applied load, and the increase in fluid viscosity with pressure. Therefore it is possible to recognize four regimes of fluid-film lubrication, depending on the magnitude of these effects and on their relative importance. In this section because of the need to represent the four fluid-film lubrication regimes graphically, the dimensionless grouping presented in Section 3.2 will need to be recast. That is, the set of dimensionless parameters given in Section 3.2 {H, U, W, G, and k} will be reduced by one parameter without any loss of generality. The dimensionless groupings to be used here thus are

Dimensionless film parameter

$$\hat{H} = H\left(\frac{W}{U}\right)^2 \qquad (3.5\text{-}1)$$

Dimensionless viscosity parameter

$$g_v = \frac{GW^3}{U^2} \qquad (3.5\text{-}2)$$

Dimensionless elasticity parameter

$$g_e = \frac{W^{8/3}}{U^2} \tag{3.5-3}$$

The ellipticity parameter remains as discussed in Section 3.1, equation (3.1-7). Therefore the reduced dimensionless group is $\{\hat{H}, g_v, g_e, k\}$.

3.5.1 Isoviscous-rigid regime

In this regime the magnitude of the elastic deformation of the surfaces is such an insignificant part of the thickness of the fluid film separating them that it can be neglected, and the maximum pressure in the contact is too low to increase fluid viscosity significantly. This form of lubrication is typically encountered in circular-arc thrust bearing pads; in industrial processes in which paint, emulsion, or protective coatings are applied to sheet or film materials passing between rollers; and in very lightly loaded rolling bearings.

The influence of conjunction geometry on the isothermal hydrodynamic film separating two rigid solids was investigated by Brewe et al. (1979). The effect of geometry on the film thickness was determined by varying the radius ratio R_y/R_x from 1 (a circular configuration) to 36 (a configuration approaching a rectangular contact). The film thickness was varied over two orders of magnitude for conditions representative of steel solids separated by a paraffinic mineral oil. It was found that the computed minimum film thickness had the same speed, viscosity, and load dependence as the classical Kapitza (1955) solution so that the new dimensionless film thickness $\hat{H}$ depends only on k. However, when the Reynolds cavitation condition ($\partial p/\partial n = 0$ and $p = 0$) was introduced at the cavitation boundary, where n represents the coordinate normal to the interface between the full film and the cavitation region, this geometrical dependence could be determined. Thus, according to Brewe et al. (1979), the dimensionless minimum-film-thickness parameter for the isoviscous-rigid regime can be written as

$$(\hat{H}_{\min})_{ir} = 128\alpha\lambda_b^2\left[0.131\tan^{-1}\left(\frac{\alpha}{2}\right) + 1.683\right]^2 \tag{3.5-4}$$

where

$$\alpha = \frac{R_y}{R_x} \approx (k)^{\pi/2} \tag{3.5-5}$$

and

$$\lambda_b = \left(1 + \frac{2}{3\alpha}\right)^{-1} \tag{3.5-6}$$

Equation (3.5-4) shows explicitly that the dimensionless minimum-film-thickness parameter $\hat{H}$ is indeed strictly a function only of the geometry of the contact described by k or equivalently by the ratio $\alpha = R_y/R_x$.

3.5.2 Piezoviscous-rigid regime

If the pressure within the contact is sufficiently high to increase the fluid viscosity within the conjunction significantly, it may be necessary to consider the pressure-viscosity characteristics of the lubricant while assuming that the solids remain rigid. For the latter part of this assumption to be valid, the deformation of the surfaces must remain an insignificant part of the fluid-film thickness. This form of lubrication may be encountered on roller end-guide flanges, in contacts in moderately loaded cylindrical tapered rollers, and between some piston rings and cylinder liners.

From Hamrock and Dowson (1981) the minimum film thickness parameter for the piezoviscous-rigid regime can be written as

$$(\hat{H}_{\min})_{pvr} = 1.66\, g_v^{2/3}\,(1 - e^{-0.68k}) \tag{3.5-7}$$

Note the absence of the dimensionless elasticity parameter g_e from equation (3.5-7).

3.5.3 Isoviscous-elastic (soft EHL) regime

In this regime the elastic deformation of the solids is a significant part of the thickness of the fluid film separating them, but the pressure within the contact is quite low and insufficient to cause any substantial increase in viscosity. This situation arises with materials of low elastic modulus (such as rubber), and it is a form of lubrication that may be encountered in seals, human joints, tires, and elastomeric material machine elements.

If the film thickness equation for soft EHL (eq. (3.4-1)) is rewritten in terms of the reduced dimensionless grouping, the minimum-film-thickness parameter for the isoviscous-elastic regime can be rewritten approximately as

$$(\hat{H}_{\min})_{ie} = 8.70\, g_e^{0.67}\,(1 - 0.85\, e^{-0.31k}) \tag{3.5-8}$$

Note the absence of the dimensionless viscosity parameter g_e from equation (3.5-8).

3.5.4 Piezoviscous-elastic (hard EHL) regime

In fully developed elastohydrodynamic lubrication the elastic deformation of the solids is often a significant part of the thickness of the fluid film separating them, and the pressure within the contact is high enough to cause a significant increase in the viscosity of the lubricant. This form of lubrication is typically encountered in ball and roller bearings, gears, and cams.

Once the film thickness equation (eq. (3.3-1)) has been rewritten in terms of the reduced dimensionless grouping, the minimum film parameter for the piezoviscous-elastic regime can be written as

$$(\hat{H}_{\min})_{pve} = 3.42\, g_v^{0.49} g_e^{0.17} (1 - e^{-0.68k}) \qquad (3.5\text{-}9)$$

An interesting observation to make in comparing equations (3.5-7) to (3.5-9) is that in each case the sum of the exponents on g_v and g_e is close to the value of 2/3 required for complete dimensional representation of these three lubrication regimes: piezoviscous rigid, isoviscous elastic, and piezoviscous elastic.

3.5.5 Contour plots

Having expressed the dimensionless minimum-film-thickness parameter for the four fluid-film regimes in equations (3.5-4) to (3.5-9), Hamrock and Dowson (1979) used these relationships to develop a map of the lubrication regimes in the form of dimensionless minimum-film-thickness parameter contours. Some of these maps are shown in figures 3.5-1 to 3.5-3 on a log-log grid of the dimensionless viscosity and elasticity parameters for ellipticity parameters of 1, 3, and 6, respectively. The procedure used to obtain these figures can be found in Hamrock and Dowson (1979). The four lubrication regimes are clearly shown in figures 3.5-1 to 3.5-3. By using these figures for given values of the parameters k, g_v, and g_e, the fluid-film lubrication regime in which any elliptical conjunction is operating can be ascertained and the approximate value of $\hat{H}_{\min}$ determined. When the lubrication regime is known, a more accurate value of $\hat{H}_{\min}$ can be obtained by using the appropriate dimensionless minimum-film-thickness equation. These results are particularly useful in initial investigations of many practical lubrication problems involving elliptical conjunctions.

3.6 Rolling-Element Bearings

Rolling-element bearings are precision, yet simple, machine elements of great utility whose mode of lubrication is elastohydrodynamic. This section describes the types of rolling-element bearings and their geometry, kinematics, load distribution, and fatigue life and demonstrates how elastohydrodynamic lubrication theory can be applied to the operation of rolling-element

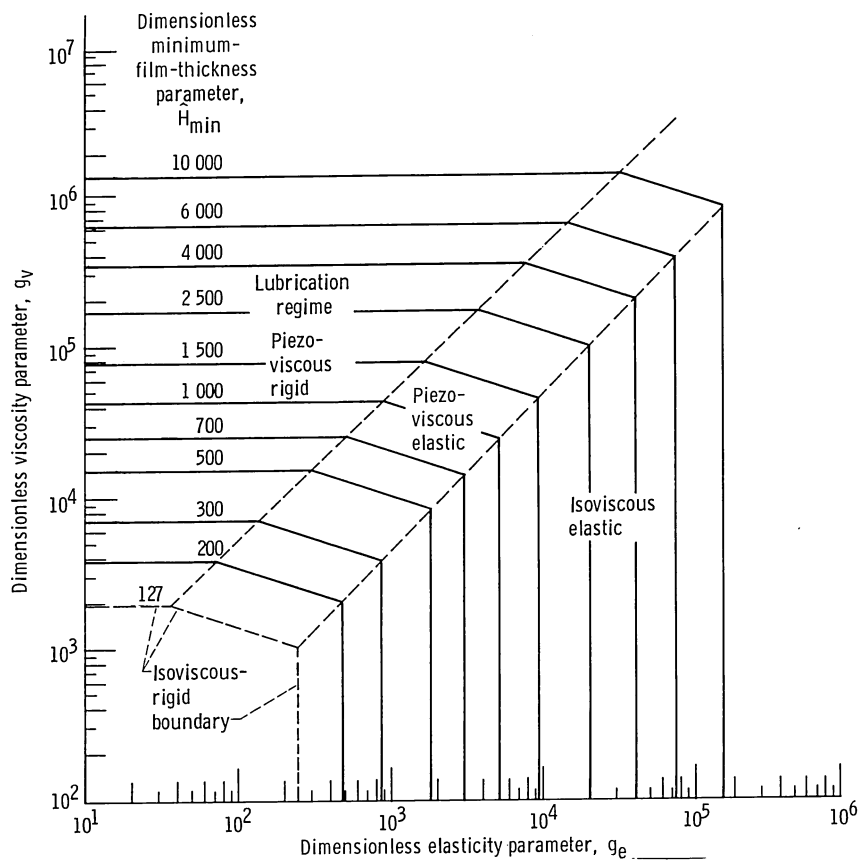

Figure 3.5-1.—Map of lubrication regimes for ellipticity parameter k of 1. (From Hamrock and Dowson, 1979.)

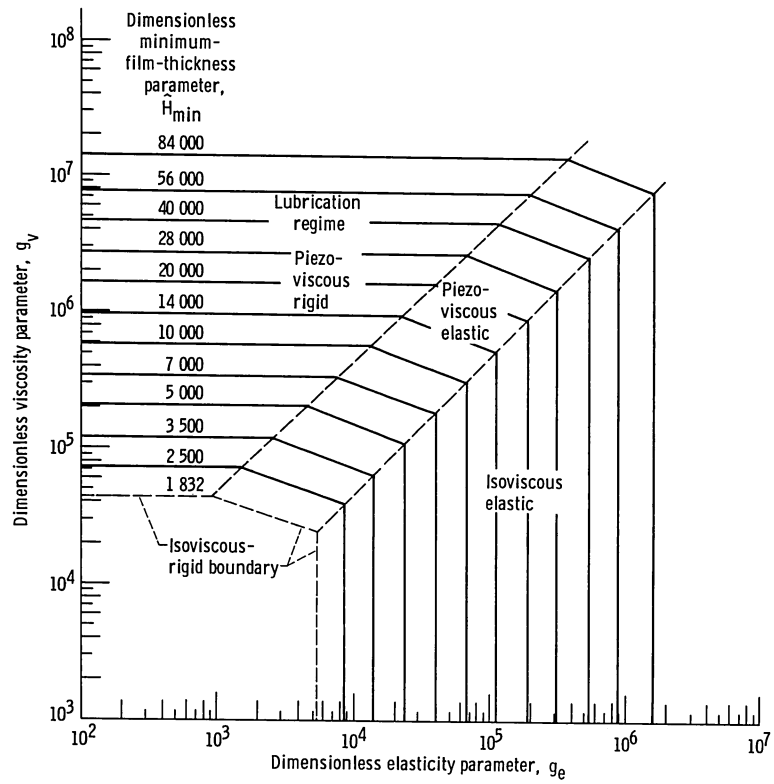

Figure 3.5-2.—Map of lubrication regimes for ellipticity parameter k of 3. (From Hamrock and Dowson, 1979.)

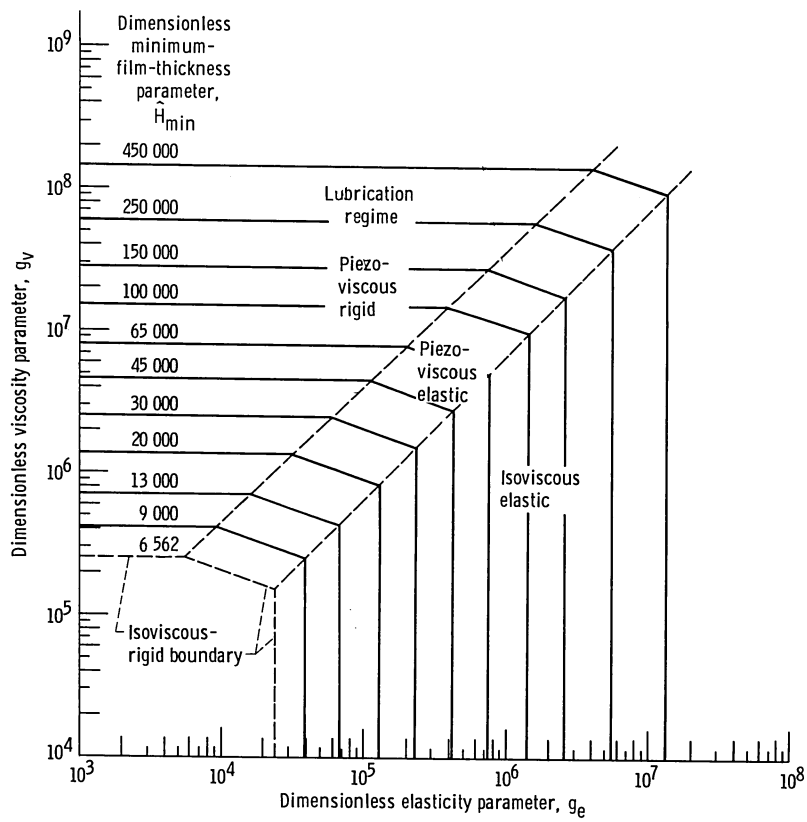

Figure 3.5-3.—Map of lubrication regimes for ellipticity parameter k of 6. (From Hamrock and Dowson, 1979.)

bearings. This section makes extensive use of Hamrock and Dowson (1981) and Hamrock and Anderson (1983).

3.6.1 Bearing types

A great variety both of design and size range of ball and roller bearings is available to the designer. The intent of this section is not to duplicate the complete descriptions given in manufacturers' catalogs, but rather to present a guide to representative bearing types along with the approximate range of sizes available. Tables 3.6-7 to 3.6-9 illustrate some of the more widely used bearing types. In addition, there are available numerous types of specialty bearings for which space does not permit a complete cataloging. Size ranges are given in metric units. Traditionally, most rolling-element bearings have been manufactured to metric dimensions, predating the efforts toward a metric standard. In addition to bearing types and approximate size ranges available, tables 3.6-1 to 3.6-9 also list approximate relative load-carrying capabilities, both radial and thrust, and where relevant, approximate tolerances to misalignment.

Rolling bearings are an assembly of several parts—an inner race, an outer race, a set of balls or rollers, and a cage or separator. The cage or separator maintains even spacing of the rolling elements. A cageless bearing, in which the annulus is packed with the maximum rolling-element complement, is called a full-complement bearing. Full-complement bearings have high load capacity but lower speed limits than bearings equipped with cages. Tapered-roller bearings are an assembly of a cup, a cone, a set of tapered rollers, and a cage.

TABLE 3.6-1. - CHARACTERISTICS OF REPRESENTATIVE RADIAL BALL BEARINGS

[From Hamrock and Anderson (1983).]

Type	Approximate range of bore sizes, mm		Relative capacity		Limiting speed factor	Tolerance to misalignment
	Minimum	Maximum	Radial	Thrust		
Conrad or deep groove 	3	1060	1.00	[a]0.7	1.0	±0°15'
Maximum capacity or filling notch 	10	130	1.2-1.4	[a]0.2	1.0	±0°3'
Magneto or counterbored outer 	3	200	0.9-1.3	[b]0.5-0.9	1.0	±0°5'
Airframe or aircraft control 	4.826	31.75	High static capacity	[a]0.5	0.2	0°
Self-aligning, internal 	5	120	0.7	[b]0.2	1.0	±2°30'
Self-aligning, external 	------	------	1.0	[a]0.7	1.0	High
Double row, maximum 	6	110	1.5	[a]0.2	1.0	±0°3'
Double row, deep groove 	6	110	1.5	[a]1.4	1.0	0°

[a]Two directions.
[b]One direction.

Ball bearings

Ball bearings are used in greater quantity than any other type of rolling bearing. For an application where the load is primarily radial with some thrust load present, one of the types in table 3.6–1 can be chosen. A Conrad, or deep-groove, bearing has a ball complement limited by the number of balls that can be packed into the annulus between the inner and outer races with the inner race resting against the inside diameter of the outer race. A stamped and riveted two-piece cage, piloted on the ball set, or a machined two-piece cage, ball piloted or race piloted, is almost always used in a Conrad bearing. The only exception is a one-piece cage with open-sided pockets that is snapped into place. A filling-notch bearing has both inner and outer races notched so that a ball complement limited only by the annular space between the races can be used. It has low thrust capacity because of the filling notch.

The self-aligning internal bearing shown in table 3.6–1 has an outer-race ball path ground in a spherical shape so that it can accept high levels of misalignment. The self-aligning external bearing has a multipiece outer race with a spherical interface. It too can accept high misalignment and has higher capacity than the self-aligning internal bearing. However, the external self-aligning bearing is somewhat less self-aligning than its internal counterpart because of friction in the multipiece outer race.

Representative angular-contact ball bearings are illustrated in table 3.6–2. An angular-contact ball bearing has a two-shouldered ball groove in one race and a single-shouldered ball groove in the other race. Thus it can

TABLE 3.6-2. - CHARACTERISTICS OF REPRESENTATIVE ANGULAR-CONTACT BALL BEARINGS

[From Hamrock and Anderson (1983).]

Type	Approximate range of bore sizes, mm		Relative capacity		Limiting speed factor	Tolerance to misalignment
	Minimum	Maximum	Radial	Thrust		
One-directional thrust 	10	320	[b]1.00-1.15	[a,b]1.5-2.3	[b]1.1-3.0	±0°2'
Duplex, back to back 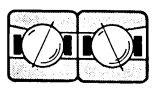	10	320	1.85	[c]1.5	3.0	0°
Duplex, face to face 	10	320	1.85	[c]1.5	3.0	0°
Duplex, tandem 	10	320	1.85	[a]2.4	3.0	0°
Two directional or split ring 	10	110	1.15	[c]1.5	3.0	±0°2'
Double row 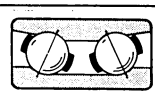	10	140	1.5	[c]1.85	0.8	0°
Double row, maximum 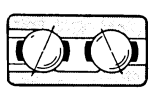	10	110	1.65	[a]0.5 [d]1.5	0.7	0°

[a]One direction.
[b]Depends on contact angle.
[c]Two directions.
[d]In other direction.

support only a unidirectional thrust load. The cutaway shoulder allows assembly of the bearing by snapping over the ball set after it is positioned in the cage and outer race. This also permits use of a one-piece, machined, race-piloted cage that can be balanced for high-speed operation. Typical contact angles vary from 15° to 25°.

Angular-contact ball bearings are used in duplex pairs mounted either back to back or face to face as shown in table 3.6-2. Duplex bearing pairs are manufactured so that they "preload" each other when clamped together in the housing and on the shaft. The use of preloading provides stiffer shaft support and helps prevent bearing skidding at light loads. Proper levels of preload can be obtained from the manufacturer. A duplex pair can support bidirectional thrust load. The back-to-back arrangement offers more resistance to moment or overturning loads than does the face-to-face arrangement.

Where thrust loads exceed the capability of a simple bearing, two bearings can be used in tandem, with each bearing supporting part of the thrust load. Three or more bearings are occasionally used in tandem, but this is discouraged because of the difficulty in achieving good load sharing. Even slight differences in operating temperature will cause a maldistribution of load sharing.

The split-ring bearing shown in table 3.6-2 offers several advantages. The split ring (usually the inner) has its ball groove ground as a circular arc with a shim between the ring halves. The shim is then removed when the bearing is assembled so that the split-ring ball groove has the shape of a gothic arch. This reduces the axial play for a given radial play and results in more accurate axial positioning of the shaft. The bearing can support bidirectional thrust loads but must not be operated for prolonged periods of time at predominantly radial loads. This results in three-point ball-race contact and relatively high frictional losses. As with the conventional angular-contact bearing, a one-piece precision-machined cage is used.

Thrust ball bearings (90° contact angle), table 3.6-3, are used almost exclusively for machinery with vertically oriented shafts. The flat-race bearing allows eccentricity of the fixed and rotating members. An additional bearing must be used for radial positioning. It has low load capacity because of the very small ball-race contacts and consequent high Hertzian stress. Grooved-race bearings have higher load capacities and are capable of supporting low-magnitude radial loads. All of the pure thrust ball bearings have modest speed capability because of the 90° contact angle and the consequent high level of ball spinning and frictional losses.

Roller bearings

Cylindrical roller bearings, table 3.6-4, provide purely radial load support in most applications. An N or U type of bearing will allow free axial movement of the shaft relative to the housing to accommodate differences in thermal expansion. An F or J type of bearing will support a light thrust load in one direction; and a T type of bearing, a light bidirectional thrust load.

Cylindrical roller bearings have moderately high radial load capacity as well as high speed capability. Their speed capability exceeds that of either spherical or tapered-roller bearings. A commonly used bearing combination for support of a high-speed rotor is an angular-contact ball bearing or duplex pair and a cylindrical roller bearing.

TABLE 3.6-3. - CHARACTERISTICS OF REPRESENTATIVE THRUST BALL BEARINGS

[From Hamrock and Anderson (1983).]

Type	Approximate range of bore sizes, mm		Relative capacity		Limiting speed factor	Tolerance to misalignment
	Minimum	Maximum	Radial	Thrust		
One directional, flat race 	6.45	88.9	0	[a]0.7	0.10	[b]0°
One directional, grooved race 	6.45	1180	0	[a]1.5	0.30	0°
Two directional, grooved race 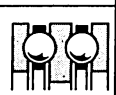	15	220	0	[c]1.5	0.30	0°

[a]One direction.
[b]Accepts eccentricity.
[c]Two directions.

TABLE 3.6-4. - CHARACTERISTICS OF REPRESENTATIVE CYLINDRICAL ROLLER BEARINGS

[From Hamrock and Anderson (1983).]

Type	Approximate range of bore sizes, mm		Relative capacity		Limiting speed factor	Tolerance to misalignment
	Minimum	Maximum	Radial	Thrust		
Separable outer ring, nonlocating (RN, RIN) 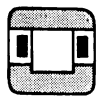	10	320	1.55	0	1.20	±0°5'
Separable inner ring, nonlocating (RU, RIU) 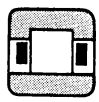	12	500	1.55	0	1.20	±0°5'
Separable outer ring, one-direction locating (RF, RIF) 	40	177.8	1.55	[a]Locating	1.15	±0°5'
Separable inner ring, one-direction locating (RJ, RIJ) 	12	320	1.55	[a]Locating	1.15	±0°5'
Self-contained, two-direction locating 	12	100	1.35	[b]Locating	1.15	±0°5'
Separable inner ring, two-direction locating (RT, RIT) 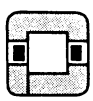	20	320	1.55	[b]Locating	1.15	±0°5'
Nonlocating, full complement (RK, RIK) 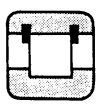	17	75	2.10	0	0.20	±0°5'
Double row, separable outer ring, nonlocating (RD) 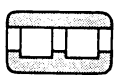	30	1060	1.85	0	1.00	0°
Double row, separable inner ring, nonlocating 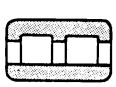	70	1060	1.85	0	1.00	0°

[a]One direction.
[b]Two directions.

As explained in the following section on bearing geometry, the rollers in cylindrical roller bearings are seldom pure cylinders. They are crowned, or made slightly barrel shaped, to relieve stress concentrations of the roller ends when any misalignment of the shaft and housing is present.

Cylindrical roller bearings may be equipped with one- or two-piece cages, usually race piloted. For greater load capacity, full-complement bearings can be used, but at a significant sacrifice in speed capability.

Spherical roller bearings, tables 3.6-5 to 3.6-7, are made as either single- or double-row bearings. The more popular bearing design uses barrel-shaped rollers. An alternative design employs hourglass-shaped rollers. Spherical roller bearings combine very high radial load capacity with modest thrust load capacity (with the exception of the thrust type) and excellent tolerance to misalignment. They find widespread use in heavy-duty rolling mill and industrial gear drives, where all of these bearing characteristics are requisite.

Tapered-roller bearings, table 3.6-8, are also made as single- or double-row bearings with combinations of one- or two-piece cups and cones. A four-row bearing assembly with two- or three-piece cups and cones is also available. Bearings are made with either a standard angle for applications in which moderate thrust loads are present or with a steep angle for high thrust capacity. Standard and special cages are available to suit the application requirements.

Single-row tapered-roller bearings must be used in pairs because a radially loaded bearing generates a thrust reaction that must be taken by a second bearing. Tapered-roller bearings are normally set up with spacers designed so that they operate with some internal play. Manufacturers' engineering manuals should be consulted for proper setup procedures.

Needle roller bearings, table 3.6-9, are characterized by compactness in the radial direction and are frequently used without an inner race. In the latter case the shaft is hardened and ground to serve as the inner race. Drawn cups, both open and closed end, are frequently used for grease retention. Drawn cups are thin walled and require substantial support from the housing. Heavy-duty roller bearings have relatively rigid races and are more akin to cylindrical roller bearings with large-length-to-diameter-ratio rollers.

Needle roller bearings are more speed limited than cylindrical roller bearings because of roller skewing at high speeds. A high percentage of needle roller bearings are full-complement bearings. Relative to a caged needle bearing, these have higher load capacity but lower speed capability.

There are many types of specialty bearings available other than those discussed here. Aircraft bearings for

TABLE 3.6-5. - CHARACTERISTICS OF REPRESENTATIVE SPHERICAL ROLLER BEARINGS

[From Hamrock and Anderson (1983).]

Type	Approximate range of bore sizes, mm		Relative capacity		Limiting speed factor	Tolerance to misalignment
	Minimum	Maximum	Radial	Thrust		
Single row, barrel or convex 	20	320	2.10	0.20	0.50	±2°
Double row, barrel or convex 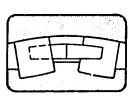	25	1250	2.40	0.70	0.50	±1°30'
Thrust 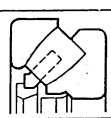	85	360	[a]0.10 [b]0.10	[a]1.80 [b]2.40	0.35-0.50	±3°
Double row, concave 	50	130	2.40	0.70	0.50	±1°30'

[a]Symmetric rollers.
[b]Asymmetric rollers.

control systems, thin-section bearings, and fractured-ring bearings are some of the more widely used bearings among the many types manufactured. A complete coverage of all bearing types is beyond the scope of this section.

Angular-contact ball bearings and cylindrical roller bearings are generally considered to have the highest speed capabilities. Speed limits of roller bearings are discussed in conjunction with lubrication methods. The lubrication system employed has as great an influence on limiting bearing speed as does the bearing design.

3.6.2 Geometry

The operating characteristics of a rolling-element bearing depend greatly on the diametral clearance of the bearing. This clearance varies for the different types of bearings discussed in the preceding section. In this section the principal geometrical relationships governing the operation of unloaded rolling-element bearings are developed. This information will be of vital interest when such quantities as stress, deflection, load capacity, and life are considered in subsequent sections. Although

TABLE 3.6-6. - CHARACTERISTICS OF STANDARDIZED DOUBLE-ROW, SPHERICAL ROLLER BEARINGS

[From Hamrock and Anderson (1983).]

Type	Roller design	Retainer design	Roller guidance	Roller-race contact
SLB 	Symmetric	Machined, roller piloted	Retainer pockets	Modified line, both races
SC 	Symmetric	Stamped, race piloted	Floating guide ring	Modified line, both races
SD 	Asymmetric	Machined, race piloted	Inner-ring center rib	Line contact, outer; point contact, inner

TABLE 3.6-7. - CHARACTERISTICS OF SPHERICAL ROLLER BEARINGS

[From Hamrock and Anderson (1983).]

Series	Types	Approximate range of bore sizes, mm		Approximate relative capacity[a]		Limiting speed factor
		Minimum	Maximum	Radial	Thrust	
202	Single-row barrel	20	320	1.0	0.11	0.5
203	Single-row barrel	20	240	1.7	.18	.5
204	Single-row barrel	25	110	2.1	.22	.4
212	SLB	35	75	1.0	.26	.6
213	SLB	30	70	1.7	.53	↓
22, 22K	SLB, SC, SD	30	320	1.7	.46	
23, 23K	SLB, SC, SD	40	280	2.7	1.0	
30, 30K	SLB, SC, SD	120	1250	1.2	.29	.7
31, 31K	SLB, SC, SD	110	1250	1.7	.54	.6
32, 32K	SLB, SC, SD	100	850	2.1	.78	.6
39, 39K	SD	120	1250	.7	.18	.7
40, 40K	SD	180	250	1.5	----	.7

[a]Load capacities are comparative within the various series of spherical roller bearings only. For a given envelope size, a spherical roller bearing has a radial capacity approximately equal to that of a cylindrical roller bearing.

bearings rarely operate in the unloaded state, an understanding of this section is vital to the appreciation of the remaining sections.

Geometry of ball bearings

Pitch diameter and clearance.—The cross section through a radial, single-row ball bearing, shown in figure 3.6-1, depicts the radial clearance and various diameters. The pitch diameter d_e is the mean of the inner- and outer-race contact diameters and is given by

$$d_e = d_i + \frac{1}{2}(d_o - d_i)$$

or

$$d_e = \frac{1}{2}(d_o + d_i) \tag{3.6-1}$$

Also from figure 3.6-1 the diametral clearance denoted by P_d can be written as

$$P_d = d_o - d_i - 2d \tag{3.6-2}$$

Diametral clearance may therefore be thought of as the maximum distance that one race can move diametrally with respect to the other when no measurable force is applied and both races lie in the same plane. Although diametral clearance is generally used in connection with single-row radial bearings, equation (3.6-2) is also applicable to angular-contact bearings.

TABLE 3.6-8. - CHARACTERISTICS OF REPRESENTATIVE TAPERED ROLLER BEARINGS

[From Hamrock and Anderson (1983).]

Type	Subtype	Approximate range of bore sizes, mm	
		Minimum	Maximum
Single row (TS) 			
	TST - Tapered bore	8	1690
	TSS - Steep angle	24	430
	TS - Pin cage	16	1270
	TSE, TSK - keyway cones		----
	TSF, TSSF - flanged cup	12	380
	TSG - steering gear (without cone)	8	1070

Two row, double cone, single cups (TDI) 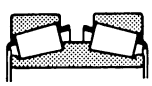			
	TDIK, TDIT, TDITP - tapered bore	30	1200
	TDIE, TDIKE - slotted double cone	30	860
	TDIS - steep angle	24	690
		55	520
Two row, double cup, single cones, adjustable (TDO) 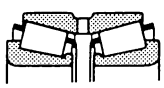	TDO	8	1830
	TDOS - steep angle	20	1430
Two row, double cup, single cones, nonadjustable (TNA) 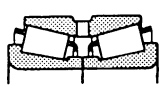			
	TNA	20	60
	TNASW - slotted cones	30	260
	TNASWE - extended cone rib	20	305
	TNASWH - slotted cones, sealed	8	70
	TNADA, TNHDADX - self-aligning cup AD	---	----
Four row, cup adjusted (TQO) 	TQO, TQOT - tapered bore	70	1500
		250	1500
Four row, cup adjusted (TQI) 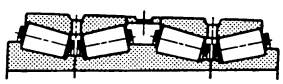	TQIT - tapered bore	---	----

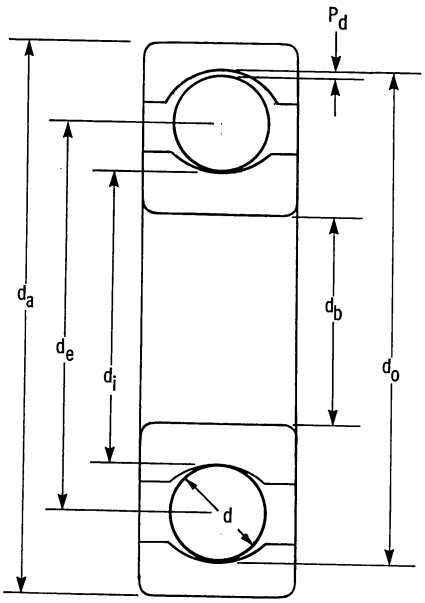

Figure 3.6-1.—Cross section through radial, single-row ball bearing. (From Hamrock and Dowson, 1981.)

Race conformity.—Race conformity is a measure of the geometrical conformity of the race and the ball in a plane passing through the bearing axis, which is a line passing through the center of the bearing perpendicular to its plane and transverse to the race. Figure 3.6-2 is a cross section of a ball bearing showing race conformity, expressed as

$$f = \frac{r}{d} \tag{3.6-3}$$

For perfect conformity, where the radius of the race is equal to the ball radius, f is equal to 1/2. The closer the race conforms to the ball, the greater the frictional heat within the contact. On the other hand, open-race curvature and reduced geometrical conformity, which reduce friction, also increase the maximum contact stresses and consequently reduce the bearing fatigue life. For this reason, most ball bearings made today haye race conformity ratios in the range $0.51 \leq f \leq 0.54$, with $f = 0.52$ being the most common value. The race conformity ratio

TABLE 3.6-9. - CHARACTERISTICS OF REPRESENTATIVE NEEDLE ROLLER BEARINGS

[From Hamrock and Anderson (1983).]

Type	Bore sizes, mm		Relative load capacity		Limiting speed factor	Misalignment tolerance
	Minimum	Maximum	Dynamic	Static		
Drawn cup, needle (Open end / Closed end)	3	185	High	Moderate	0.3	Low
Drawn cup, needle, grease retained	4	25	High	Moderate	0.3	Low
Drawn cup, roller (Open end / Closed end)	5	70	Moderate	Moderate	0.9	Moderate
Heavy-duty roller	16	235	Very high	Moderate	1.0	Moderate
Caged roller	12	100	Very high	High	1.0	Moderate
Cam follower	12	150	Moderate to high	Moderate to high	0.3-0.9	Low
Needle thrust	6	105	Very high	Very high	0.7	Low

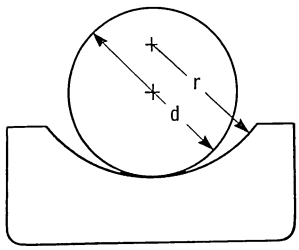

Figure 3.6-2.—Cross section of ball and outer race, showing race conformity. (From Hamrock and Dowson, 1981.)

for the outer race is usually made slightly smaller than that for the inner race to compensate for the larger conformity ratio in the plane of the bearing between the outer race and ball than between the inner race and ball. This tends to equalize the contact stresses at the inner- and outer-race contacts. The difference in race conformities does not normally exceed 0.02.

Contact angle.—Radial bearings have some axial play since they are generally designed to have a diametral clearance, as shown in figure 3.6-3. This implies a free-contact angle different from zero. Angular-contact bearings are specifically designed to operate under thrust loads. The clearance built into the unloaded bearing, along with the race conformity ratio, determines the bearing free-contact angle. Figure 3.6-3 shows a radial bearing with contact due to the axial shift of the inner and outer rings when no measurable force is applied.

Before the free-contact angle is discussed, it is important to define the distance between the centers of curvature of the two races in line with the center of the ball in figures 3.6-3(a) and (b). This distance—denoted by x in figure 3.6-3(a) and by D in figure 3.6-3(b)—depends on race radius and ball diameter. Denoting quantities referred to the inner and outer races by subscripts i and o, respectively, we see from figures 3.6-3(a) and (b) that

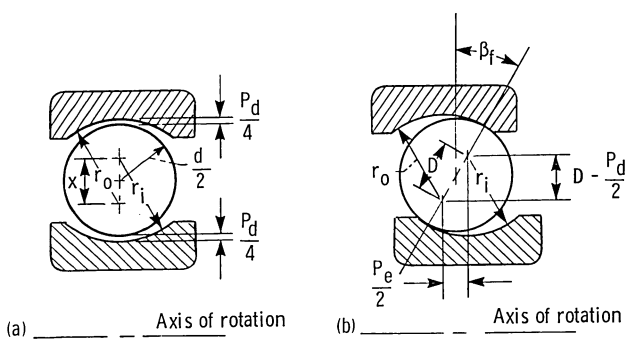

(a) Initial position.
(b) Shifted position.

Figure 3.6-3.—Cross section of radial ball bearing, showing ball-race contact due to axial shift of inner and outer rings. (From Hamrock and Dowson, 1981.)

$$\frac{P_d}{4}+d+\frac{P_d}{4}=r_o-x+r_i$$

or

$$x=r_o+r_i-d-\frac{P_d}{2}$$

and

$$d=r_o-D+r_i$$

or

$$D=r_o+r_i-d \tag{3.6-4}$$

From these equations, we can write

$$x=D-\frac{P_d}{2}$$

This distance, shown in figure 3.6-3, will be useful in defining the contact angle.

By using equation (3.6-3), we can write equation (3.6-4) as

$$D=Bd \tag{3.6-5}$$

where

$$B=f_o+f_i-1 \tag{3.6-6}$$

The quantity B is known as the total conformity ratio and is a measure of the combined conformity of both the outer and inner races to the ball. Calculations of bearing deflection in later sections depend on the quantity B.

The free-contact angle β_f (fig. 3.6-3) is defined as the angle made by a line through the points of contact of the ball and both races with a plane perpendicular to the bearing axis of rotation when no measurable force is applied. Note that the centers of curvature of both the outer and inner races lie on the line defining the free-contact angle. From figure 3.6-3 the expression for the free-contact angle can be written as

$$\cos\beta_f=\frac{D-P_d/2}{D} \tag{3.6-7}$$

By using equations (3.6-2) and (3.6-4), we can write equation (3.6-7) as

$$\beta_f=\cos^{-1}\left[\frac{r_o+r_i-\frac{1}{2}(d_o-d_i)}{r_o+r_i-d}\right] \tag{3.6-8}$$

Equation (3.6-8) shows that if the size of the balls is increased and everything else remains constant, the free-contact angle is decreased. Similarly, if the ball size is decreased, the free-contact angle is increased.

From equation (3.6-7) the diametral clearance P_d can be written as

$$P_d = 2D(1 - \cos \beta_f) \tag{3.6-9}$$

This is an alternative definition of the diametral clearance given in equation (3.6-2).

Endplay.—Free endplay P_e is the maximum axial movement of the inner race with respect to the outer when both races are coaxially centered and no measurable force is applied. Free endplay depends on total curvature and contact angle, as shown in figure 3.6-3, and can be written as

$$P_e = 2D \sin \beta_f \tag{3.6-10}$$

The variation of free-contact angle and free endplay with the ratio $P_d/2d$ is shown in figure 3.6-4 for four values of total conformity normally found in single-row ball bearings. Eliminating β_f in equations (3.6-9) and (3.6-10) enables the establishment of the following relationships between free endplay and diametral clearance:

$$P_d = 2D - \left[(2D)^2 - P_e^2\right]^{1/2}$$

$$P_e = \left(4DP_d - P_d^2\right)^{1/2}$$

Shoulder height.—The shoulder height of ball bearings is illustrated in figure 3.6-5. Shoulder height, or race depth, is the depth of the race groove measured from the shoulder to the bottom of the groove and is denoted by s in figure 3.6-5. From this figure the equation defining the shoulder height can be written as

$$s = r(1 - \cos \theta) \tag{3.6-11}$$

The maximum possible diametral clearance for complete retention of the ball-race contact within the race under zero thrust load is given by

$$(P_d)_{max} = \frac{2Ds}{r}$$

Curvature sum and difference.—A cross section of a ball bearing operating at a contact angle β is shown in figure 3.6-6. Equivalent radii of curvature for both inner- and outer-race contacts in, and normal to, the direction of rolling can be calculated from this figure. The radii of curvature for the ball-inner-race contact are

$$r_{ax} = r_{ay} = \frac{d}{2} \tag{3.6-12}$$

$$r_{bx} = \frac{d_e - d \cos \beta}{2 \cos \beta} \tag{3.6-13}$$

$$r_{by} = -f_i d = -r_i \tag{3.6-14}$$

The radii of curvature for the ball-outer-race contact are

$$r_{ax} = r_{ay} = \frac{d}{2} \tag{3.6-15}$$

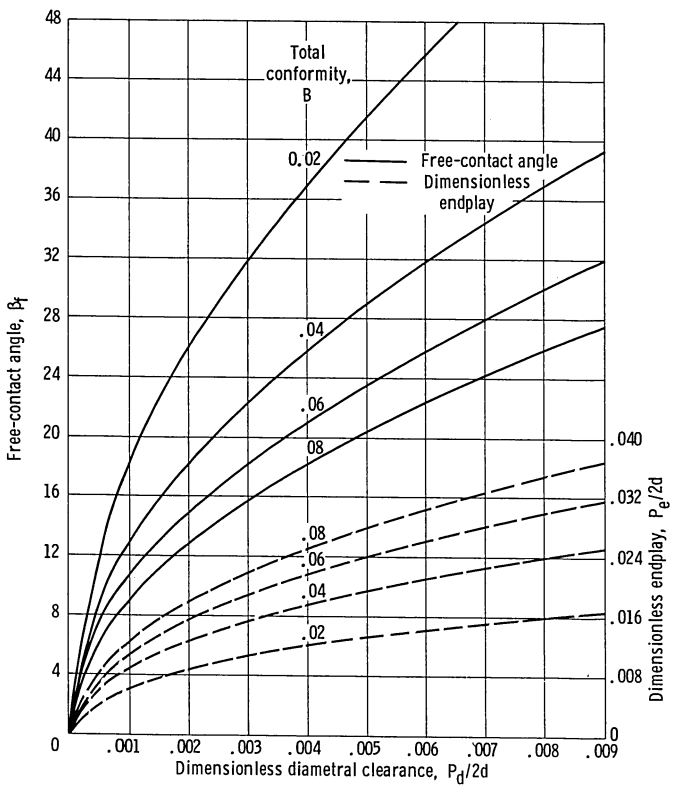

Figure 3.6-4.—Chart for determining free-contact angle and endplay. (From Hamrock and Dowson, 1981.)

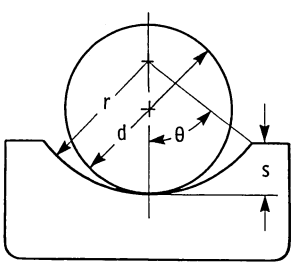

Figure 3.6-5.—Shoulder height in ball bearing. (From Hamrock and Dowson, 1981.)

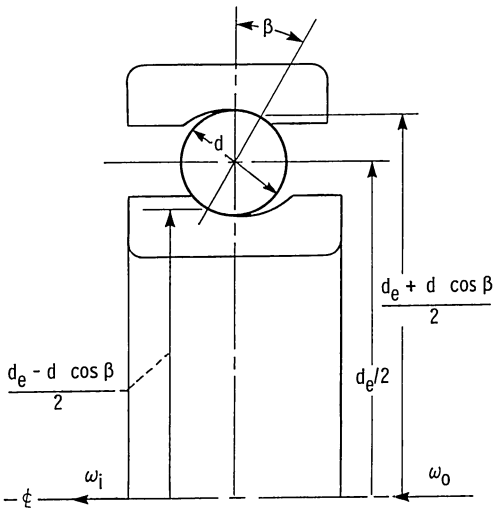

Figure 3.6-6.—Cross section of ball bearing. (From Hamrock and Dowson, 1981.)

$$r_{bx} = -\frac{d_e + d \cos \beta}{2 \cos \beta} \tag{3.6-16}$$

$$r_{by} = -f_o d = -r_o \tag{3.6-17}$$

In equations (3.6-13) and (3.6-16), β is used instead of β_f since these equations are also valid when a load is applied to the contact. By setting $\beta = 0°$ equations (3.6-12) to (3.6-17) are equally valid for radial ball bearings. For thrust ball bearings, $r_{bx} = \infty$ and the other radii are defined as given in the preceding equations.

Equations (3.1-4) and (3.1-5) effectively redefine the problem of two ellipsoidal solids approaching one another in terms of an equivalent ellipsoidal solid of radii R_x and R_y approaching a plane. From the radius-of-curvature expressions the radii R_x and R_y for the contact example discussed earlier can be written for the ball-inner-race contact as

$$R_x = \frac{d(d_e - d \cos \beta)}{2d_e} \tag{3.6-18}$$

$$R_y = \frac{f_i d}{2f_i - 1} \tag{3.6-19}$$

and for the ball-outer-race contact as

$$R_x = \frac{d(d_e + d \cos \beta)}{2d_e} \tag{3.6-20}$$

$$R_y = \frac{f_o d}{2f_o - 1} \tag{3.6-21}$$

Roller bearings

The equations developed for the pitch diameter d_e and diametral clearance P_d for ball bearings in equations (3.6-1) and (3.6-2), respectively, are directly applicable for roller bearings.

Crowning.—To prevent high stresses at the edges of the rollers in cylindrical roller bearings, the rollers are usually crowned as shown in figure 3.6-7. A fully crowned roller is shown in figure 3.6-7(a) and a partially crowned roller, in figure 3.6-7(b). In this figure the crown curvature is greatly exaggerated for clarity. The crowning of rollers also gives the bearing protection against the effects of slight misalignment. For cylindrical rollers $r_{ay}/d \approx 10^2$. In contrast, for spherical rollers in spherical roller bearings, as shown in figure 3.6-8, $r_{ay}/d \approx 4$. In figure 3.6-7 the roller effective length l_r is the length presumed to be in contact with the races under loading. Generally the roller effective length can be written as

$$l_r = l_t - 2r_c$$

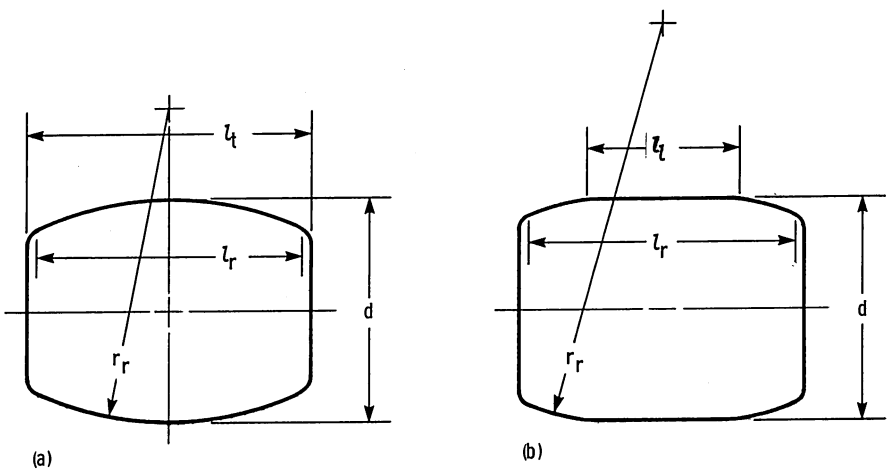

(a) Spherical roller (fully crowned).
(b) Cylindrical roller (partially crowned.

Figure 3.6-7.—Spherical and cylindrical rollers. (From Hamrock and Anderson, 1983.)

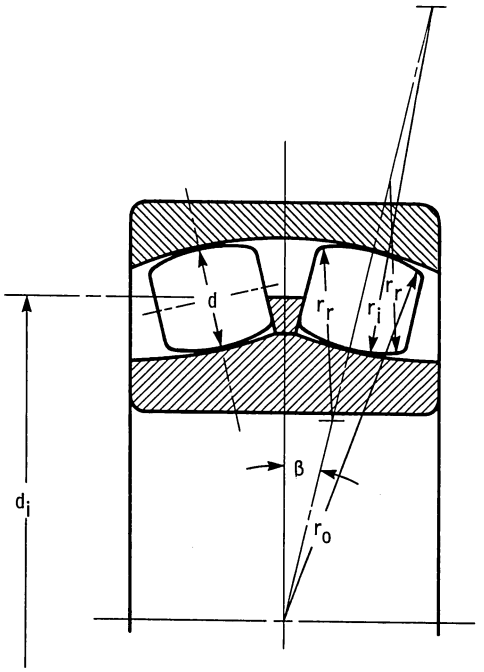

Figure 3.6-8.—Spherical roller bearing geometry. (From Hamrock and Anderson, 1983.)

where r_c is the roller corner radius or the grinding undercut, whichever is larger.

Race conformity.—Race conformity applies to roller bearings much like it applies to ball bearings. It is a measure of the geometrical conformity of the race and the roller. Figure 3.6-8 shows a cross section of a spherical roller bearing. From this figure the race conformity can be written as

$$f = \frac{r}{2r_{ay}}$$

In this equation if subscripts i or o are added to f and r, we obtain the values for the race conformity for the inner- and outer-race contacts.

Free endplay and contact angle.—Cylindrical roller bearings have a contact angle of zero and can take thrust load only by virtue of axial flanges. Tapered-roller bearings must be subjected to a thrust load or the inner and outer rings (the cone and cup) will not remain assembled; therefore tapered-roller bearings do not exhibit free diametral play. Radial spherical roller bearings are, however, normally assembled with free diametral play and hence exhibit free endplay. The diametral play P_d for a spherical roller bearing is the same as that obtained for ball bearings as expressed in equation (3.6-2). This diametral play as well as endplay is shown in figure 3.6-9 for a spherical roller bearing. From this figure we can write that

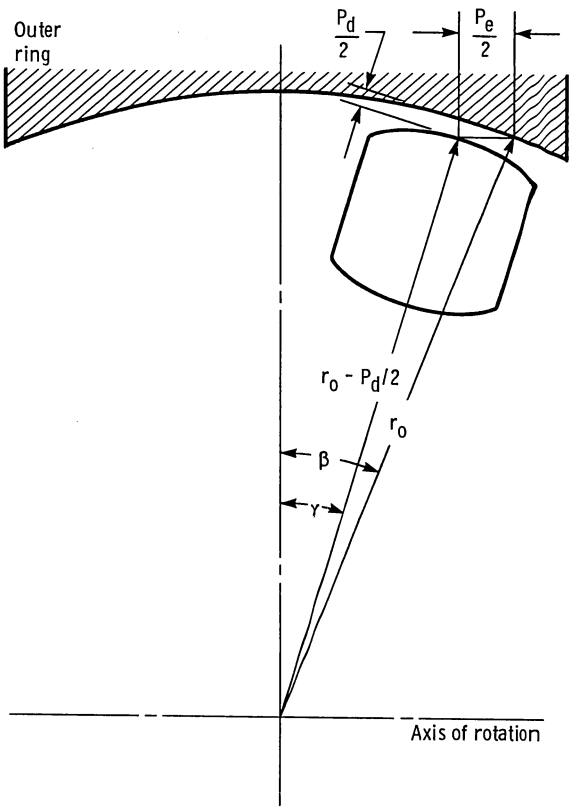

Figure 3.6-9.—Schematic diagram of spherical roller bearing, showing diametral play and endplay. (From Hamrock and Anderson, 1983.)

$$r_o \cos\beta = \left(r_o - \frac{P_d}{2}\right)\cos\gamma$$

or

$$\beta = \cos^{-1}\left[\left(1 - \frac{P_d}{2r_o}\right)\cos\gamma\right]$$

Also from figure 3.6-9 the free endplay can be written as

$$P_e = 2r_o(\sin\beta - \sin\gamma) + P_d \sin\gamma$$

Curvature sum and difference.—The same procedure will be used for defining the curvature sum and difference for roller bearings as was used for ball bearings. For spherical roller bearings, as shown in figure 3.6-8, the radii of curvature for the roller–inner-race contact can be written as

$$r_{ax} = \frac{d}{2}$$

$$r_{ay} = f_i\left(\frac{r_i}{2}\right)$$

$$r_{bx} = \frac{d_e - d\cos\beta}{2\cos\beta}$$

$$r_{by} = -2f_i r_{ay}$$

For the spherical roller bearing shown in figure 3.6-8 the radii of curvature for the roller-outer-race contact can be written as

$$r_{ax} = \frac{d}{2}$$

$$r_{ay} = f_o\left(\frac{r_o}{2}\right)$$

$$r_{bx} = -\frac{d_e + d\cos\beta}{2\cos\beta}$$

$$r_{by} = -2f_o r_{ay}$$

Knowing the radii of curvature for the respective contact condition, we can write the curvature sum and difference directly from equations (3.1-2) and (3.1-3). Furthermore, the radius-of-curvature expressions R_x and R_y for spherical roller bearings can be written for the roller-inner-race contact as

$$R_x = \frac{d(d_e - d\cos\beta)}{2d_e} \tag{3.6-22}$$

$$R_y = \frac{2r_{ay}f_i}{2f_i - 1} \tag{3.6-23}$$

and for the roller-outer-race contact as

$$R_x = \frac{d(d_e + d\cos\beta)}{2d_e} \tag{3.6-24}$$

$$R_y = \frac{2r_{ay}f_o}{2f_o - 1} \tag{3.6-25}$$

3.6.3. Kinematics

The relative motions of the separator, the balls or rollers, and the races of rolling-element bearings are important to understanding their performance. The relative velocities in a ball bearing are somewhat more complex than those in roller bearings, the latter being analogous to the specialized case of a zero- or fixed-value contact-angle ball bearing. For that reason the ball bearing is used as an example here to develop approximate expressions for relative velocities. These are useful for rapid but reasonably accurate calculation of elastohydrodynamic film thickness, which can be used with surface roughnesses to calculate the lubrication life factor.

When a ball bearing operates at high speeds, the centrifugal force acting on the ball creates a difference between the inner- and outer-race contact angles, as shown in figure 3.6-10, in order to maintain force

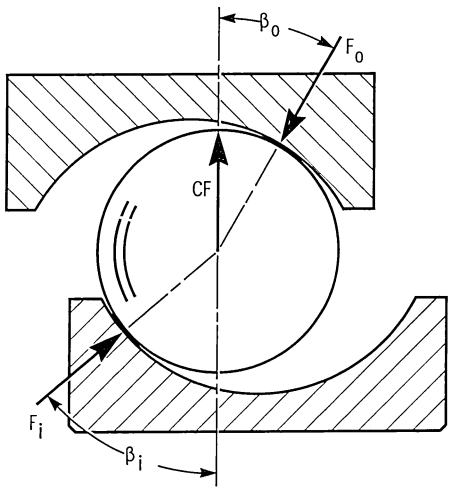

Figure 3.6-10.—Contact angles in a ball bearing at appreciable speeds. (From Hamrock and Anderson, 1983.)

equilibrium on the ball. For the most general case of rolling and spinning at both inner- and outer-race contacts, the rolling and spinning velocities of the ball are as shown in figure 3.6-11.

The equations for ball and separator angular velocity for all combinations of inner- and outer-race rotation were developed by Jones (1964). Without introducing additional relationships to describe the elastohydrodynamic conditions at both ball-race contacts, however, the ball-spin-axis orientation angle φ cannot be obtained. As mentioned, this requires a lengthy numerical solution except for the two extreme cases of outer- or inner-race control. These are illustrated in figure 3.6-12.

Race control assumes that pure rolling occurs at the controlling race, with all of the ball spin occurring at the other race contact. The orientation of the ball rotational axis is then easily determinable from bearing geometry. Race control probably occurs only in dry bearings or dry-

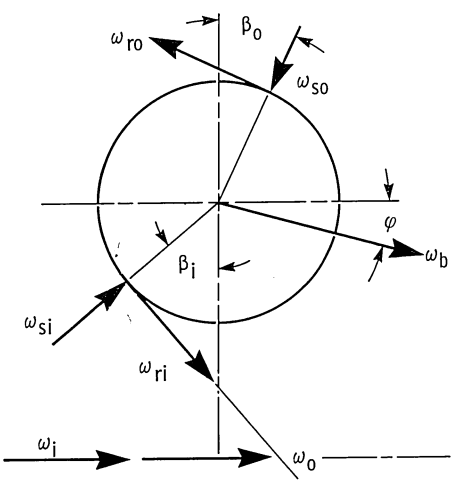

Figure 3.6-11.—Angular velocities of a ball. (From Hamrock and Anderson, 1983.)

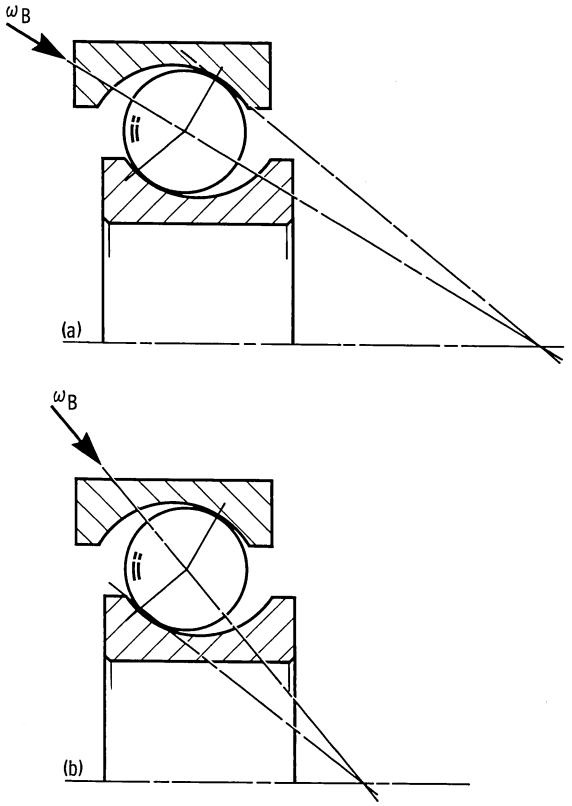

(a) Outer-race control.
(b) Inner-race control.

Figure 3.6-12.—Ball-spin-axis orientations for outer- and inner-race control. (From Hamrock and Anderson, 1983.)

film-lubricated bearings where Coulomb friction conditions exist in the ball-race contact ellipses. Pure rolling will occur at the race contact with the higher magnitude spin-opposing moment. This is usually the inner race at low speeds and the outer race at high speeds.

In oil-lubricated bearings in which elastohydrodynamic films exist in both ball-race contacts, rolling with spin occurs at both contacts. Therefore precise ball motions can only be determined through use of a computer analysis. We can approximate the situation with a reasonable degree of accuracy, however, by assuming that the ball rolling axis is normal to the line drawn through the centers of the two ball-race contacts. This is shown in figure 3.6–6.

The angular velocity of the separator or ball set ω_c about the shaft axis can be shown to be (Anderson, 1970)

$$\omega_c = \frac{(v_i + v_o)/2}{d_e/2}$$

$$= \frac{1}{2}\left[\omega_i\left(1 - \frac{d\cos\beta}{d_e}\right) + \omega_o\left(1 + \frac{d\cos\beta}{d_e}\right)\right] \quad (3.6\text{–}26)$$

where v_i and v_o are the linear velocities of the inner and outer contacts. The angular velocity of a ball about its own axis ω_b is

$$\omega_b = \frac{v_i - v_o}{d_e/2}$$

$$= \frac{d_e}{2d}\left[\omega_i\left(1 - \frac{d\cos\beta}{d_e}\right) - \omega_o\left(1 + \frac{d\cos\beta}{d_e}\right)\right] \quad (3.6\text{–}27)$$

To calculate the velocities of the ball-race contacts, which are required for calculating elastohydrodynamic film thicknesses, it is convenient to use a coordinate system that rotates at ω_c. This fixes the ball-race contacts relative to the observer. In the rotating coordinate system the angular velocities of the inner and outer races become

$$\omega_{ir} = \omega_i - \omega_c = \left(\frac{\omega_i - \omega_o}{2}\right)\left(1 + \frac{d\cos\beta}{d_e}\right)$$

$$\omega_{or} = \omega_o - \omega_c = \left(\frac{\omega_o - \omega_i}{2}\right)\left(1 - \frac{d\cos\beta}{d_e}\right)$$

The surface velocities entering the ball–inner-race contact for pure rolling are

$$u_{ai} = u_{bi} = \left(\frac{d_e - d\cos\beta}{2}\right)\omega_{ir} \quad (3.6\text{–}28)$$

or

$$u_{ai} = u_{bi} = \frac{d_e(\omega_i - \omega_o)}{4}\left(1 - \frac{d^2\cos^2\beta}{d_e^2}\right) \quad (3.6\text{–}29)$$

and those at the ball–outer-race contact are

$$u_{ao} = u_{bo} = \left(\frac{d_e + d\cos\beta}{2}\right)\omega_{or}$$

or

$$u_{ao} = u_{bo} = \frac{d_e(\omega_o - \omega_i)}{4}\left(1 - \frac{d^2\cos^2\beta}{d_e^2}\right) \quad (3.6\text{–}30)$$

For a cylindrical roller bearing $\beta = 0°$ and equations (3.6–25), (3.6–27), (3.6–29), and (3.6–30) become, if d is roller diameter,

$$\omega_c = \frac{1}{2}\left[\omega_i\left(1 - \frac{d}{d_e}\right) + \omega_o\left(1 + \frac{d}{d_e}\right)\right]$$

$$\omega_R = \frac{d_e}{2d}\left[\omega_i\left(1 - \frac{d}{d_e}\right) + \omega_o\left(1 + \frac{d}{d_e}\right)\right]$$

$$u_{ai} = u_{bi} = \frac{d_e(\omega_i - \omega_o)}{4}\left(1 - \frac{d^2}{d_e^2}\right)$$

$$u_{ao} = u_{bo} = \frac{d_e(\omega_o - \omega_i)}{4}\left(1 - \frac{d^2}{d_e^2}\right) \tag{3.6-31}$$

For a tapered-roller bearing equations directly analogous to those for a ball bearing can be used if d is the average diameter of the tapered roller, d_e is the diameter at which the geometric center of the rollers is located, and β is the angle, as shown in figure 3.6-13.

3.6.4 Static load distribution

Having defined a simple analytical expression for the deformation in terms of load in Section 3.1, it is possible to consider how the bearing load is distributed among the rolling elements. Most rolling-element bearing applications involve steady-state rotation of either the inner or outer race or both; however, the speeds of rotation are usually not so great as to cause ball or roller centrifugal forces or gyroscopic moments of significant magnitudes. In analyzing the loading distribution on the rolling elements, it is usually satisfactory to ignore these effects in most applications. In this section the load-deflection relationships for ball and roller bearings are given, along with radial and thrust load distributions of statically loaded rolling elements.

Load-deflection relationships

For an elliptical contact the load-deflection relationship given in equation (3.1-13) can be written as

$$F = K_{1.5}\delta^{3/2} \tag{3.6-32}$$

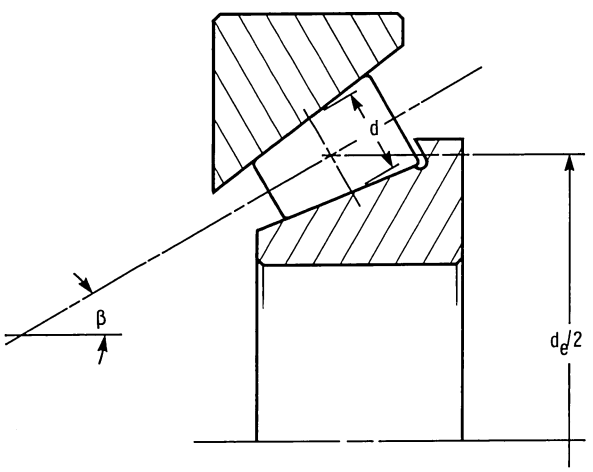

Figure 3.6-13.—Simplified geometry for tapered-roller bearing. (From Hamrock and Anderson, 1983.)

where

$$K_{1.5} = \pi k E' \left(\frac{2\Sigma R}{9\mathfrak{F}3}\right)^{1/2} \tag{3.6-33}$$

Similarly for a rectangular contact, equation (3.1-18) gives

$$F = K_1\delta$$

where

$$K_1 = \left(\frac{\pi l E'}{2}\right)\left[\frac{1}{\frac{2}{3} + \ln\left(\frac{2r_{ax}}{b}\right) + \ln\left(\frac{2r_{bx}}{b}\right)}\right] \tag{3.6-34}$$

In general then,

$$F = K_j\delta^j \tag{3.6-35}$$

in which $j = 1.5$ for ball bearings and 1.0 for roller bearings. The total normal approach between two races separated by a rolling element is the sum of the deformations under load between the rolling element and both races. Therefore

$$\delta = \delta_o + \delta_i \tag{3.6-36}$$

where

$$\delta_o = \left[\frac{F}{(K_j)_o}\right]^{1/j} \tag{3.6-37}$$

$$\delta_i = \left[\frac{F}{(K_j)_i}\right]^{1/j} \tag{3.6-38}$$

Substituting equations (3.6-36) to (3.6-38) into equation (3.6-35) gives

$$K_j = \frac{1}{\left\{\left[\frac{1}{(K_j)_o}\right]^{1/j} + \left[\frac{1}{(K_j)_i}\right]^{1/j}\right\}^j}$$

Recall that $(K_j)_o$ and $(K_j)_i$ are defined by equation (3.6-33) or (3.6-34) for an elliptical or rectangular contact, respectively. From these equations we observe that $(K_j)_o$ and $(K_j)_i$ are functions of only the geometry of the contact and the material properties. The radial and thrust load analyses are presented in the following two sections and are directly applicable for radially loaded ball and roller bearings and thrust-loaded ball bearings.

Radially loaded ball and roller bearings

A radially loaded rolling element with radial clearance P_d is shown in figure 3.6-14. In the concentric position a uniform radial clearance between the rolling element and the races of $P_d/2$ is evident. The application of a small radial load to the shaft causes the inner ring to move a distance $P_d/2$ before contact is made between a rolling element located on the load line and the inner and outer races. At any angle there will still be a radial clearance c that, if P_d is small as compared with the radius of the tracks, can be expressed with adequate accuracy by

$$c=(1-\cos\psi)\frac{P_d}{2}$$

On the load line where $\psi=0$ the clearance is zero; but when $\psi=90°$ the clearance retains its initial value of $P_d/2$.

The application of further load will cause elastic deformation of the balls and the elimination of clearance around an arc $2\psi_c$. If the interference or total elastic compression on the load line is δ_{max}, the corresponding elastic compression of the ball δ_ψ along a radius at angle ψ to the load line will be given by

$$\delta_\psi=(\delta_{max}\cos\psi-c)=\left(\delta_{max}+\frac{P_d}{2}\right)\cos\psi-\frac{P_d}{2}$$

This assumes that the races are rigid. Now, it is clear from figure 3.6-14 that $\delta_{max}+P_d/2$ represents the total relative radial displacement of the inner and outer races. Hence

$$\delta_\psi=\delta\cos\psi-\frac{P_d}{2} \qquad (3.6\text{-}39)$$

The relationship between load and elastic compression along the radius at angle ψ to the load vector is given by equation (3.6-35) as

$$F_\psi=K_j\delta_\psi^j$$

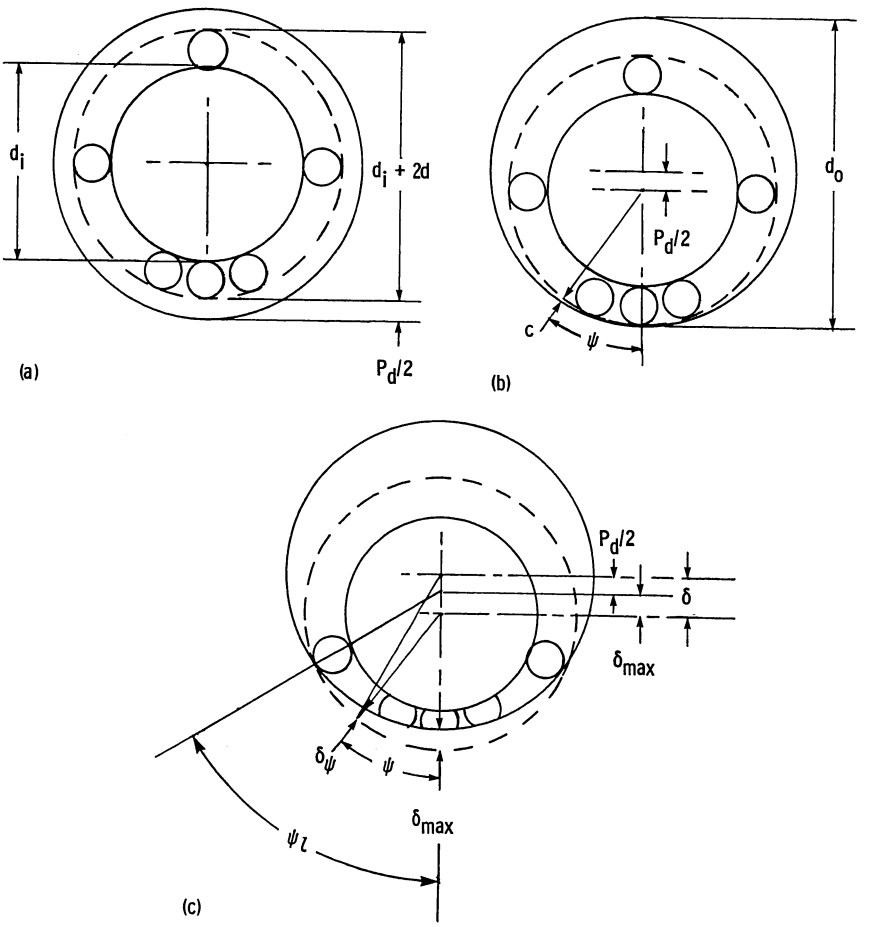

(a) Concentric arrangement.
(b) Initial contact.
(c) Interference.

Figure 3.6-14.—Radially loaded rolling-element bearing. (From Hamrock and Dowson, 1981.)

Substituting equation (3.6-39) into this equation gives

$$F_\psi = K_j\left(\delta \cos \psi - \frac{P_d}{2}\right)^j$$

For static equilibrium the applied load must equal the sum of the components of the rolling-element loads parallel to the direction of the applied load.

$$F_r = \Sigma F_\psi \cos \psi$$

therefore

$$F_r = K_j \sum \left(\delta \cos \psi - \frac{P_d}{2}\right)^j \cos \psi \qquad (3.6\text{-}40)$$

The angular extent of the bearing arc $2\psi_l$ in which the rolling elements are loaded is obtained by setting the root expression in equation (3.6-40) equal to zero and solving for ψ.

$$\psi_l = \cos^{-1}\left(\frac{P_d}{2\delta}\right)$$

The summation in equation (3.6-40) applies only to the angular extent of the loaded region. This equation can be written for a roller bearing as

$$F_r = \left(\psi_l - \frac{P_d}{2\delta}\sin \psi_l\right)\frac{nK_1\delta}{2\pi} \qquad (3.6\text{-}41)$$

and similarly in integral form for a ball bearing as

$$F_r = \frac{n}{\pi}K_{1.5}\delta^{3/2}\int_0^{\psi_l}\left(\cos \psi - \frac{P_d}{2\delta}\right)^{3/2}\cos \psi \, d\psi$$

The integral in the equation can be reduced to a standard elliptic integral by the hypergeometric series and the beta function. If the integral is numerically evaluated directly, the following approximate expression is derived:

$$\int_0^{\psi_l}\left(\cos \psi - \frac{P_d}{2\delta}\right)^{3/2}\cos \psi \, d\psi = 2.491\left\{\left[1+\left(\frac{P_d/2\delta - 1}{1.23}\right)^2\right]^{1/2} - 1\right\}$$

This approximate expression fits the exact numerical solution to within ±2 percent for a complete range of $P_d/2\delta$.

The load carried by the most heavily loaded ball is obtained by substituting $\psi = 0°$ in equation (3.6-40) and dropping the summation sign

$$F_{max} = K_j\delta^j\left(1 - \frac{P_d}{2\delta}\right)^j \qquad (3.6\text{-}42)$$

Dividing the maximum ball load (eq. (3.6-42)) by the total radial load for a roller bearing (eq. (3.6-41)) gives

$$F_r = \frac{\left(\psi_l - \frac{P_d}{2\delta}\sin \psi_l\right)nF_{max}}{2\pi(1 - P_d/2\delta)} \qquad (3.6\text{-}43)$$

and similarly for a ball bearing

$$F_r = \frac{nF_{max}}{Z} \qquad (3.6\text{-}44)$$

where

$$Z = \frac{\pi(1 - P_d/2\delta)^{3/2}}{2.491\left\{\left[1+\left(\frac{1 - P_d/2\delta}{1.23}\right)^2\right]^{1/2} - 1\right\}} \qquad (3.6\text{-}45)$$

For *roller bearings* when the diametral clearance P_d is zero, $\psi_l = \pi/2$ and equation (3.6-43) gives

$$F_r = \frac{nF_{max}}{4} \qquad (3.6\text{-}46)$$

For *ball bearings* when the diametral clearance P_d is zero, the value of Z in equation (3.6-44) becomes 4.37. This is the value derived by Stribeck (1901) for ball bearings of zero diametral clearance. The approach used by Stribeck was to evaluate the finite summation for various numbers of balls. He then derived the celebrated Stribeck equation for static load-carrying capacity by writing the more conservative value of 5 for the theoretical value of 4.37:

$$F_r = \frac{nF_{max}}{5} \qquad (3.6\text{-}47)$$

In using equation (3.6-47), it should be remembered that Z was considered to be a constant and that the effects of clearance and applied load on load distribution were not taken into account. However, these effects were considered in obtaining equation (3.6-44).

Thrust-loaded ball bearings

The static-thrust-load capacity of a ball bearing may be defined as the maximum thrust load that the bearing can endure before the contact ellipse approaches a race shoulder, as shown in figure 3.6-15, or the load at which the allowable mean compressive stress is reached, which-

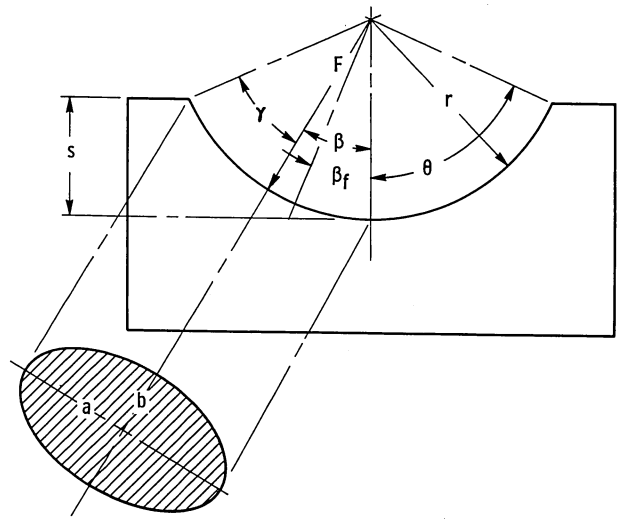

Figure 3.6-15.—Contact ellipse in bearing race. (From Hamrock and Dowson, 1981.)

ever is smaller. Both the limiting shoulder height and the mean compressive stress must be calculated to find the static-thrust-load capacity.

In the contact ellipse in a bearing race under a load (fig. 3.6-15) each ball is subjected to an identical thrust component F_t/n, where F_t is the total thrust load. The initial contact angle before the application of a thrust load is denoted by β_f. Under load the normal ball thrust load F acts at the contact angle β and is written as

$$F=\frac{F_t}{n}\sin\beta \tag{3.6-48}$$

A cross section through an angular-contact bearing under a thrust load F_t is shown in figure 3.6-16. From this figure the contact angle after the thrust load has been applied can be written as

$$\beta=\cos^{-1}\left(\frac{D-P_d/2}{D+\delta}\right) \tag{3.6-49}$$

The initial contact angle was given in equation (3.6-7). Using that equation and rearranging terms in equation (3.6-49) give, solely from geometry (fig. 3.6-16),

$$\delta=D\left(\frac{\cos\beta_f}{\cos\beta}-1\right)$$

$$\delta=\delta_o+\delta_i$$

$$\delta=\left[\frac{F}{(K_j)_o}\right]^{1/j}+\left[\frac{F}{(K_j)_i}\right]^{1/j}$$

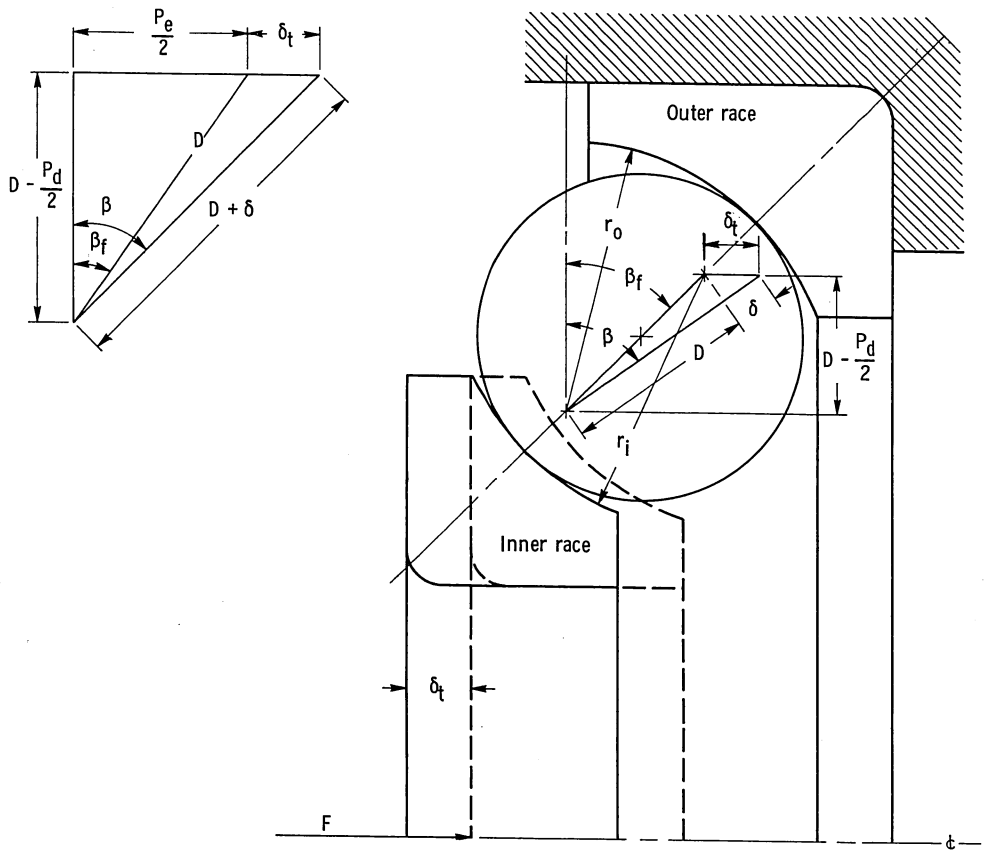

Figure 3.6-16.—Angular-contact ball bearing under thrust load. (From Hamrock and Dowson, 1981.)

$$K_j = \frac{1}{\left\{\left[\frac{1}{(K_j)_o}\right]^{1/j} + \left[\frac{1}{(K_j)_i}\right]^{1/j}\right\}^j}$$

$$K_j = \frac{1}{\left[\frac{4.5\,\mathfrak{F}_o^3}{\pi k_o E_o'(R_o\mathcal{E}_o)^{1/2}}\right]^{2/3} + \left[\frac{4.5\,\mathfrak{F}_i^3}{\pi k_i E_i'(R_i\mathcal{E}_i)^{1/2}}\right]^{2/3}} \tag{3.6-50}$$

$$F = K_j D^{3/2}\left(\frac{\cos\beta_f}{\cos\beta} - 1\right)^{3/2} \tag{3.6-51}$$

where

$$K_{1.5} = \pi k E'\left(\frac{R\mathcal{E}}{4.5\,\mathfrak{F}^3}\right)^{1/2} \tag{3.6-52}$$

and k, $\mathcal{E}$, and $\mathfrak{F}$ are given by equations (3.1-7), (3.1-8), and (3.1-9), respectively.

From equations (3.6-48) and (3.6-51), we can write

$$\frac{F_t}{n\sin\beta} = F$$

$$\frac{F_t}{nK_jD^{3/2}} = \sin\beta\left(\frac{\cos\beta_f}{\cos\beta} - 1\right)^{3/2} \tag{3.6-53}$$

This equation can be solved numerically by the Newton-Raphson method. The iterative equation to be satisfied is

$$\beta' - \beta = \frac{\dfrac{F_t}{nK_{1.5}D^{3/2}} - \sin\beta\left(\dfrac{\cos\beta_f}{\cos\beta} - 1\right)^{3/2}}{\cos\beta\left(\dfrac{\cos\beta_f}{\cos\beta} - 1\right)^{3/2} + \dfrac{3}{2}\cos\beta_f\tan^2\beta\left(\dfrac{\cos\beta_f}{\cos\beta} - 1\right)^{1/2}} \tag{3.6-54}$$

In this equation convergence is satisfied when $\beta' - \beta$ becomes essentially zero.

When a thrust load is applied, the shoulder height is limited to the distance by which the pressure-contact ellipse can approach the shoulder. As long as the following inequality is satisfied, the pressure-contact ellipse will not exceed the shoulder height limit:

$$\theta > \beta + \sin^{-1}\left(\frac{D_y}{fd}\right)$$

From figure 3.6-5 and equation (3.6-3) the angle used to define the shoulder height θ can be written as

$$\theta = \cos^{-1}\left(\frac{1-s}{fd}\right)$$

From figure 3.6-16 the axial deflection δ_t corresponding to a thrust load can be written as

$$\delta_t = (D+\delta)\sin\beta - D\sin\beta_f \tag{3.6-55}$$

Substituting equation (3.6-50) into equation (3.6-55) gives

$$\delta_t = \frac{D\sin(\beta-\beta_f)}{\cos\beta}$$

Having determined β from equation (3.6-54) and β_f from equation (3.6-8), we can easily evaluate the relationship for δ_t.

Preloading

The use of angular-contact bearings as duplex pairs preloaded against each other is discussed in Section 3.6.1. As shown in table 3.6-2 duplex bearing pairs are used in either back-to-back or face-to-face arrangements. Such bearings are usually preloaded against each other by providing what is called "stickout" in the manufacture of the bearing. This is illustrated in figure 3.6-17 for a bearing pair used in a back-to-back arrangement. The

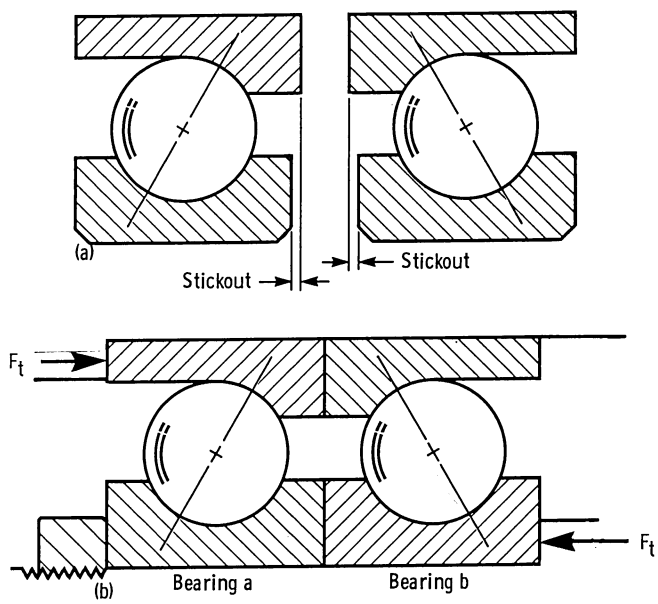

(a) Separated.
(b) Mounted and preloaded.

Figure 3.6-17.—Angular-contact bearings in back-to-back arrangement, shown individually as manufactured and as mounted with preload. (From Hamrock and Anderson, 1983.)

magnitude of the stickout and the bearing design determine the level of preload on each bearing when the bearings are clamped together as in figure 3.6-17. The magnitude of preload and the load-deflection characteristics for a given bearing pair can be calculated by using equations (3.6-7), (3.6-32), (3.6-48), and (3.6-50) to (3.6-53).

The relationship of initial preload, system load, and final load for bearings a and b is shown in figure 3.6-18. The load-deflection curve follows the relationship $\delta = KF^{3/2}$. When a system thrust load F_t is imposed on the bearing pairs, the magnitude of load on bearing b increases while that on bearing a decreases until the difference equals the system load. The physical situation demands that the change in each bearing deflection be the same ($\Delta a = \Delta b$ in fig. 3.6-18). The increments in bearing load, however, are not the same. This is important because a system thrust load far greater than twice the preload is always required before one bearing becomes unloaded. Prevention of bearing unloading, which can result in skidding and early failure, is an objective of preloading.

3.6.5 Rolling bearing fatigue life

Contact fatigue theory

Rolling fatigue is a material failure caused by the application of repeated stresses to a small volume of material. A unique failure type, it is essentially a process of seeking out the weakest point at which the first failure will occur. A typical spall is shown in figure 3.6-19. We can surmise that on a microscale there will be a wide dispersion in material strength or resistance to fatigue because of inhomogeneities in the material. Because bearing materials are complex alloys, we would not expect

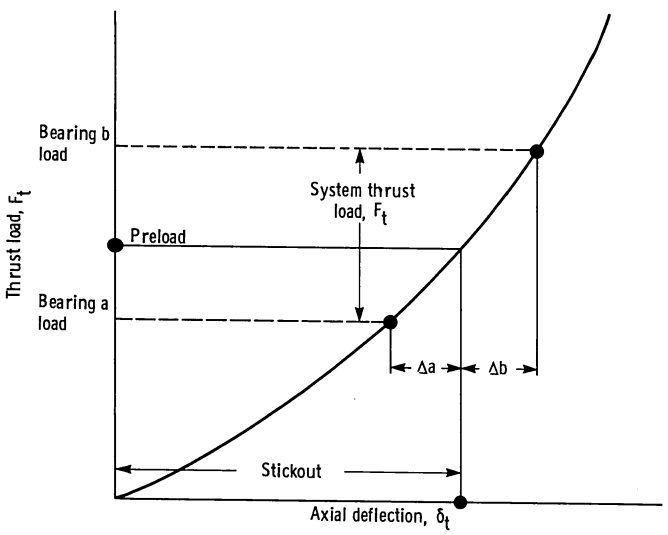

Figure 3.6-18.—Thrust load-axial deflection curve for a typical ball bearing. (From Hamrock and Anderson, 1983.)

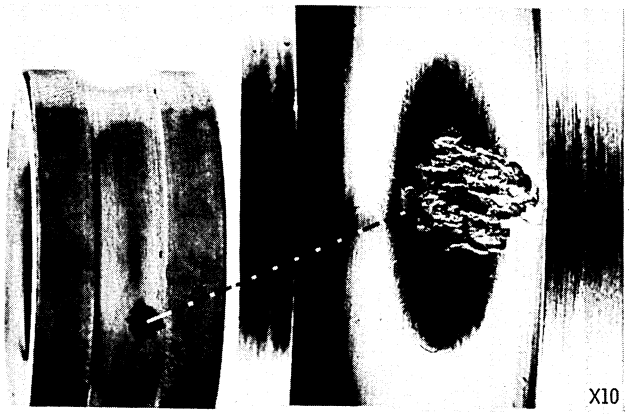

Figure 3.6-19.—Typical fatigue spall.

them to be homogeneous or equally resistant to failure at all points. Therefore the fatigue process can be expected to be one in which a group of supposedly identical specimens exhibit wide variations in failure time when stressed in the same way. For this reason it is necessary to treat the fatigue process statistically.

To be able to predict how long a typical bearing will run under a specific load, we must have the following two essential pieces of information:

(1) An accurate, quantitative estimate of the life dispersion or scatter

(2) The life at a given survival rate or reliability level. This translates into an expression for the "load capacity," or the ability of the bearing to endure a given load for a stipulated number of stress cycles or revolutions. If a group of supposedly identical bearings is tested at a specific load and speed, there will be a wide scatter in bearing lives, as shown in figure 3.6-20.

The Weibull distribution

Weibull (1949) postulates that the fatigue lives of a homogeneous group of rolling-element bearings are dispersed according to the following relation:

$$\ln \ln \frac{1}{S} = e_1 \ln \frac{L}{A}$$

where S is the probability of survival, L is the fatigue life, and e_1 and A are constants. The Weibull distribution results from a statistical theory of strength based on probability theory, where the dependence of strength on volume is explained by the dispersion in material strength. This is the "weakest link" theory.

Consider a volume being stressed that is broken up into m similar volumes

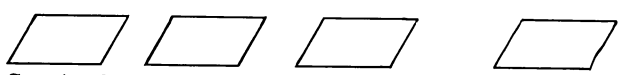

$$S_1 = 1 - M_1, S_2 = 1 - M_2, S_3 = 1 - M_3, \cdots, S_m = 1 - M_m$$

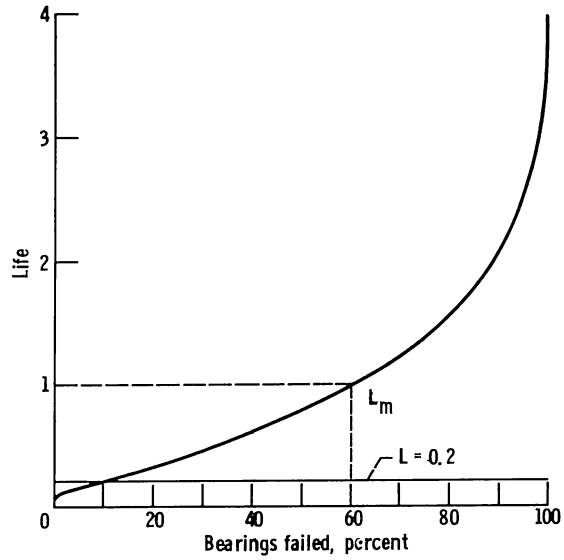

Figure 3.6-20.—Distribution of bearing fatigue failures. (From Hamrock and Anderson, 1983.)

The M's represent the probability of failure and the S's, the probability of survival. For the entire volume we can write

$$S=S_1 \cdot S_2 \cdot S_3 \cdot \cdots S_m$$

Then

$$1-M=(1-M_1)(1-M_2)(1-M_3)\cdots(1-M_m)$$

$$1-M=\prod_{i=1}^{m}(1-M_i)$$

$$S=\prod_{i=1}^{m}(1-M_i)$$

The probability of a crack starting in the i^{th} volume is

$$M_i=f(x)\,v_i$$

where $f(x)$ is a function of the stress level, the number of stress cycles, and the depth into the material where the maximum stress occurs and v_i is the elementary volume. Therefore

$$S=\prod_{i=1}^{m}\left[1-f(x)\,v_i\right]$$

$$\ln S=\sum_{i=1}^{m}\ln\left[1-f(x)\,v_i\right]$$

Now if $f(x)\,v_i<<1$, then $\ln\left[1-f(x)\,v_i\right]=-f(x)\,v_i$ and

$$\ln S=-\sum_{i=1}^{m}f(x)\,v_i$$

Let $v_i \to 0$; then

$$\sum_{i=1}^{m}f(x)\,v_i=\int f(x)\,dv=f(x)\,V$$

Lundberg and Palmgren (1947) assume that $f(x)$ could be expressed as a power function of shear stress τ_0, number of stress cycles J, and depth to the maximum shear stress Z_0.

$$f(x)=\frac{\tau_0^{c_1}J^{c_2}}{Z_0^{c_3}}$$

They also choose as the stressed volume

$$V=D_y Z_0 l_v$$

Then

$$\ln S=-\frac{\tau_0^{c_1}J^{c_2}D_y l_v}{Z_0^{c_3-1}}$$

or

$$\ln\frac{1}{S}=\frac{\tau_0^{c_1}J^{c_2}D_y l_v}{Z_0^{c_3-1}} \tag{3.6-56}$$

For a specific bearing and load (e.g., stress) τ_0, D_y, l_v, and Z_0 are all constant so that

$$\ln\frac{1}{S}\approx J^{c_2}$$

Designating J as life L in stress cycles gives

$$\ln\frac{1}{S}=\left(\frac{L}{A}\right)^{c_2}$$

or

$$\ln\ln\frac{1}{S}=c_2\ln\left(\frac{L}{A}\right) \tag{3.6-57}$$

This is the Weibull distribution, which relates probability of survival and life. It has two principal functions. First, bearing fatigue lives plot as a straight line on Weibull coordinates (log log vs. log), so that the life at any reliability level can be determined. Of most interest are the L_{10} life ($S=0.9$) and the L_{50} life ($S=0.5$). Bearing load ratings are based on the L_{10} life. Second, equation (3.6-57) can be used to determine what the L_{10} life must

be to obtain a required life at any reliability level. The L_{10} life is calculated, from the load on the bearing and the bearing dynamic capacity or load rating given in manufacturers' catalogs and engineering journals, by using the equation

$$L=\left(\frac{C}{F_e}\right)^m$$

where

C basic dynamic capacity or load rating
F_e equivalent bearing load
m 3 for elliptical contacts and 10/3 for rectangular contacts

A typical Weibull plot is shown in figure 3.6-21.

Lundberg-Palmgren theory

The Lundberg-Palmgren theory, on which bearing ratings are based, is expressed by equation (3.6-56). The exponents in this equation are determined experimentally from the dispersion of bearing lives and the dependence of life on load, geometry, and bearing size. As a standard of reference, all bearing load ratings are expressed in terms of the specific dynamic capacity C, which, by definition, is the load that a bearing can carry for 1 million inner-race revolutions with a 90 percent chance of survival.

Factors on which specific dynamic capacity and bearing life depend are

(1) Size of rolling element
(2) Number of rolling elements per row

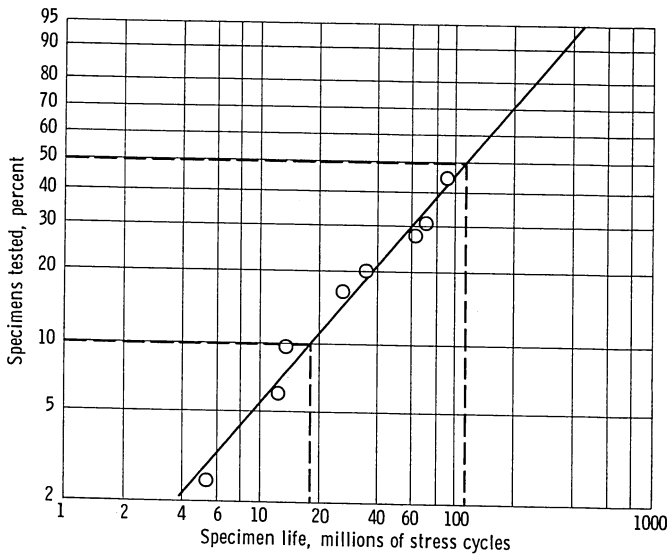

Figure 3.6-21.—Typical Weibull plot of bearing fatigue failures. (From Hamrock and Dowson, 1981.)

(3) Number of rows of rolling elements
(4) Conformity between rolling elements and races
(5) Contact angle under load
(6) Material properties
(7) Lubricant properties
(8) Operating temperature
(9) Operating speed

Only factors (1) to (5) are incorporated in bearing dynamic capacities developed from the Lundberg-Palmgren theory. The remaining factors must be taken into account in the life adjustment factors discussed later.

The formulas for specific dynamic capacity as developed by Lundberg-Palmgren (1947, 1952) are as follows:

For radial ball bearings with $d \leq 25$ mm,

$$C=f_c(i\cos\beta)^{0.7}n^{2/3}\left(\frac{d}{0.0254}\right)^{1.8}$$

where

d diameter of rolling element, m
i number of rows of rolling elements
n number of rolling elements per row
β contact angle
f_c coefficient dependent on material and bearing type

For radial ball bearings with $d \geq 25$ mm,

$$C=f_c(i\cos\beta)^{0.7}n^{2/3}\left(\frac{d}{0.0254}\right)^{1.4}$$

For radial roller bearings,

$$C=f_c(i\cos\beta)^{0.78}n^{3/4}\left(\frac{d}{0.0254}\right)^{1.07}\left(\frac{l_t}{0.0254}\right)^{0.78}$$

where l_t is roller length in meters.

For thrust ball bearings with $\beta \neq 90°$,

$$C=f_c(i\cos\beta)^{0.7}(\tan\beta)n^{2/3}\left(\frac{d}{0.0254}\right)^{1.8}$$

For thrust roller bearings with $\beta \neq 90°$,

$$C=f_c(i\cos\beta)^{0.78}(\tan\beta)n^{3/4}\left(\frac{l_t}{0.0254}\right)^{0.78}$$

For thrust ball bearings with $\beta = 90°$,

$$C=f_c i^{0.7}n^{2/3}\left(\frac{d}{0.0254}\right)^{1.8}$$

For thrust roller bearings with $\beta = 90°$,

$$C = f_c i^{0.78} n^{3/4} \left(\frac{d}{0.0254}\right)^{1.07} \left(\frac{l_t}{0.0254}\right)^{0.78}$$

For ordinary bearing steels such as SAE 52100 with mineral oil lubrication, f_c can be evaluated by using tables 3.6-10 and 3.6-11, but a more convenient method is to use tabulated values from the most recent Antifriction Bearing Manufacturers Association (AFBMA) documents on dynamic load ratings and life (ISO, 1976). The value of C is calculated or determined from bearing manufacturers' catalogs. The equilvalent load F_e can be calculated from the equation

$$F_e = XF_r + YF_t$$

Factors X and Y are given in bearing manufacturers' catalogs for specific bearings.

In addition to specific dynamic capacity C, every bearing has a specific static capacity, usually designated as C_0. Specific static capacity is defined as the load that, under static conditions, will result in a permanent deformation of 0.0001 times the rolling-element diameter. For some bearings C_0 is less than C, so it is important to avoid exposing a bearing to a static load that exceeds C_0. Values of C_0 are also given in bearing manufacturers' catalogs.

The AFBMA method

Shortly after publication of the Lundberg-Palmgren theory, the AFBMA began efforts to standardize methods for establishing bearing load ratings and making life predictions. Standardized methods of establishing load ratings for ball bearings (AFBMA, 1960a) and roller bearings (AFBMA, 1960b) were devised, based essentially on the Lundberg-Palmgren theory. These early standards are published in their entirety in Jones (1964). In recent years significant advances have been made in rolling-element bearing material quality and in our understanding of the role of lubrication in bearing life through the development of elastohydrodynamic theory. Therefore the original AFBMA standards in AFBMA (1960a and b) have been updated with life adjustment factors. These factors have been incorporated into ISO (1976), which is discussed in the following section.

Life adjustment factors

A comprehensive study of the factors affecting the fatigue life of bearings, which were not taken account of in the Lundberg-Palmgren theory, is reported in Bamberger et al. (1971). In that reference it was assumed that the various environmental or bearing design factors are multiplicative in their effect on bearing life. The following equation results:

$$L_A = (\tilde{D})(\tilde{E})(\tilde{F})(\tilde{G})(\tilde{H}) L_{10}$$

or

$$L_A = (\tilde{D})(\tilde{E})(\tilde{F})(\tilde{G})(\tilde{H})(C/F_e)^m$$

where

$\tilde{D}$ materials factor
$\tilde{E}$ metallurgical processing factor
$\tilde{F}$ lubrication factor
$\tilde{G}$ speed effect factor
$\tilde{H}$ misalignment factor
F_e bearing equivalent load
m load-life exponent; either 3 for ball bearings or 10/3 for roller bearings

Factors $\tilde{D}$, $\tilde{E}$, and $\tilde{F}$ are briefly reviewed here. The reader is referred to Bamberger et al. (1971) for a complete discussion of all five life adjustment factors.

Materials factors $\tilde{D}$ and $\tilde{E}$.—For over a century, AISI 52100 steel has been the predominant material for rolling-element bearings. In fact, the basic dynamic capacity as defined by AFBMA in 1949 is based on an air-melted 52100 steel, hardened to at least Rockwell C 58. Since that time, better control of air-melting processes and the introduction of vacuum remelting processes have resulted in more homogeneous steels with fewer impurities. Such steels have extended rolling-element bearing fatigue lives to several times the AFBMA or catalog life. Life improvements of 3 to 8 times are not uncommon. Other steel compositions, such as AISI M-1 and AISI M-50, chosen for their higher temperature capabilities and resistance to corrosion, also have shown greater resistance to fatigue pitting when vacuum melting techniques are employed. Case-hardened materials, such as AISI 4620, AISI 4118, and AISI 8620, used primarily for roller bearings, have the advantage of a tough, ductile steel core with a hard, fatigue-resistant surface.

The recommended $\tilde{D}$ factors for various alloys processed by air melting are shown in table 3.6-12. Insufficient definitive life data were found for case-hardened materials to recommend $\tilde{D}$ factors for them. It is recommended that the user refer to the bearing manufacturer for the choice of a specific case-hardened material.

The metallurgical processing variables considered in the development of the $\tilde{E}$ factor included melting practice (air and vacuum melting) and metal working (thermomechanical working). Thermomechanical working of M-50 has also been shown to result in improved life, but it is costly and still not fully developed as a processing technique. Bamberger et al. (1971) recommend an $\tilde{E}$

TABLE 3.6-10. - CAPACITY FORMULAS FOR RECTANGULAR AND ELLIPTICAL CONTACTS

[From Hamrock and Anderson (1983). Units in kg and mm.]

Function	Elliptical contact of ball bearings			Rectangular contact of roller bearings		
C	$f_c f_a i^{0.7} N^{2/3} d^{1.8}$			$f_c f_a i^{7/9} N^{3/4} d^{29/27} \ell_{t,i}^{7/9}$		
f_c	$g_c f_1 f_2 \left(\frac{d_i}{d_i - d}\right)^{0.41}$			$g_c f_1 f_2$		
g_c	$\left[1 + \left(\frac{C_i}{C_o}\right)^{10/8}\right]^{-0.8}$			$\left[1 + \left(\frac{C_i}{C_o}\right)^{9/2}\right]^{-2/9}$		
C_i/C_o	$f_3 \left[\frac{d_i(d_o - d)}{d_o(d_i - d)}\right]^{0.41}$			$f_3 \left(\frac{\ell_{t,i}}{\ell_{t,o}}\right)^{7/9}$		
	Radial	Thrust		Radial	Thrust	
		$\beta \neq 90°$	$\beta = 90°$		$\beta \neq 90°$	$\beta = 90°$
γ	$\frac{d \cos \beta}{d_e}$		$\frac{d}{d_e}$	$\frac{d \cos \beta}{d_e}$		$\frac{d}{d_e}$
f_a	$(\cos \beta)^{0.7}$	$(\cos \beta)^{0.7} \tan \beta$	1	$(\cos \beta)^{7/9}$	$(\cos \beta)^{7/9} \tan \beta$	1
f_1	3.7-4.1	6-10		18-25	36-60	
f_2	$\frac{\gamma^{0.3}(1 - \gamma)^{1.39}}{(1 + \gamma)^{1/3}}$		$\gamma^{0.3}$	$\frac{\gamma^{2/9}(1 - \gamma)^{29/27}}{(1 + \gamma)^{1/3}}$		$\gamma^{2/9}$
f_3	$104 f_4$	f_4	1	$1.14 f_4$	f_4	1
f_4	$\left(\frac{1 - \gamma}{1 + \gamma}\right)^{1.72}$			$\left(\frac{1 - \gamma}{1 + \gamma}\right)^{38/37}$		

TABLE 3.6-11. - CAPACITY FORMULAS FOR MIXED RECTANGULAR AND ELLIPTICAL CONTACTS

[From Hamrock and Anderson (1983). $C = C_i[1 + (C_i/C_o)^4]^{1/4}$; units in kg and mm.]

Function	Radial bearing	Thrust bearing		Radial bearing	Thrust bearing	
		$\beta \neq 90°$	$\beta = 90°$		$\beta \neq 90°$	$\beta = 90°$
	Inner race			Outer race		
γ	$\frac{d \cos \beta}{d_e}$		$\frac{d}{d_e}$	$\frac{d \cos \beta}{d_e}$		$\frac{d}{d_e}$
	Rectangular contact C_i			Elliptical contact C_o		
C_i or C_o	$f_1 f_2 f_a i^{7/9} N^{3/4} D^{29/27} \ell_{t,i}^{7/9}$			$f_1 f_2 f_a \left(\frac{2R}{D} \frac{r_o}{r_o - R}\right)^{0.41} i^{0.7} N^{2/3} D^{1.8}$		
f_a	$(\cos \beta)^{7/9}$	$(\cos \beta)^{7/9} \tan \beta$	1	$(\cos \beta)^{0.7}$	$(\cos \beta)^{0.7} \tan \beta$	1
f_1	18-25	36-60		3.5-3.9	6-10	
f_2	$\frac{\gamma^{2/9}(1 - \gamma)^{29/27}}{(1 + \gamma)^{1/3}}$		$\gamma^{3/9}$	$\frac{\gamma^{0.3}(1 + \gamma)^{1.39}}{(1 - \gamma)^{1/3}}$		$\gamma^{0.3}$
	Point contact C_i			Line contact C_o		
C_i or C_o	$f_1 f_2 f_a \left(\frac{2R}{D} \frac{r_i}{r_i - R}\right)^{0.41} i^{0.7} n^{2/3} d^{1.8}$			$f_1 f_2 f_a i^{7/9} n^{3/4} d^{29/27} \ell_{t,o}^{7.9}$		
f_a	$(\cos \alpha)^{0.7}$	$(\cos \alpha)^{0.7} \tan \alpha$	1	$(\cos \alpha)^{7/9}$	$(\cos \alpha)^{7/9} \tan \alpha$	1
f_1	3.7-4.1	6-10		15-22	36-60	
f_2	$\frac{\gamma^{0.3}(1 - \gamma)^{1.39}}{(1 + \gamma)^{1/3}}$		$\gamma^{0.3}$	$\frac{\gamma^{2/9}(1 + \gamma)^{29/27}}{(1 - \gamma)^{1/3}}$		$\gamma^{2/9}$

TABLE 3.6-12. - MATERIAL FACTOR FOR THROUGH-HARDENED BEARING MATERIALS

[From Bamberger et al. (1971); air-melted materials assumed.]

Material	$\tilde{D}$-Factor
52100	2.0
M-1	.6
M-2	.6
M-10	2.0
M-50	2.0
T-1	.6
Halmo	2.0
M-42	.2
WB 49	.6
440C	0.6-0.8

factor of 3 for consumable-electrode-vacuum-melted materials.

The translation of these factors into a standard (ISO, 1976) is discussed later.

Lubrication factor $\tilde{F}$.—Until approximately 1960 the role of the lubricant between surfaces in rolling contact was not fully appreciated. Metal-to-metal contact was presumed to occur in all applications with attendant required boundary lubrication. The development of elastohydrodynamic lubrication theory showed that lubricant films of thicknesses of the order of microinches and tens of microinches occur in rolling contact. Since surface finishes are of the same order of magnitude as the lubricant film thicknesses, the significance of rolling-element bearing surface roughnesses to bearing performance became apparent. Tallian (1967) first reported on the importance to bearing life of the ratio of elastohydrodynamic lubrication film thickness to surface roughness. Figure 3.6-22 shows life as a percentage of calculated L_{10} life as a function of Λ, where

$$\Lambda = \frac{h_{\min}}{\left(\Delta_a^2 + \Delta_b^2\right)^{1/2}} \tag{3.6-58}$$

Figure 3.6-23, from Bamberger et al. (1971) presents a curve of the recommended $\tilde{F}$ factor as a function of the Λ parameter. A mean of the curves presented in Tallian (1967) for ball bearings and in Skurka (1970) for roller bearings is recommended for use. A formula for calculating the minimum film thickness $h_{\min}$ in the hard-EHL regime is given in equation (3.3-1).

The results of Bamberger et al. (1971) have not been fully accepted into the current AFBMA standard represented by ISO (1976). The standard presents the following:

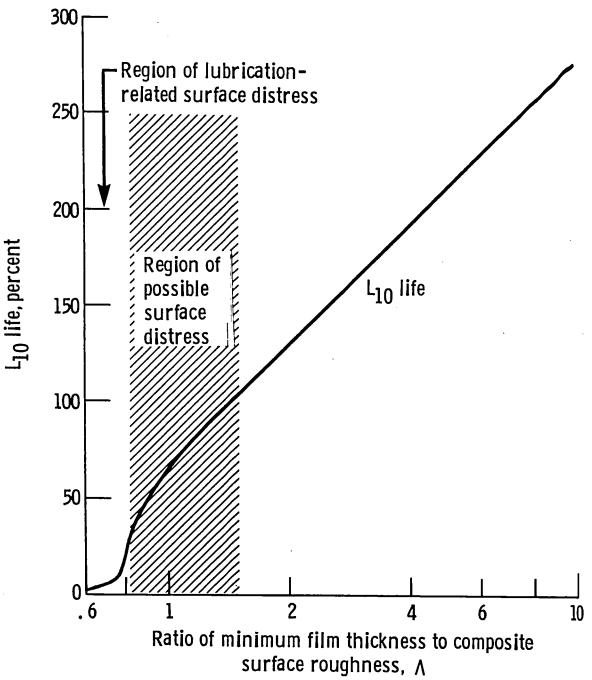

Figure 3.6-22.—Chart for determining group fatigue life L_{10}. (From Tallian, 1967.)

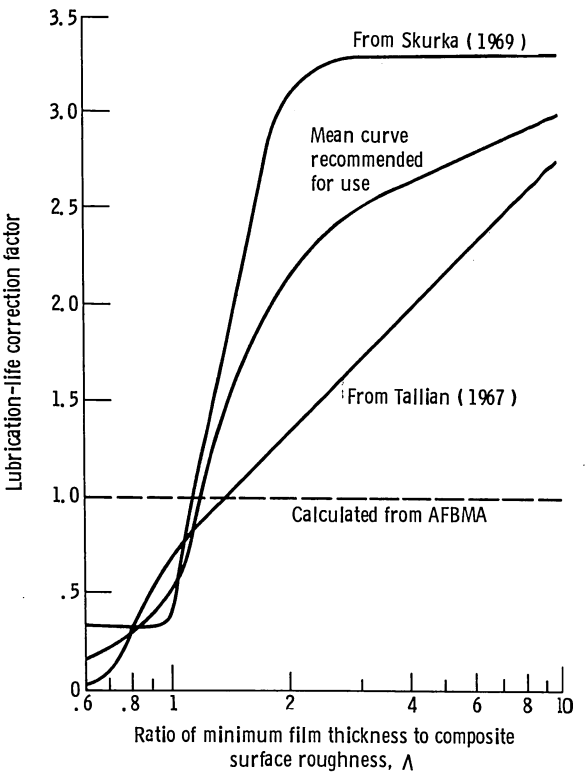

Figure 3.6-23.—Chart for determining lubrication-life correction factor. (From Bamberger, et al., 1971.)

(1) Life and dynamic load rating formulas for radial and thrust ball bearings and radial and thrust roller bearings

(2) Tables of f_c for all cases

(3) Tables of X and Y factors for calculating equivalent loads

(4) Load rating formulas for multirow bearings

(5) Life correction factors for high-reliability levels a_1, materials a_2, and lubrication or operating conditions a_3

Procedures for calculating a_2 and a_3 are less than definitive, reflecting the need for additional research, life data, and operating experience.

3.6.6 Applications

In this section two applications of the film thickness equations developed throughout this chapter are presented to illustrate how the fluid-film lubrication conditions in machine elements can be analyzed. Specifically a typical roller bearing problem and a typical ball bearing problem are considered.

Cylindrical roller bearing problem

The equations for elastohydrodynamic film thickness that have been developed earlier relate primarily to elliptical contacts, but they are sufficiently general to allow them to be used with adequate accuracy in line-contact problems, as would be found in a cylindrical roller bearing. Therefore the minimum elastohydrodynamic film thicknesses on the inner and outer races of a cylindrical roller bearing with the following dimensions are calculated:

Inner-race diameter, d_i, mm (m) 64 (0.064)
Outer-race diameter, d_o, mm (m) 96 (0.096)
Diameter of cylindrical rollers, d, mm (m).....16 (0.016)
Axial length of cylindrical rollers, l, mm (m) 16 (0.016)
Number of rollers in complete bearing, n.....9

A bearing of this kind might well experience the following operating conditions:

Radial load, F_r, N 10 800
Inner-race angular velocity, ω_i, rad/s 524
Outer-race angular velocity, ω_o, rad/s 0
Lubricant viscosity at atmospheric pressure at operating temperature of bearings, η_0, N s/m^2 .....0.01
Viscosity-pressure coefficient, ξ, m^2/N.....2.2×10^{-8}
Modulus of elasticity for both rollers and races, E, N/m^2 .....2.075×10^{11}
Poisson's ratio, ν 0.3

Calculation.—From equation (3.6-46), the most heavily loaded roller can be expressed as

$$F_{max}=\frac{4F_r}{n}=\frac{4(10\ 800\ \text{N})}{9}=4800\ \text{N} \tag{3.6-46}$$

Therefore the radial load per unit length on the most heavily loaded roller is

$$F'_{max}=\frac{4800\ \text{N}}{0.016\ \text{m}}=0.3\ \text{MN/m} \tag{3.6-46}$$

From figure 3.6-24 we can write the radii of curvature as

$r_{ax}=0.008$ m, $\quad r_{ay}=\infty$

$r_{bx,i}=0.032$ m, $\quad r_{by,i}=\infty$

$r_{bx,o}=0.048$ m, $\quad r_{by,o}=\infty$

Then

$$\frac{1}{R_{x,i}}=\frac{1}{0.008}+\frac{1}{0.032}=\frac{5}{0.032}$$

giving $R_{x,i}=0.0064$ m;

$$\frac{1}{R_{x,o}}=\frac{1}{0.008}-\frac{1}{0.048}=\frac{5}{0.048} \tag{3.1-4}$$

giving $R_{x,o}=0.0096$ m; and

$$\frac{1}{R_{y,i}}=\frac{1}{R_{y,o}}=\frac{1}{\infty}+\frac{1}{\infty}=0 \tag{3.1-5}$$

giving $R_{y,i}=R_{y,o}=\infty$.

From the input information the effective modulus of elasticity can be written as

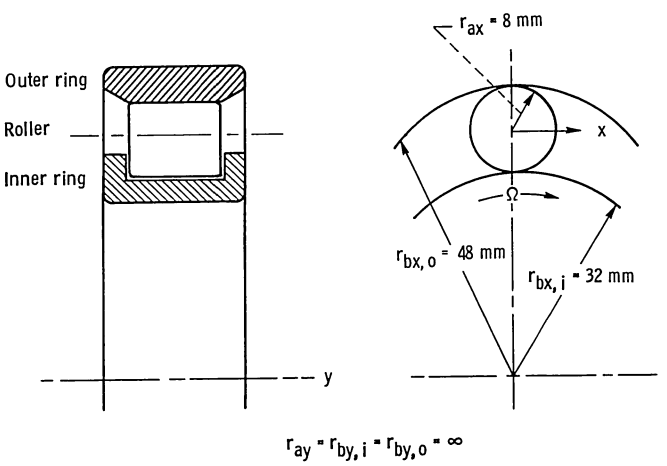

Figure 3.6-24.—Roller bearing example. $r_{ay}=r_{by,i}=r_{by,o}=\infty$.

$$E' = \frac{2}{\frac{1-\nu_a^2}{E_a} + \frac{1-\nu_b^2}{E_b}} = 2.28 \times 10^{11}\ \text{N/m}^2 \qquad (3.1\text{-}14)$$

For pure rolling the surface velocity u relative to the lubricated conjunctions for a cylindrical roller is

$$u = |\omega_i - \omega_o| \frac{(d_e^2 - d^2)}{4d_e} \qquad (3.6\text{-}30)$$

where d_e is the pitch diameter and d is the roller diameter.

$$d_e = \frac{d_o + d_i}{2} = \frac{0.096 + 0.064}{2} = 0.08\ \text{m} \qquad (3.6\text{-}1)$$

Hence

$$u = \frac{0.08^2 - 0.16^2}{4 \times 0.08}|524 - 0| = 10.061\ \text{m/s} \qquad (3.6\text{-}30)$$

The dimensionless speed, materials, and load parameters for the inner- and outer-race conjunctions thus become

$$U_i = \frac{\eta_0 u}{E' R_{x,i}} = \frac{0.01 \times 10.061}{2.28 \times 10^{11} \times 0.0064} = 6.895 \times 10^{-11} \qquad (3.2\text{-}4)$$

$$G_i = \xi E' = 5016 \qquad (3.2\text{-}5)$$

$$W_i = \frac{F}{E'(R_{x,i})^2} = \frac{4800}{2.28 \times 10^{11} \times (0.0064)^2} = 5.140 \times 10^{-4} \qquad (3.2\text{-}3)$$

$$U_o = \frac{\eta_0 u}{E' R_{x,o}} = \frac{0.01 \times 10.061}{2.28 \times 10^{11} \times 0.0096} = 4.597 \times 10^{-11} \qquad (3.2\text{-}4)$$

$$G_o = \xi E' = 5016 \qquad (3.2\text{-}5)$$

$$W_o = \frac{F}{E'(R_{x,o})^2} = \frac{4800}{2.28 \times 10^{11} \times (0.0096)^2} = 2.284 \times 10^{-4} \qquad (3.2\text{-}3)$$

The appropriate elliptical-contact elastohydrodynamic film thickness equation for a fully flooded conjunction is developed in Section 3.3 and recorded as equation (3.3-1):

$$H_{\min} = \frac{h_{\min}}{R_x} = 3.63\ U^{0.68} G^{0.49} W^{-0.073} (1 - e^{-0.68k}) \qquad (3.3\text{-}1)$$

For a roller bearing, $k = \infty$ and this equation reduces to

$$H_{\min} = 3.63\ U^{0.68} G^{0.49} W^{-0.073}$$

The dimensionless film thickness for the roller–inner-race conjunction is

$$H_{\min} = \frac{h_{\min}}{R_{x,i}} = 3.63 \times 1.231 \times 10^{-7} \times 65.04 \times 1.738 = 50.5 \times 10^{-6}$$

and hence

$$h_{\min} = 0.0064 \times 50.5 \times 10^{-6} = 0.32\ \mu\text{m}$$

The dimensionless film thickness for the roller–outer-race conjunction is

$$H_{\min} = \frac{h_{\min}}{R_{x,o}} = 3.63 \times 9.343 \times 10^{-8} \times 65.04 \times 1.844 = 40.7 \times 10^{-6}$$

and hence

$$h_{\min} = 0.0096 \times 40.7 \times 10^{-6} = 0.39\ \mu\text{m}$$

It is clear from these calculations that the smaller minimum film thickness in the bearing occurs at the roller–inner-race conjunction, where the geometrical conformity is less favorable. It was found that, if the ratio of minimum film thickness to composite surface roughness is greater than 3, an adequate elastohydrodynamic film is maintained. This implies that a composite surface roughness of $<0.1\ \mu$m is needed to assure that an elastohydrodynamic film is maintained.

Radial ball bearing problem

Consider a single-row, radial, deep-groove ball bearing with the following dimensions:

Inner-race diameter, d_i, m 0.052291
Outer-race diameter, d_o, m 0.077706
Ball diameter, d, m 0.012700

Number of balls in complete bearing, n 9
Inner-groove radius, r_i, m 0.006604
Outer-groove radius, r_o, m 0.006604
Contact angle, β, deg 0
rms surface finish of balls, Δ_b, μm 0.0625
rms surface finish of races, Δ_a, μm 0.175

A bearing of this kind might well experience the following operating conditions:

Radial load, F_r, N 8900
Inner-race angular velocity, β_i, rad/s 400
Outer-race angular velocity, β_o, rad/s 0
Lubricant viscosity at atmospheric pressure and effective operating temperature of bearing, η_0, N s/m^2 ..... 0.04
Viscosity-pressure coefficient, ξ, m^2/N ..... 2.3×10^{-8}
Modulus of elasticity for both balls and races, E, N/m^2 ..... 2×10^{11}
Poisson's ratio for both balls and races, ν 0.3

The essential features of the geometry of the inner and outer conjunctions (figs. 3.6-1 and 3.6-2) can be ascertained as follows:

Pitch diameter (eq. (3.6-1))

$$d_e=0.5(d_o+d_i)=0.065 \text{ m}$$

Diametral clearance (eq. (3.6-2))

$$P_d=d_o-d_i-2d=1.5\times10^{-5} \text{ m}$$

Race conformity (eq. (3.6-3))

$$f_i=f_o=\frac{r}{d}=0.52$$

Equivalent radius (eq. (3.6-18))

$$R_{x,i}=\frac{d(d_e-d)}{2d_e}=0.00511 \text{ m}$$

Equivalent radius (eq. (3.6-20))

$$R_{x,o}=\frac{d(d_e+d)}{2d_e}=0.00759 \text{ m}$$

Equivalent radius (eq. (3.6-19))

$$R_{y,i}=\frac{f_i d}{2f_i-1}=0.165 \text{ m}$$

Equivalent radius (eq. (3.6-21))

$$R_{y,o}=\frac{f_o d}{2f_o-1}=0.165 \text{ m}$$

The curvature sum

$$\frac{1}{R_i}=\frac{1}{R_{x,i}}+\frac{1}{R_{y,i}}=201.76 \qquad (3.1\text{-}4)$$

gives $R_i=4.956\times10^{-3}$ m, and the curvature sum

$$\frac{1}{R_o}=\frac{1}{R_{x,o}}+\frac{1}{R_{y,o}}=137.81 \qquad (3.1\text{-}4)$$

gives $R_o=7.256\times10^{-3}$ m. Also, $\alpha_i=R_{y,i}/R_{x,i}=32.35$ and $\alpha_o=R_{y,o}/R_{x,o}=21.74$

The nature of the Hertzian contact conditions can now be assessed.

Ellipticity parameters

$$k_i=\alpha_i^{2/\pi}=9.42$$
$$k_o=\alpha_o^{2/\pi}=7.09 \qquad (3.1\text{-}7)$$

Elliptic integrals

$$q=\frac{\pi}{2}-1$$
$$\mathcal{E}_i=1+\frac{q}{\alpha_i}=1.0188$$
$$\mathcal{E}_o=1+\frac{q}{\alpha_o}=1.0278 \qquad (3.1\text{-}8)$$
$$\mathcal{F}_i=\frac{\pi}{2}+q\ln\alpha_i=3.6205$$
$$\mathcal{F}_o=\frac{\pi}{2}+q\ln\alpha_o=3.3823 \qquad (3.1\text{-}9)$$

The effective elastic modulus E' is given by

$$E'=\frac{2}{\frac{1-\nu_a^2}{E_a}+\frac{1-\nu_b^2}{E_b}}=2.198\times10^{11} \text{ N/m}^2$$

To determine the load carried by the most heavily loaded ball in the bearing, it is necessary to adopt an iterative procedure based on the calculation of local static compression and the analysis presented in Section 3.6.4. Stribeck (1901) found that the value of Z was about 4.37 in the expression

$$F_{\max}=\frac{ZF_r}{n}$$

where

F_{max} load on most heavily loaded ball
F_r radial load on bearing
n number of balls

However, it is customary to adopt a value of $Z=5$ in simple calculations in order to produce a conservative design, and this value will be used to begin the iterative procedure.

Stage 1

Assume $Z=5$. Then

$$F_{max}=\frac{5F_r}{9}=\frac{5}{9}\times 8900=4944\text{ N} \qquad (3.6\text{-}44)$$

The maximum local elastic compression is

$$\delta_i=\mathfrak{F}_i\left[\left(\frac{9}{2\Sigma_i R_i}\right)\left(\frac{F_{max}}{\pi k_i E'}\right)^2\right]^{1/3}$$

$$=2.902\times 10^{-5}\text{ m}$$

$$\delta_o=\mathfrak{F}_o\left[\left(\frac{9}{2\Sigma_o R_o}\right)\left(\frac{F_{max}}{\pi k_o E'}\right)^2\right]^{1/3} \qquad (3.1\text{-}13)$$

$$=2.877\times 10^{-5}\text{ m}$$

The sum of the local compressions on the inner and outer races is

$$\delta=\delta_i+\delta_o=5.779\times 10^{-5}\text{ m}$$

A better value for Z can now be obtained from

$$Z=\frac{\pi(1-P_d/2\delta)^{3/2}}{2.491\left\{\left[1+\left(\frac{1-P_d/2\delta}{1.23}\right)^2\right]^{1/2}-1\right\}}$$

since $P_d/2\delta=(1.5\times 10^{-5})/(5.779\times 10^{-5})=0.1298$

Thus

$Z=4.551$

Stage 2

$Z=4.551$

$$F_{max}=\frac{4.551\times 8900}{9}=4500\text{ N}$$

$\delta_i=2.725\times 10^{-5}$ m

$\delta_o=2.702\times 10^{-5}$ m

$\delta=5.427\times 10^{-5}$ m

$\frac{P_d}{2\delta}=0.1382$

Thus

$Z=4.565$

Stage 3

$Z=4.565$

$$F_{max}=\frac{4.565\times 8900}{9}=4514\text{ N}$$

$\delta_i=2.731\times 10^{-5}$ m

$\delta_o=2.708\times 10^{-5}$ m

$\delta=5.439\times 10^{-5}$ m

$\frac{P_d}{2\delta}=0.1379$

and hence

$Z=4.564$

This value is very close to the previous value from stage 2 of 4.565, and a further iteration confirms its accuracy.

Stage 4

$Z=4.564$

$$F_{max}=\frac{4.564\times 8900}{9}=4513\text{ N}$$

$\delta_i=2.731\times 10^{-5}$ m

$\delta_o=2.707\times 10^{-5}$ m

$\delta=5.438\times 10^{-5}$ m

$\frac{P_d}{2\delta}=0.1379$

and hence

$$Z = 4.564$$

The load on the most heavily loaded ball is thus 4513 N.

Elastohydrodynamic minimum film thickness.—For pure rolling

$$u = |\omega_o - \omega_i| \frac{d_e^2 - d^2}{4d_e} = 6.252 \text{ m/s} \qquad (3.6\text{-}28)$$

The dimensionless speed, materials, and load parameters for the inner- and outer-race conjunctions thus become

$$U_i = \frac{\eta_0 u}{E' R_{x,i}}$$

$$= \frac{0.04 \times 6.252}{2.198 \times 10^{11} \times 5.11 \times 10^{-3}} = 2.227 \times 10^{-10} \qquad (3.2\text{-}4)$$

$$G_i = \xi E' = 2.3 \times 10^{-8} \times 2.198 \times 10^{11} = 5055 \qquad (3.2\text{-}5)$$

$$W_i = \frac{F}{E' (R_{x,i})^2}$$

$$= \frac{4513}{2.198 \times 10^{11} \times (5.11)^2 \times 10^{-6}} = 7.863 \times 10^{-4} \qquad (3.2\text{-}3)$$

$$U_o = \frac{\eta_0 u}{E' R_{x,o}}$$

$$= \frac{0.04 \times 6.252}{2.198 \times 10^{11} \times 7.59 \times 10^{-3}} = 1.499 \times 10^{-10} \qquad (3.2\text{-}4)$$

$$G_o = \xi E' = 2.3 \times 10^{-8} \times 2.198 \times 10^{11} = 5055 \qquad (3.2\text{-}5)$$

$$W_o = \frac{F}{E' (R_{x,o})^2}$$

$$= \frac{4513}{2.198 \times 10^{11} \times (7.59)^2 \times 10^{-6}} = 3.564 \times 10^{-4} \qquad (3.2\text{-}3)$$

The dimensionless minimum elastohydrodynamic film thickness in a fully flooded elliptical contact is given by equation (3.3-1)

$$H_{\min} = \frac{h_{\min}}{R_x} = 3.63\ U^{0.68} G^{0.49} W^{-0.073} (1 - e^{-0.68k}) \qquad (3.3\text{-}1)$$

Ball-inner-race conjunction

$$(H_{\min})_i = 3.63 \times 2.732 \times 10^{-7} \times 65.29 \times 1.685 \times 0.9983$$

$$= 1.09 \times 10^{-4} \qquad (3.3\text{-}1)$$

Thus

$$(h_{\min})_i = 1.09 \times 10^{-4} R_{x,i} = 0.557\ \mu\text{m}$$

The lubrication factor Λ discussed in Section 3.6.5 was found to play a significant role in determining the fatigue life of rolling-element bearings. In this case

$$\Lambda_i = \frac{(h_{\min})_i}{(\Delta_a^2 + \Delta_b^2)^{1/2}}$$

$$= \frac{0.557 \times 10^{-6}}{[(0.175)^2 + (0.06225)^2]^{1/2} \times 10^{-6}} = 3.00 \qquad (3.6\text{-}58)$$

Ball-outer-race conjunction

$$(H_{\min})_o = \frac{(h_{\min})_o}{R_{x,o}}$$

$$= 3.63\ U_o^{0.68} G^{0.49} W^{-0.073} (1 - e^{-0.68k_o})$$

$$= 3.63 \times 2.087 \times 10^{-7} \times 65.29 \times 1.785 \times 0.9919$$

$$= 0.876 \times 10^{-4} \qquad (3.3\text{-}1)$$

Thus

$$(h_{\min})_o = 0.876 \times 10^{-4} R_{x,o} = 0.665\ \mu\text{m}$$

In this case, the lubrication factor Λ is given by

$$\Lambda_o = \frac{0.665 \times 10^{-6}}{[(0.175)^2 + (0.0625)^2]^{1/2} \times 10^{-6}} = 3.58 \qquad (3.6\text{-}58)$$

Once again, it is evident that the smaller minimum film thickness occurs between the most heavily loaded ball and the inner race. However, in this case the minimum elastohydrodynamic film thickness is about three times the composite surface roughness, and the bearing lubrication can be deemed to be entirely satisfactory.

4 Boundary Lubrication

If the pressures in fluid-film-lubricated machine elements are too high, the running speeds too low, or the surface roughness too great, penetration of the lubricant

film will occur. Contact will take place between asperities, leading to a rise in friction and wear rate. Figure 4.0-1 (obtained from Bowden and Tabor, 1973) shows the behavior of coefficient of friction in the different lubrication regimes. It is to be noted in this figure that in boundary lubrication, although the friction is much higher than in the hydrodynamic regime, it is still much lower than for unlubricated surfaces. As the running conditions are made more severe, the amount of lubricant breakdown increases until the system scores or seizes so badly that the machine element can no longer operate successfully.

Figure 4.0-2 shows the wear rate in the different lubrication regimes as determined by the operating load. In the hydrodynamic and elastohydrodynamic lubrication regimes, since there is no asperity contact, there is little or no wear. In the boundary lubrication regime the degree of asperity interaction and wear rate increases as the load increases. The transition from boundary lubrication to an unlubricated condition is marked by a drastic change in wear rate. Machine elements cannot operate successfully in the unlubricated region. Together figures 4.0-1 and 4.0-2 show that both friction and wear can be greatly decreased by providing a boundary lubricant to unlubricated surfaces.

Understanding boundary lubrication depends first on recognizing that bearing surfaces have asperities that are large compared with molecular dimensions. On the smoothest machined surfaces these asperities may be 25 nm (0.025 μm) high; on rougher surfaces they may be ten to several hundred times higher. Figure 4.0-3 illustrates typical surface roughness as a random distribution of hills and valleys with varying heights, spacing, and slopes. In the absence of hydrodynamic or elastohydrodynamic pressures these hills or asperities must support all of the load between the bearing surfaces. Understanding boundary lubrication also depends on recognizing that bearing surfaces are often covered by boundary lubricant films such as are idealized in figure 4.0-3. These films separate the bearing materials and, by shearing preferentially, provide some control of friction, wear, and surface damage.

Many mechanisms, such as door hinges, operate totally under conditions (high load, low speed) of boundary lubrication. Others are designed to operate under full hydrodynamic or elastohydrodynamic lubrication. However, as the oil film thickness is a function of speed, the film will be unable to provide complete separation of the surfaces during startup and rundown and the condition of boundary lubrication will exist. The problem from the boundary lubrication standpoint is to provide a boundary film with the proper physical characteristics to control friction and wear. The work of Bowden and Tabor (1973), Godfrey (1968), and Jones (1982) was relied upon in writing the sections that follow.

4.1 Formation of Films

The most important aspect of boundary lubrication is the formation of surface films that will protect the contacting surfaces. There are three ways of forming a boundary lubricant film: physical adsorption, chemisorption, and chemical reaction. The surface action that determines the behavior of boundary lubricant films is the energy binding the film molecules to the surface, a measure of the film strength. The formation of films is presented in the order of film strength, the weakest being presented first.

4.1.1 Physical adsorption

Physical adsorption involves intermolecular forces analogous to those involved in condensing vapors to liquids. A layer of lubricant one or more molecules thick

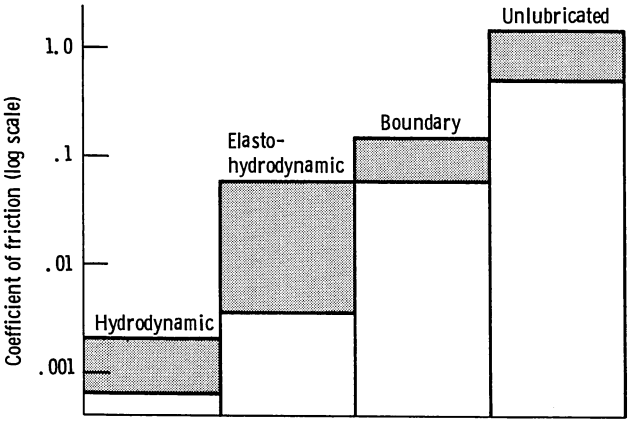

Figure 4.0-1.—Schematic drawing showing how type of lubrication shifts from hydrodynamic to elastohydrodynamic to boundary lubrication as severity of running conditions is increased. (From Bowden and Tabor, 1973.)

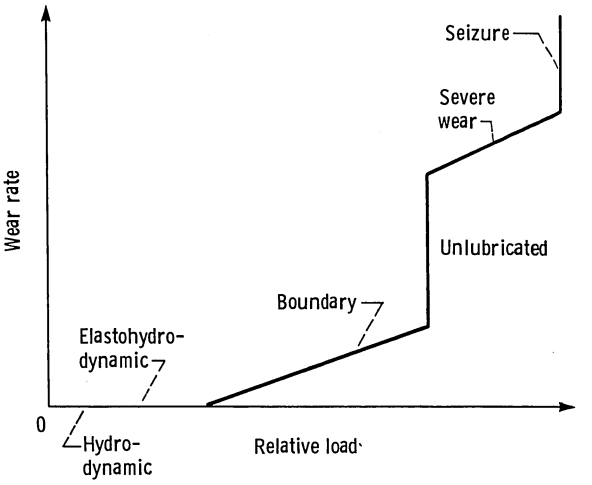

Figure 4.0-2.—Chart for determining wear rate for various lubrication regimes. (From Beerbower, 1972.)

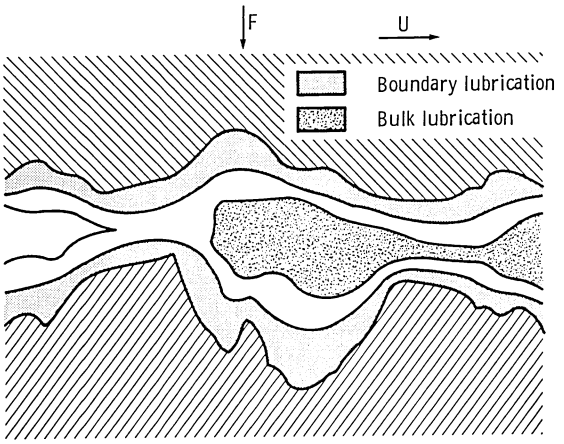

Figure 4.0-3.—Lubricated bearing surfaces. (From Fein and Villforth, 1973.)

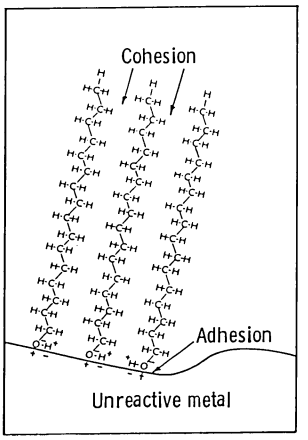

Figure 4.1-1.—Physical adsorption of hexadecanol. (From Godfrey, 1968.)

becomes attached to the surfaces of the solids, and this provides a modest protection against wear. Physical adsorption is usually rapid, reversible, and nonspecific. Energies involved in physical adsorption are in the range of heats of condensation. Physical adsorption may be monomolecular or multilayer. There is no electron transfer in this process. An idealized example of physical adsorption of hexadecanol on an unreactive metal is shown in figure 4.1-1. Because of the weak bonding energies involved, physically adsorbed species are usually not very effective boundary lubricants.

4.1.2 Chemical adsorption

Chemically adsorbed films are generally produced by adding animal and vegetable fats and oils to the base oils. These additives contain long-chain fatty acid molecules, which exhibit great affinity for metals at their active ends. The usual configuration of these polar molecules resembles that of a carpetpile with the molecules standing perpendicular to the surface. Such fatty acid molecules form metal soaps that are low-shear-strength materials with coefficients of friction in the range 0.10 to 0.15. The soap film is dense because of the preferred orientation of the molecules. For example, on a steel surface stearic acid will form a monomolecular layer of iron stearate, a soap containing 10^{14} molecules/cm^2 of surface. The effectiveness of these layers is limited by the melting point of the soap (180° C for iron stearate). It is clearly essential to choose an additive that will react with the bearing metals, so that less reactive inert metals like gold and platinum are not effectively lubricated by fatty acids.

Examples of fatty acid additives are stearic, oleic, and lauric acid. The soap films formed by these acids might reduce the coefficient of friction to 50 percent of that obtained by a straight mineral oil. They provide satisfactory boundary lubrication at moderate loads, temperatures, and speeds and are often successful in situations showing evidence of mild surface distress.

Chemisorption of a film on a surface is usually specific, may be rapid or slow, and is not always reversible. Energies involved are large enough to imply that a chemical bond has formed (i.e., electron transfer has taken place). In contrast to physical adsorption chemisorption may require an activation energy. A film may be physically adsorbed at low temperatures and chemisorbed at higher temperatures. In addition physical adsorption may occur on top of a chemisorbed film. An example of a film of stearic acid chemisorbed on an iron oxide surface to form iron stearate is shown in figure 4.1-2.

4.1.3 Chemical reaction

Films formed by chemical reaction are strongest and are used in the most severe operating conditions. If the load and sliding speeds are high, significant contact temperatures will be developed. It has already been noted that films formed by physical and chemical adsorption cease to be effective above certain transition tempera-

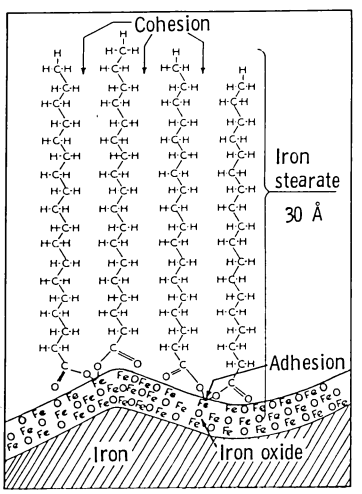

Figure 4.1-2.—Chemisorption of stearic acid on iron surface to form iron stearate. (From Godfrey, 1968.)

tures, but some additives start to react and form new high-melting-point inorganic solids at high temperatures. For example, sulfur will start to react at about 100° C to form sulfides with melting points of over 1000° C. Lubricants containing additives like sulfur, chlorine, phosphorous, and zinc are often referred to as extreme-pressure (EP) lubricants since they are effective under the most arduous conditions.

The formation of a chemical reaction film is specific, may be rapid or slow (depending on temperature, reactivity, and other conditions), and is irreversible. An idealized example of a reacted film of iron sulfide on an iron surface is shown in figure 4.1-3.

4.2 Physical Properties of Boundary Films

The two physical properties of boundary films that are most important in determining their effectiveness in protecting surfaces are melting point and shear strength. It is assumed that the film thicknesses involved are sufficient to allow these properties to be well defined.

4.2.1 Melting point

The melting point of a surface film appears to be one discriminating physical property governing failure temperature for a wide range of materials including inorganic salts. It is based on the observation that only a surface film that is solid can properly interfere with potentially damaging asperity contacts. Conversely, a liquid film allows high friction and wear. Under practical conditions, physically adsorbed additives are known to be effective only at low temperatures, and chemisorbed additives at moderate temperatures. High-melting-point inorganic materials are used for high-temperature lubricants.

The correlation of melting point with failure temperature has been established for a variety of organic films. Figure 4.2-1 (obtained from Russell et al., 1965) shows the friction transition for copper lubricated with pure hydrocarbons. Friction data for two hydrocarbons (mesitylene and dotriacontane) are given as a function of temperature. In this figure the boundary film failure occurs at the melting point of each hydrocarbon.

In contrast, chemisorption of fatty acids on reactive metals yields failure temperature based on the softening

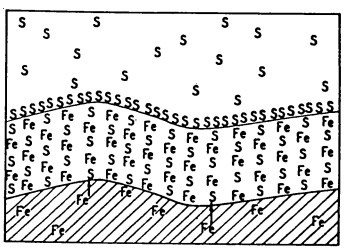

Figure 4.1-3.—Formation of inorganic film by reaction of sulfur with iron to form iron sulfide. (From Godfrey, 1968.)

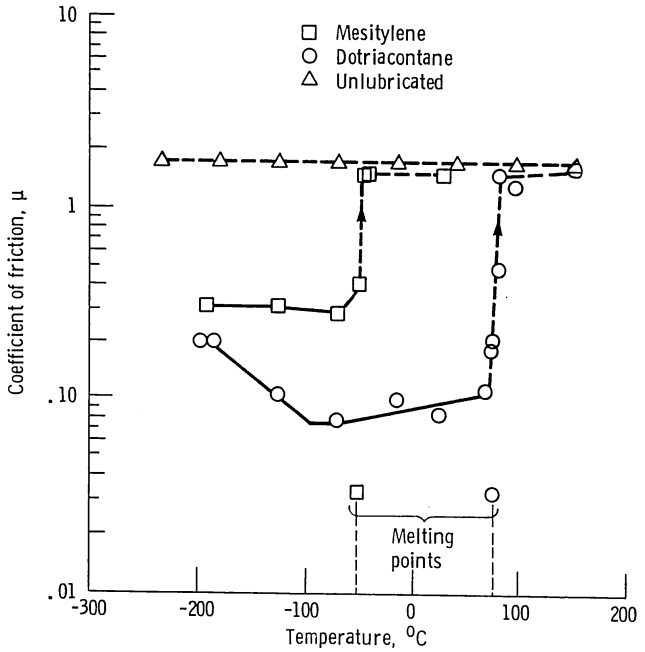

Figure 4.2-1.—Chart for determining friction of copper lubricated with hydrocarbons in dry helium. (From Russell et al., 1965.)

point of the soap rather than the melting point of the parent fatty acid.

4.2.2 Shear strength

The shear strength of a boundary lubricating film should be directly reflected in the friction coefficient. In general, this is true with low-shear-strength soaps yielding low friction and high-shear-strength salts yielding high friction. However, the important parameter in boundary friction is the ratio of shear strength of the film to that of the substrate. This relationship is shown in figure 4.2-2, where the ratio is plotted on the horizontal axis with a value of 1 at the left and zero at the right.

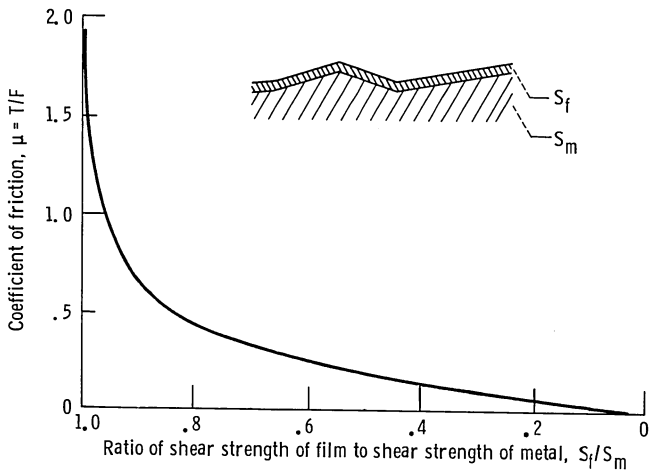

Figure 4.2-2.—Chart for determining friction as function of shear strength ratio. (From Godfrey, 1968.)

These results are in agreement with experience. For example, on steel an MoS_2 film gives low friction and Fe_2O_3 gives high friction. The results from figure 4.2-2 also indicate how the same friction value can be obtained with various combinations provided that the ratio is the same. It is also important to recognize that shear strength is affected by pressure and temperature.

4.3 Film Thickness

Boundary film thickness can vary from a few angstroms (adsorbed gas) to thousands of angstroms (chemical reaction films). In general, as the thickness of a boundary film increases, the coefficient of friction decreases. This effect is shown in figure 4.3-1, in which the coefficient of friction is plotted against oxide film thickness formed on a copper surface. However, continued increases in thickness may result in an increase in friction. This effect is shown in the lower plot of figure 4.3-1, in which the coefficient of friction is plotted against indium film thickness on a copper surface. Note that the shear strength of all boundary films decreases as their thickness increases, which may be related to the effect shown.

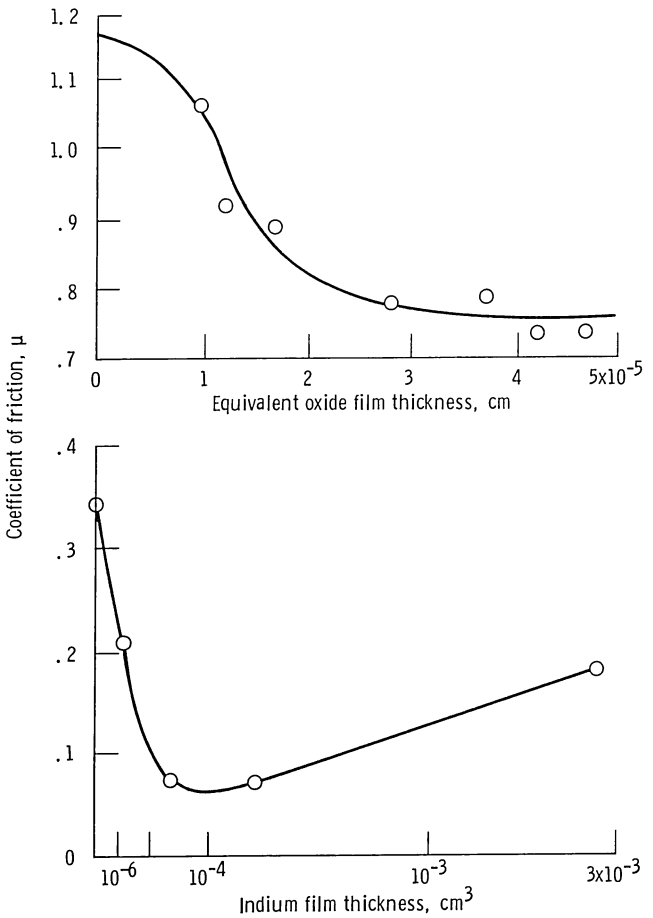

Figure 4.3-1.—Chart for determining relationship of friction and thickness of films on copper surfaces. (From Kragelski, 1965.)

For physically adsorbed or chemisorbed films, surface protection is usually enhanced by increasing film thickness. The frictional transition temperature of multilayers also increases with increasing number of layers.

For thick chemically reacted films there is an optimum thickness for minimum wear that depends on temperature, concentration, or load conditions. The relationship between wear and lubricant (or additive) reactivity is shown in figure 4.3-2. Here, if reactivity is not great enough to produce a thick enough film, adhesion wear occurs. On the other hand, if the material is too reactive, very thick films are formed and corrosive wear ensues.

4.4 Effect of Operating Variables

The effect of load, speed, temperature, and atmosphere can be important for the friction and wear of boundary lubrication films. Such effects are considered in this section.

4.4.1 On friction

Load

The coefficient of friction is essentially constant with increasing load.

Speed

In general, in the absence of viscosity effects, friction changes little with speed over a sliding speed range of 0.005 to 1.0 cm/sec. When viscosity effects do come into play, two types of behavior are observed, as shown in figure 4.4-1. Relatively nonpolar materials such as mineral oils show a decrease in friction with increasing speed, while polar fatty acids show the opposite trend. At

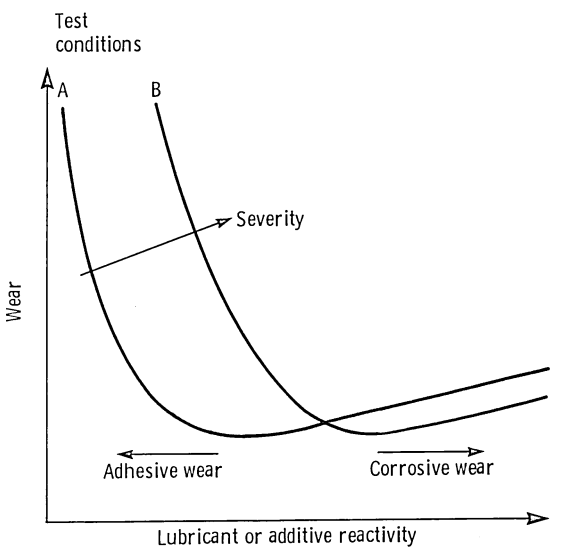

Figure 4.3-2.—Relationship between wear and lubricant reactivity. (From Rowe, 1973.)

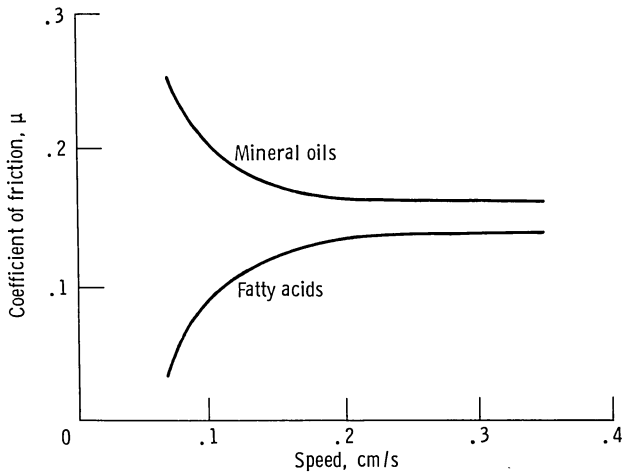

Figure 4.4-1.—Effect of speed on coefficient of friction. (From Clayton, 1951.)

higher speeds viscous effects will be present, and increases in friction are normally observed.

Temperature

It is difficult to make general comments on the effect of temperature on boundary friction since so much depends on the other conditions and the type of materials present. Temperature can cause disruption, desorption, or decomposition of boundary films. It can also provide activation energy for chemisorption or chemical reactions.

Atmosphere

The presence of oxygen and water vapor in the atmosphere can greatly affect the chemical processes that occur in the boundary layer. These processes can, in turn, affect the friction coefficient.

4.4.2 On wear

Load

It is generally agreed that wear increases with increasing load, but no simple relationship seems to exist, at least before the transition to severe wear occurs. At this point a discontinuity of wear versus load is observed (fig. 4.0-2).

Speed

For practical purposes, wear rate in a boundary lubrication regime is essentially independent of speed. This assumes no boundary film failure due to contact temperature rise.

Temperature

As was the case for friction, there is no way to generalize the effect of temperature on wear. The same statement that pertains to friction also pertains to wear.

Atmosphere

Oxygen has been shown to be an important ingredient in boundary lubrication experiments involving load-carrying additives. The presence of oxygen or moisture in the atmosphere has a great effect on the wear properties of lubricants containing aromatic species.

4.5 Extreme-Pressure (EP) Lubricants

The best boundary lubricant films cease to be effective above 200° to 250° C. At these high temperatures the lubricant film may oxidize. To operate under more severe conditions, extreme-pressure (EP) lubricants might be considered.

EP lubricants usually consist of a small quantity of an EP additive dissolved in a lubricating oil, usually referred to as the base oil. The most common additives used for this purpose contain phosphorus, chlorine, or sulfur. In general, these materials function by reacting with the surface to form a surface film that prevents metal-to-metal contact. If in addition the surface film formed has a low shear strength, it will not only protect the surface, but will also give a low coefficient of friction. Chloride films give a lower coefficient of friction ($\mu = 0.2$) than sulfide films ($\mu = 0.5$). Sulfide films, however, are more stable, are unaffected by moisture, and retain their lubricating properties to very high temperatures.

Although EP additives function by reacting with the surface, they must not be too reactive; otherwise chemical corrosion may be more troublesome than frictional wear. They should only react when there is a danger of seizure, usually noticed by a sharp rise in local or global temperature. For this reason it is often an advantage to incorporate in a lubricant a small quantity of a fatty acid that can provide effective lubrication at temperatures below those at which the additive becomes reactive. Bowden and Tabor (1973) describe this behavior in figure 4.5-1, where the coefficient of friction is plotted against temperature. Curve A is for paraffin oil (the base oil) and shows that the friction is initially high and increases as the temperature is raised. Curve B is for a fatty acid dissolved in the base oil: it reacts with the surface to form a metallic soap, which provides good lubrication from room temperature up to the temperature at which the soap begins to soften. Curve C is for a typical extreme-pressure additive in the base oil: this reacts very slowly below the critical temperature T_c so that in this range the lubrication is poor, while above T_c the protective film is formed and effective lubrication is provided to a very high temperature. Curve D is the result

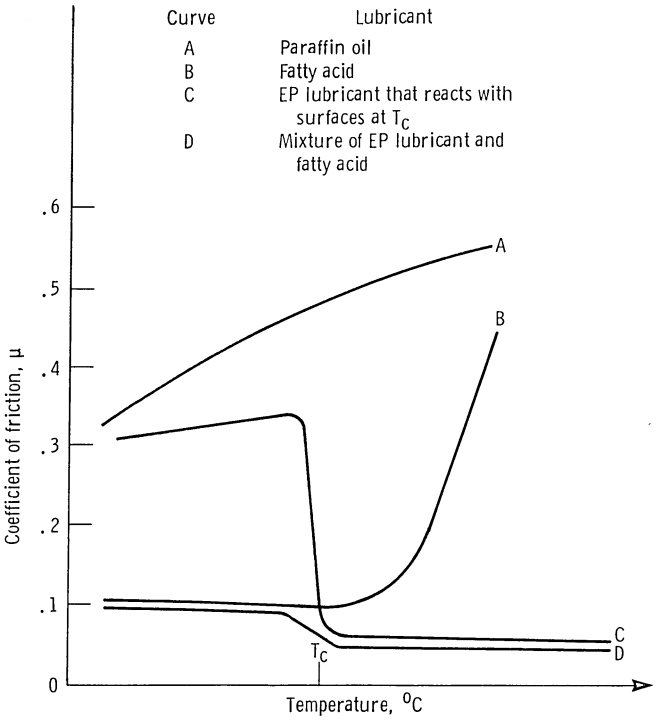

Figure 4.5-1.—Graph showing frictional behavior of metal surfaces with various lubricants. (From Bowden and Tabor, 1973.)

obtained when the fatty acid is added to the EP solution. Good lubrication is provided by the fatty acid below T_c; above this temperature the greater part of the lubrication is due to the additive. At still higher temperatures, a deterioration of lubricating properties will also occur for both curves C and D.

References

AFBMA (1960a) "Method of Evaluating Load Ratings for Roller Bearings," AFBMA Standard System No. 11. (Anti-Friction Bearing Manufacturers Association, Inc., New York).

AFBMA (1960b) "Method of Evaluating Load Ratings for Ball Bearings," AFBMA Standard System No. 9, Revision No. 4. (Anti-Friction Bearing Manufacturers Association, Inc., New York).

Aihara, S., and Dowson, D. (1979), "A Study of Film Thickness in Grease Lubricated Elastohydrodynamic Contacts," in *Proceedings of Fifth Leeds-Lyon Symposium on Tribology on Elastohydrodynamics and Related Topics,* D. Dowson, C. M. Taylor, M. Godet, and D. Berthe, eds., Mechanical Engineering Publications, Bury St. Edmunds, Suffolk, 104-115.

Allaire, P. E., and Flack, R. D. (1980) "Journal Bearing Design for High Speed Turbomachinery," *Bearing Design—Historical Aspects, Present Technology and Future Problems,* W. J. Anderson, ed., American Society of Mechanical Engineers, New York, 111-160.

Anderson, W. J. (1970) "Elastohydrodynamic Lubrication Theory as a Design Parameter for Rolling Element Bearings," ASME Paper 70-DE-19.

Bamberger, E. N., Harris, T. A., Kacmarsky, W. M., Moyer, C. A., Parker, R. J., Sherlock, J. J., and Zaretsky, E. V. (1971) *Life Adjustment Factors for Ball and Roller Bearings—An Engineering Design Guide,* American Society for Mechanical Engineers, New York.

Barus, C. (1893) "Isotherms, Isopeistics and Isometrics Relative to Viscosity," Am. J. Sci., vol. 45, 87-96.

Beerbower, A. (1972) "Boundary Lubrication," *Scientific and Technical Application Forecasts,* Department of Army, DAC-19-69-C-0033.

Bisson, E. E., and Anderson, W. J. (1964) *Advanced Bearing Technology,* NASA SP-38.

Bowden, F. P., and Tabor, D. (1973) *Friction—An Introduction to Tribology,* Heinemann, London.

Brewe, D. E., Hamrock, B. J., and Taylor, C. M. (1979) "Effect of Geometry on Hydrodynamic Film Thickness," J. Lubr. Technol., vol. 101 (2), 231-239.

Cameron, A., and Gohar, R. (1966) "Theoretical and Experimental Studies of the Oil Film in Lubricated Point Contacts," Proc. R. Soc. London, ser. A, vol. 291, 520-536.

Clayton, D. (1951) "An Introduction to Boundary and Extreme Pressure Lubrication," Physics of Lubrication, Br. J. Appl. Phys., vol. 2, Suppl. 1, 25.

Dowson, D. (1965) "Elastohydrodynamic Lubrication—An Introduction and a Review of Theoretical Studies," Institution of Mechanical Engineers, London, Proc., vol. 180, pt. 3B, 7-16.

Dowson, D., and Higginson, G. R. (1966) *Elastohydrodynamic Lubrication, the Fundamentals of Roller and Gear Lubrication,* Pergamon, Oxford.

Engineering Sciences Data Unit (ESDU) (1965) "General Guide to the Choice of Journal Bearing Type," Engineering Sciences Data Unit, Item 65007, Institution of Mechanical Engineers, London, England.

Engineering Sciences Data Unit (ESDU) (1967) "General Guide to the Choice of Thrust Bearing Type," Engineering Sciences Data Unit, Item 67033, Institution of Mechanical Engineers, London.

Engineering Sciences Data Unit (ESDU) (1978) "Contact Stresses," Engineering Sciences Data Unit, Item 78035, Institution of Mechanical Engineers, London.

Fein, R. S., and Villforth, F. J., (1973) "Lubrication Fundamentals," Lubrication (Texaco Inc.), New York, 77-88.

Fleming, D. P. and Hamrock, B. J. (1974) "Optimization of Self-Acting Herringbone Journal Bearings for Maximum Stability," *6th International Gas Bearing Symposium,* Southhampton, Paper C1, 1-11.

Godfrey, D. (1968) "Boundary Lubrication," in *Interdisciplinary Approach to Friction and Wear,* NASA SP-181, P. M. Ku, ed., 335-384.

Gross, W. A., Matsch, L. A., Castelli, V., Eshel, A., and Wildmann, M. (1980) *Fluid Film Lubrication,* Wiley, New York.

Grubin, A. N. (1949) "Fundamentals of the Hydrodynamic Theory of Lubrication of Heavily Loaded Cylindrical Surfaces," in *Investigation of the Contact Machine Components,* Kh. F. Ketova, ed., translation of Russian Book No. 30, Central Scientific Institute of Technology and Mechanical Engineering, Moscow, Ch. 2. (Available from Dept. of Scientific and Industrial Research, Great Britain, Transl. CTS-235, and from Special Libraries Association, Chicago, Transl. R-3554.)

Gunter, E. J., Hinkle, J. G., and Fuller, D. D. (1964) "Design Guide for Gas-Lubricated Tilting-Pad Journal and Thrust Bearings with Special Reference to High Speed Rotors," Franklin Institute Research Laboratories Report I-A2392-3-1.

Hamrock, B. J. (1972) "Optimization of Self-Acting Step Thrust Bearings for Load Capacity and Stiffness," ASLE Trans., vol. 15, no. 3, 159-170.

Hamrock, B. J. (1983) "Optimum Parallel Step-Sector Bearing Lubricated with an Incompressible Fluid," NASA TM-83356.

Hamrock, B. J., and Anderson, W. J. (1973) "Analysis of an Arched Outer-Race Ball Bearing Considering Centrifugal Forces," ASME Journal of Lubrication Technology, vol. 95, no. 3, 265-276.

Hamrock, B. J., and Anderson, W. J. (1983) "Rolling-Element Bearings," NASA RP-1105.

Hamrock, B. J., and Brewe, D. (1983) "Simplified Solution for Stresses and Deformations," J. Lubr. Technol., vol. 105, no. 2, 171-177.

Hamrock, B. J., and Dowson, D. (1976) "Isothermal Elastohydrodynamic Lubrication of Point Contacts, Part I-Theoretical Formulation," J. Lubr. Technol., vol. 98, no. 22, 223-229.

Hamrock, B. J., and Dowson, D. (1977) "Isothermal Elastohydrodynamic Lubrication of Point Contacts, Part III-Fully Flooded Results," J. Lubr. Technol., vol. 99, no. 2, 264-276.

Hamrock, B. J., and Dowson, D. (1978) "Elastohydrodynamic Lubrication of Elliptical Contacts for Materials of Low Elastic Modulus, Part I-Fully Flooded Conjunction," J. Lubr. Technol. vol. 100, no. 2, 236-245.

Hamrock, B. J., and Dowson, D. (1979) "Minimum Film Thickness in Elliptical Contacts for Different Regimes of Fluid-Film Lubrication," in *Proceedings of Fifth Leeds-Lyon Symposium on Tribology on Elastohydrodynamics and Related Topics,* D. Dowson, C. M. Taylor, M. Godet, and D. Berthe, eds, Mechanical Engineering Publications, Bury St. Edmunds, Suffolk, 22-27.

Hamrock, B. J., and Dowson, D. (1981) *Ball Bearing Lubrication—The Elastohydrodynamics of Elliptical Contacts,* Wiley, New York.

Hamrock, B. J., and Fleming, D. P. (1971) "Optimization of Self-Acting Herringbone Grooved Journal Bearings for Minimum Radial Load," in *Proceedings of Fifth International Gas Bearing Symposium,* Southampton, paper 13.

Hardy, W. B., and Doubleday, I. (1922a) "Boundary Lubrication—The Temperature Coefficient," Proc. R. Soc., vol. A101, 487-492.

Hardy, W. B., and Doubleday, I. (1922b) "Boundary Lubrication—The Paraffin Series," Proc. R. Soc., vol. A104, 25-39.

Hertz, H., (1881) "The Contact of Elastic Solids," J. Reine Angew. Math., vol. 92, 156-171.

ISO (1976) "Rolling Bearings, Dynamic Load Ratings and Rating Life," ISO/TC4/JC8, Revision of ISOR281. Issued by International Organization for Standardization, Technical Committee ISO/TC4.

Jones, A. B. (1946) "Analysis of Stresses and Deflections," New Departure Engineering Data, General Motors Corp., Bristol, Conn.

Jones, A. B. (1964) "The Mathematical Theory of Rolling Element Bearings," in *Mechanical Design and Systems Handbook,* H. A. Rothbart, ed., McGraw-Hill, New York, 13-1 to 13-76.

Jones, W. R. (1982) "Boundary Lubrication—Revisited," NASA TM-82858.

Jones, W. R., Johnson, R. L., Winer, W. O, and Sanborn, D. M. (1975) "Pressure-Viscosity Measurements for Several Lubricants to 5.5×10^8 Newtons Per Square Meter (8×10^4 psi) and 149° C (300° F), ASLE Trans., vol. 18, no. 4, 249-262.

Kapitza, P. L. (1955) "Hydrodynamic Theory of Lubrication During Rolling," Zh. Tekh. Fiz., vol. 25, no. 4, 747-762.

Kragelski, I. V. (1965) *Friction and Wear,* Buttersworths, 158-163.

Lundberg, G., and Palmgren, A. (1947) "Dynamic Capacity of Rolling Bearings," Acta Polytechnica, Mechanical Engineering Series, vol. I, no. 3.

Lundberg, G., and Palmgren, A. (1952) "Dynamic Capacity of Rolling Bearings," Acta Polytechnica, Mechanical Engineering Series, vol. II, no. 4.

Newton, I. (1687) *Philosophiae Naturalis Principia Mathematica,* Imprimature S. Pepys. Reg. Soc. Praess, 5 Julii 1866. Revised and supplied with a historical and explanatory appendix by F. Cajori, edited by R. T. Crawford (1934), and published by the University of California Press, Berkeley and Los Angeles (1966).

Petrov, N. P. (1883) "Friction in Machines and the Effect of the Lubricant," Inzh. Zh. St-Petreb., vol. 1, 71-140; vol. 2, 227-279; vol. 3, 377-436; vol. 4, 535-564.

Petrusevich, A. J. (1951) "Fundamental Conclusion from the Contact-Hydrodynamic Theory of Lubrication," Zv. Akad, Nauk, SSSR(OTN), vol. 2, 209.

Pinkus, O., and Sternlicht, B. (1961) *Theory of Hydrodynamic Lubrication,* McGraw Hill, New York.

Raimondi, A. A., and Boyd, J. (1955) "Applying Bearing Theory to the Analysis and Design of Pad-Type Bearings," Trans. ASME, April, 287-309.

Raimondi, A. A., and Boyd, J. (1958) "A Solution for the Finite Journal Bearing and Its Application to Analysis and Design; III, Trans. ASLE, vol. 1, no. 1, 194-209.

Reiger, N. F. (1967) *Design of Gas Bearings,* Mechanical Technology, Inc., Latham, New York.

Reynolds, O. (1886) "On the Theory of Lubrication and Its Application to Mr. Beauchamp Tower's Experiments, Including an Experimental Determination of the Viscosity of Olive Oil," Philos, Trans. R. Soc. London, vol. 177, 157-234.

Rippel, H. C., (1963) *Cast Bronze Hydrostatic Bearing Design Manual,* Cast Bronze Bearing Institute, Inc., Cleveland, Ohio.

Rowe, C. N. (1973) "Wear Corrosion and Erosion," *Interdisciplinary Approach to Liquid Lubricant Technology,* ed., P. M. Ku, NASA SP-237, 469-527.

Russell, J. A., Campbell, W. C., Burton, R. A., and Ku, P. M. (1965) "Boundary Lubrication Behavior of Organic Films at Low Temperatures," ASLE Trans., vol. 8, no. 1, 48.

Skurka, J. C., (1970) "Elastohydrodynamic Lubrication of Roller Bearings," J. Lubr. Technol., vol. 92, no. 2, 281-291.

Stribeck, R. (1901) "Kugellager fur beliebige Belastungen," VDI-Zeitschrift, vol. 45, no. 3, 73-125.

Tallian, T. E. (1967) "On Competing Failure Modes in Rolling Contact," Trans. ASLE, vol. 10, 418-439.

Tallian, T., Sibley, L., and Valori, R. (1965) "Elastohydrodynamic Film Effect on the Load-Life Behavior of Rolling Contacts," ASME Paper 65-LUB-11.

Tower, B. (1883) "First Report on Friction Experiments (Friction of Lubricated Bearings)." Proc. Inst. Mech. Eng., London, 632-659.

Weibull, W. (1949) "A Statistical Representation of Fatigue Failures in Solids," Trans. Roy. Inst. Tech., Stockholm, vol. 27.

Wilson, A. R., (1979) "The Relative Thickness of Grease and Oil Films in Rolling Bearings," Proc. Inst. Mech. Eng., London, vol. 193, no. 17, 185-192.

1. Report No.	2. Government Accession No.	3. Recipient's Catalog No.
NASA RP-1126		

4. Title and Subtitle	5. Report Date
Lubrication of Machine Elements	August 1984
	6. Performing Organization Code: 506-53-1B

7. Author(s)	8. Performing Organization Report No.
Bernard J. Hamrock	E-1949
	10. Work Unit No.

9. Performing Organization Name and Address	11. Contract or Grant No.
National Aeronautics and Space Administration Lewis Research Center Cleveland, Ohio 44135	13. Type of Report and Period Covered: Reference Publication

12. Sponsoring Agency Name and Address	14. Sponsoring Agency Code
National Aeronautics and Space Administration Washington, D.C. 20546	

15. Supplementary Notes

Published as Chapter 23 in Kent Handbook of Mechanical Engineering, John Wiley & Sons, 1984.

16. Abstract

By 1950 two distinct regimes of lubrication were generally recognized. The understanding of hydrodynamic lubrication began with the classical experiments of Tower (1883), in which the existence of a film was detected from measurements of pressure within the lubricant, and of Petrov (1883), who reached the same conclusion from friction measurements. Reynolds (1886) used a reduced form of the Navier-Stokes equations and the continuity equation to generate a second-order differential equation for the pressure in the narrow, converging gap of a bearing contact. Such a pressure enables a load to be transmitted between the surfaces with very low friction since the surfaces are completely separated by a film of fluid. In such as situation it is the physical properties of the lubricant, notably the dynamic viscosity, that dictate the behavior of the contact. The understanding of boundary lubrication is normally attributed to Hardy and Doubleday (1922a and b), who found that very thin films adhering to surfaces were often sufficient to assist relative sliding. Boundary lubrication is at the opposite end of the lubrication spectrum from hydrodynamic lubrication. In boundary lubrication it is the physical and chemical properties of thin films of molecular proportions and the surfaces to which they are attached that determine contact behavior. The lubricant viscosity is not an influential parameter. In the last 30 years research has been devoted to a better understanding and more precise definition of other lubrication regimes between these extremes. One such regime, elastohydrodynamic lubrication, occurs in nonconformal contacts, where the pressures are high and the bearing surfaces deform elastically. In this situation the viscosity of the lubricant may raise considerably, and this further assists the formation of an effective fluid film. Significant progress has been made in our understanding of the mechanism of elastohydrodynamic lubrication, generally viewed as reaching maturity. This report briefly describes the science of these three lubrication regimes (hydrodynamic, elastohydrodynamic, and boundary) and then demonstrates how this science is used in the design of machine elements.

17. Key Words (Suggested by Author(s))	18. Distribution Statement
Boundary lubrication; Hydrodynamic lubrication; Elastohydrodynamic lubrication; Lubrication	Unclassified - unlimited STAR category 37

19. Security Classif. (of this report)	20. Security Classif. (of this page)	21. No. of pages	22. Price*
Unclassified	Unclassified	91	A05

*For sale by the National Technical Information Service, Springfield, Virginia 22161

NASA-Langley, 1984

National Aeronautics and Space Administration

Washington, D.C.
20546

Official Business
Penalty for Private Use, $300

THIRD-CLASS BULK RATE

Postage and Fees Paid
National Aeronautics and
Space Administration
NASA-451

U.S.MAIL

10 1 RP,D, 840810 S00715BS
PRINCETON UNIV
ENGINEERING QUADRANGLE
ATTN: ENGINEERING LIBRARY
P O BOX 710
PRINCETON NJ 08544

NASA

POSTMASTER: If Undeliverable (Section 158 Postal Manual) Do Not Return